CONCEPTUAL DESIGN AND EVALUATION OF A NOVEL MULTI-MATERIAL BIOPRINTING SYSTEM

A Thesis Submitted to the
College of Graduate and Postdoctoral Studies
In Partial Fulfillment of the Requirements
For the Degree of Master of Science
In the Department of Mechanical Engineering
University of Saskatchewan
Saskatoon

By

NICHOLAS BETANCOURT

PERMISSION TO USE

In presenting this thesis/dissertation in partial fulfillment of the requirements for a Postgraduate degree from the University of Saskatchewan, I agree that the Libraries of this University may make it freely available for inspection. I further agree that permission for copying of this thesis/dissertation in any manner, in whole or in part, for scholarly purposes may be granted by the professor or professors who supervised my thesis/dissertation work or, in their absence, by the Head of the Department or the Dean of the College in which my thesis work was done. It is understood that any copying or publication or use of this thesis/dissertation or parts thereof for financial gain shall not be allowed without my written permission. It is also understood that due recognition shall be given to me and to the University of Saskatchewan in any scholarly use which may be made of any material in my thesis/dissertation.

Requests for permission to copy or to make other uses of materials in this thesis/dissertation in whole or part should be addressed to:

Head of the Department of Mechanical Engineering

57 Campus Drive

University of Saskatchewan

Saskatoon, Saskatchewan S7N 5A9 Canada

OR

Dean

College of Graduate and Postdoctoral Studies

University of Saskatchewan

116 Thorvaldson Building, 110 Science Place

Saskatoon, Saskatchewan S7N 5C9 Canada

ABSTRACT

Millions of people suffer from damaged tissues or organs. The gold standard for treatment is tissue/organ transplantation; however, the demand for donated tissues and organs eclipses the number of donors. Scaffold-based tissue engineering aims to produce tissue/organ substitutes or scaffolds for transplants or implantation for promoting tissue regeneration. Extrusion-based bioprinting has recently emerged to create scaffolds by printing biomaterials with living cells in a layer-by-layer pattern. A significant limitation of existing extrusion-based techniques is their material distribution, e.g., printing scaffolds from only one material. Multi-material bioprinting is essential to mimic the complex anisotropic and heterogeneous features of native tissues. Researchers have taken steps towards making multi-material scaffolds; however, current methods are limited in terms of the material distribution and longitudinal/circumferential organization in the printed filaments.

This M.Sc. work aims to study the design of a multi-material bioprinting system with spatial control of material in longitudinal and circumferential directions. The design was conceived through a methodical approach, from technical specifications to conceptual-, embodiment-, and detail-design stages. The system will employ a combination of a desktop 3D printer for x-y-z control, a multi-channel pressure controller for on-the-fly adjustments, a custom printhead for organizing multiple inlets to a single outlet, and a carriage to affix the printhead assembly to the x-y-z- controller. For the proposed system, spatial control of material comes from several configurations of the custom modular printhead and the flow controller. Axiomatic Design principles are then used to compare and evaluate the proposed systems against existing systems in terms of material control and ease of configurability. Specified functional requirements and design ranges quantify longitudinal and circumferential material control and ease of configurability. Then, the system ranges for the functional requirements were built using the reported data of the existing systems. Axiom 1 shows that side-by-side, core-and-shell, and advanced techniques lack functional independence. Then, Axiom 2 shows that the proposed technique has the probability of completing the specified functions, granting it as the single-best design. The resulting design, justified by the evaluation and comparison, shows that this work is promising in helping researchers realize intricate scaffold designs with specific material control.

ACKNOWLEDGEMENTS

The work in this thesis would not have been possible without the guidance and expertise of my supervisor, Dr. Daniel Chen. Thank you, Dr. Chen, for pushing me every step of the way and for introducing me to the field of tissue engineering. You helped me find my passion. Your patience and enthusiasm in research and teaching are inspiring.

Thank you to the members of my advisory committee, Dr. Duncan Cree and Dr. Donald Bergstrom, for their kind words, encouragement, and research advice.

Thank you to the entire Biofabrication Group for sharing your expansive knowledge of research with me. In particular, thank you to Mr. Reza Gharraei Khosroshahi for assisting me with the mixing considerations and detailed design of the printhead components. Also, thank you to Mr. Doug Bitner for aiding in the procurement and selection of equipment for the bioprinting system, as well as sharing technical advice on prototyping.

I acknowledge the financial support from the University of Saskatchewan Devolved M.Sc. Scholarship from the Department of Mechanical Engineering and the support from Natural Science and Research Council (NSERC) to the Biofabrication Group.

DEDICATION

I dedicate this thesis to my loving family and friends who believed in me and challenged me during my graduate studies.

Gido, you taught me how to think like a problem solver and to never give up.

Baba, you showed me the importance of being strong.

Abuela, me mostraste cómo enfrentar los desafíos de la vida con resiliencia y elegancia.

Mom, your unrelenting work ethic is what I hope to achieve one day.

Papa, me enseñaste sobre vivir con pasión, compasión y estilo.

Natalia, you're an example of taking dreams into your own hands.

Paige, you take every day to the fullest and don't take a moment for granted.

Thank you.

Your unconditional love and support can not be quantified – this work is for you.

TABLE OF CONTENTS

LIST OF TABLES

LIST OF FIGURES

LIST OF ABBREVIATIONS

Abbreviation

3D – Three Dimensional

AM - Acetoxymethyl

CAD - Computer-Aided Design

CR - Constraint Requirement

CT - Computed Tomography

Da - Dalton (Unit)

DP - Design Parameter

ECM - Extracellular Matrix

FCBPSS - Function, Context, Behaviour, Principle, Structure

FDM - Fused Deposition Modelling

FR - Functional Requirement

GelMA - Gelatin Meth Acryloyl

ISO - International Organization for Standardization

LAP - Lithium Phenyl-2,4,6-trimethyl-benzoyl Phosphinate

MRI - Magnetic Resonance Imaging

MW - Molecular Weight (unit)

PCL - Polycaprolactone

PEGDA – Poly (Ethylene Glycol) Diacrylate

PEGTA - Pentaerythritol Triacrylate

PETG - Polyethylene Terephthalate Glycol

PLGA - Poly (Lactic-co-Glycolic Acid)

PR - Performance Requirement

USB - Universal Serial Bus

UV - Ultraviolet

α-TCP - Alpha-Tricalcium Phosphate

µm – micrometre (unit)

1.0 INTRODUCTION

This chapter provides a brief introduction to the M.Sc. work, including the background and motivation, research issues and objectives, and an overview of the methodology used to address the issues and fulfil the objectives.

1.1 Background and Motivation

Millions of people suffer from damaged tissues or organs and require donors for treatment. The demand for donations eclipses the number of donors with no significant signs of evening out (Canadian Blood Services 2018). Scaffold-based tissue engineering aims to produce a permanent substitute for implantation by creating cell-laden structures made of biomaterials and organized in a way to promote new tissue generation while the scaffold degrades over time. Initial studies with human recipients of engineered bladders show that this work is promising and provides an exciting step forward to wide adoption (Atala 2011). Figure 1.1 shows the principles of tissues of scaffold-based tissue engineering, starting with the harvest from a patient and expansion of cells in culture to the fabrication, maturation, and implantation of the cell-laden scaffold to the patient for tissue/organ repair (X. Chen 2018).

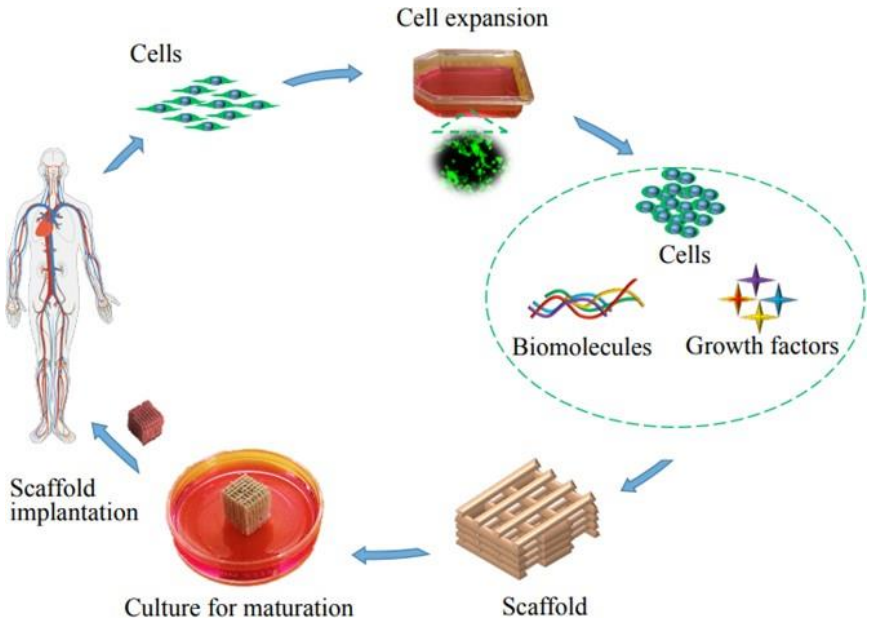

Figure 1.1: Principle of Scaffold-based Tissue Engineering (X. Chen 2018)

Tissue scaffolds, such as those shown in Figure 1.1, are typically made by layer-by-layer deposition of cell-laden material using additive manufacturing techniques, dubbed bioprinting. A

common bioprinting method is extrusion-based bioprinting, wherein scaffold material is ejected from syringe and lands onto the printing stage via mechanical forces; pneumatic, screw, or piston. Together, a dispenser controller, position controller, and temperature controller make an extrusion bioprinting system that can create three dimensional (3D) tissue scaffolds. Notably, most scaffolds made with extrusion-based bioprinting systems are printed or created from a single material and do not resemble native tissue.

Multi-material biofabrication is needed to match the anisotropic and heterogeneous features of native tissues. Researchers have made multi-material scaffolds through side-by-side bioprinting, core-and-shell bioprinting, and advanced techniques like rapid continuous bioprinting, embedded bioprinting, and pre-set nozzle extrusion, as shown in Figure 1.2. (Duan et al. 2013; Gao et al. 2015; W. Liu et al. 2018).

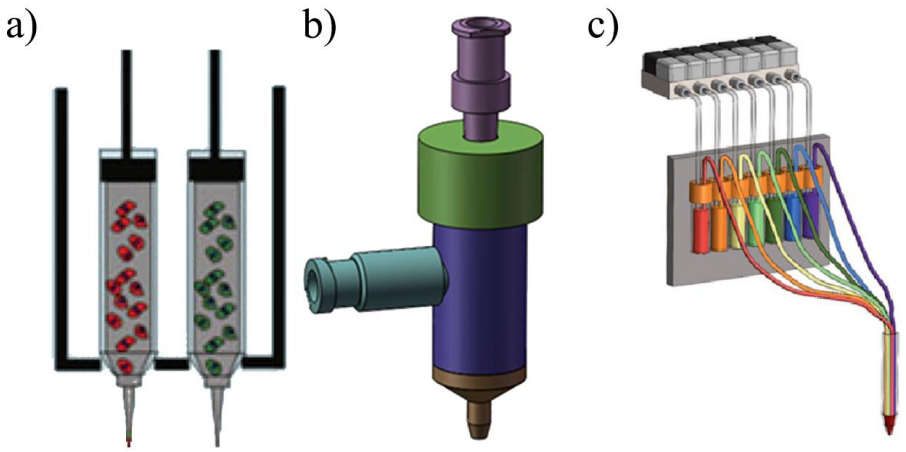

Figure 1.2: Existing Multi-material Bioprinting Systems a) Side-by-side (Duan et al. 2013) b) Core-and-shell (Gao et al. 2015) c) Advanced (W. Liu et al. 2018)

The working principle for side-by-side bioprinting is depositing one material at a time either adjacently in the same layer or by alternating materials in layers. Core-and-shell bioprinting employs two concentric nozzles to deposit a single filament with enhanced mechanical properties or increased vasculature. Advanced bioprinting methods such as rapid continuous bioprinting demonstrate on-the-fly adjustment and improved spatial control of deposited material during fabrication. Overall, the most significant issue of the existing systems is their lack of spatial control of material in the longitudinal and circumferential directions, limiting scaffold designs and development.

1.2 Research Issues

The primary research issues addressed with this M.Sc. study were, first:

1. *Single-material bioprinting does not adequately replicate the heterogeneous and anisotropic features of native tissue and organs.*

This issue of single-material bioprinting has been tackled by researchers before; leading to the second research issue:

2. *Current multi-material bioprinting systems extruded fibres with simple material organizations of either straight homogenous, fixed core-and-shell, or gradient along the longitudinal direction.*

It follows that a bioprinting system should be designed and built to address these issues. Such a system should overcome the main limitations of side-by-side bioprinting, core-and-shell bioprinting, and other advanced bioprinting methods.

The limitation with side-by-side printing is the slow fabrication speed associated with swapping tools. The printing technique that is produced should have an “on-the-fly” swapping mechanism to decrease fabrication time, which would be more practical for commercial use.

Core-and-shell bioprinting has a limited resolution of approximately 300 µm, so their structures do not resemble native tissue; however, this technique addresses vasculature, a significant research issue in tissue engineering. Further, core-and-shell bioprinting methods have fixed organization of the needles such that they only produce concentric coaxial type fibres.

The advanced printing methods, like embedded printing, rapid continuous printing, and pre-set extrusion, have an issue that their material control is either in the circumferential or longitudinal direction, and only one material is tested. For this M.Sc. project, similar issues arise as there will be merely testing the system's feasibility and illustrating control of acellular material. However, the design process for the bioprinting technique discussed here will consider different materials with viscosities and cells.

1.3 Research Objectives

To address the aforementioned research issues, the M.Sc. research aims to study the design of multi-material bioprinting systems with two specific objectives set as follows.

1. *Design of a novel multi-material extrusion-based printing system with longitudinal and circumferential control of the filament.*

The design process starts with a thorough literature review on existing multi-material bioprinting systems to build the system's technical specifications, meaning the breakdown of functions, constraints, and performance requirements. Next is to build the system's conceptual design; to assign design parameters to functional requirements in solving the principle of the solution. Following is the embodiment design phase, which adds volume, dimension, and scale to the conceptual design, giving the concept breath. Last, the detailed design gives fine specification to the embodiment such that it is manufacturable.

2. *Evaluate and compare the design of the proposed multi-material bioprinting system against existing systems based on the Axiomatic Design principles.*

It is essential to meaningfully compare and evaluate the proposed bioprinting system against existing bioprinting systems before prototyping. For this, Axiomatic Design principles provide an effective approach to determine the best design for given functional requirements and design parameters. Axiom 1 - Independence Axiom is used to identify the functional independence of the design parameters from functional requirements, while Axiom 2 - Information Axiom is used to compare a system’s information content or probability for achieving the functional requirements to a specified level. Together, the Axiomatic Design Principles demonstrate the differences among bioprinting systems and determine the best design for a given application.

1.4 Organization of the Thesis

A clear methodology was taken to accomplish the two research objectives. The steps and tasks are detailed in the following four chapters. Objective 1 is achieved and presented by Chapter 2 and 3, while Objective 2 by Chapter 4; Chapter 5 summarizes the conclusions drawn from this thesis and the suggestions for future work after this thesis.

Chapter 2 offers a brief review of relevant literature by

- Conducting a thorough literature review on existing multi-material bioprinting systems, along with their pros and cons.

Chapter 3 presents the study on the design of the bioprinting system in the following stages

- Building the technical specification of a new multi-material bioprinting system
- Developing the conceptual design of the new multi-material bioprinting system
- Establishing the embodiment of the new multi-material bioprinting system
- Forming the detailed design for manufacturing of the prototype bioprinting system
- Identifying necessary equipment to procure for the prototype system and selecting material to manufacture the prototype

Chapter 4 puts forward a comparison and evaluation of the proposed bioprinting system against others under Axiomatic Design

- Under Axiom 1- Independence axiom
    - Impose common functional requirements that meaningfully evaluate the multi-material bioprinting systems for their application
    - Assign design parameters for the multi-material bioprinting systems to achieve the functional requirements and build design matrices
    - Categorize the design matrices from their shape – diagonal matrices are uncoupled, triangle matrices are decoupled, and all other matrices are coupled.
- Under Axiom 2 - Information Axiom
    - Define the “design range” of the functional requirements
    - Determine the “system range” of the functional requirements for each of the groups of multi-material bioprinting systems from the literature

- Calculate the information content “bits” of the functional requirements for each of the groups of multi-material bioprinting systems
- Calculate the total information content for each of the groups of multi-material bioprinting systems and select the group with the lowest information content as the best system for the imposed functional requirements

Chapter 5 summarizes the work presented in this thesis, and the main conclusions are drawn. Followed are discussions on the limitations of the study and suggestions for future work.

2.0 REVIEW OF MULTI-MATERIAL BIOPRINTING SYSTEMS

The purpose of this review is to report on existing fabrication methods for multi-material tissue scaffolds in extrusion-based bioprinting. First, a general background in tissue engineering and extrusion-based bioprinting introduces the reader to the research area. Following this, the need for multi-material bioprinting systems is discussed, including an investigation of existing techniques. Last are suggestions for the research area, focusing on the research gap addressed by this M.Sc. study.

2.1 Introduction

Damaged or injured tissue leads to conditions causing millions of people around the globe to suffer – from osteoarthritis to heart attacks, stroke, burns, and more. The gold standard for treating patients with heavily damaged tissues or organs is complete or partial transplantation. However, the worldwide demand for organ donation and transplantation continues to rise, while the number of donors is not significantly increasing. At the end of 2017, over 4 300 Canadians were left on transplant waiting lists, but less than 3 000 organ transplants were done in that year; 242 patients died waiting (Canadian Blood Services 2018). From the same report, Canadian Blood Services showed that the national rate of deceased organ donation increased by 5%. In comparison, the living donation rate fell by 3%, although almost 90% of surveyed Canadians approve of organ and tissue donation after death. Tissue engineering addresses this issue by providing permanent substitutes for human organs/tissues with a lab-grown alternative (Atala and Yoo 2015).

The general goal of tissue engineering, or scaffold-based tissue engineering, to be specific, is to manufacture a construct (scaffold) that acts as an analog to the damaged native tissue/organ. The scaffold is then mixed with cells and cultured, yielding a biologically functional construct, which, after implanted, degrades at a similar rate to the new tissue growth (X. Chen 2018). First, cells from the patient are harvested and expanded in culture. Then the cells are added with printable biomaterials (usually polymers) and the appropriate growth factors forming “bioink” (X. Chen 2018). Using an additive manufacturing method with a computer-aided-design (CAD) model derived from medical images, usually magnetic resonance imaging (MRI) or computed tomography (CT), the bioink is deposited layer-by-layer to form the scaffold, further cultured and mature before being introduced to the patient. Tissue scaffolds have a porous structure to

facilitate the transfer of nutrients and cellular wastes (Hollister 2005). The size of pores depends on the size of the cell-seeded/incorporated with the structure (Loh and Choong 2013). Consideration of pore continuity and connectivity is crucial for effective scaffold design (Sobral et al. 2011). Finally, the scaffold is further cultured, and the matured scaffold is implanted to the patient for guiding new tissue growth while the construct degrades at a similar rate.

There are three main requirements to characterize the performance of a tissue scaffold: biological, mechanical, and architectural requirements. Biological requirements include the ability of the scaffold to facilitate cell functions (growth, attachment, proliferation) and tissue regeneration with the implanted cells while not negatively influencing the host cells. Mechanical requirements of the scaffold include its mechanical strength as well as how degradation affects the strength. Last, the architectural requirements of scaffolds include both their internal and external geometries. The external geometry, or macrostructure, is evaluated by how closely it resembles the host structure. The internal geometry, or microstructure, is assessed on how effectively the pores can encourage easy transport of nutrients and passage of cell waste. Medical imaging is used extensively to properly understand and replicate the complex external structure of tissues and organs (Murphy and Atala 2014).

2.1.1 Extrusion Bioprinting

Various types of materials have been used in scaffold tissue engineering, with natural materials being suited for satisfying biological requirements (promoting cell adhesion, proliferation) and synthetic materials providing, primarily, more robust and more tailorable mechanical properties (Freed et al. 1994; Drury and Mooney 2003; Stoddart et al. 2009; Ge et al. 2012; Van Blitterswijk 2014). A critical aspect of tissue-scaffold development from these materials is the deposition method to build up 3D structures. Common additive manufacturing or “bioprinting” methods for scaffold tissue engineering vary as well, including modified inkjet (or droplet-based) printers, extrusion printing systems, and laser-based systems (Coburn et al. 2011; Cui et al. 2012; Xu et al. 2012; Ning and Chen 2017). Table 2.1 briefly compares conventional bioprinting systems, listing their relative benefits and limitations to each other; note that extrusion bioprinting is the focus of this review.

Table 1.1: Brief Comparison of Common Bioprinting Systems

System	Benefits	Limitations	Sources
Droplet	Moderately high printing resolution (50 µm) Fast fabrication speed Low operation cost	Unable to achieve a continuous flow Only compatible with low viscosity inks Low cell densities	(Derakhshanfar et al. 2018; Ning and Chen 2017; Ozbolat and Hospodiuk 2016; Ozbolat, Moncal, and Gudapati 2017; X. Chen 2018; Malda et al. 2013)
Laser	Highest printing resolution (5 µm) Can deposit both solid and liquid materials	Can cause thermal damage to cells in bioink Time-consuming for multiple cell types	
Extrusion	Printing with high cell densities Able to use biomaterials with a wide range of viscosities Simple construction Ease of operation	Relatively low resolution (100 µm). Needle clogging Slow speed for large constructs Gelation and solidification requirements	

Extrusion bioprinting is a deposition method based on the principle of ejecting biomaterial layer-by-layer from a syringe to a stage via mechanical forces. Standard extrusion bioprinting systems consist of four main components: a dispensing head that holds the bioink, a positioning system

that moves the dispensing head in x-y-z directions, a printing stage that can have its temperature-controlled, and a computer where the user can adjust the deposition parameters, the position of the head, and temperature of the syringe or stage. Figure 2.1 shows a schematic view of a typical extrusion bioprinting system (Ning and Chen 2017).

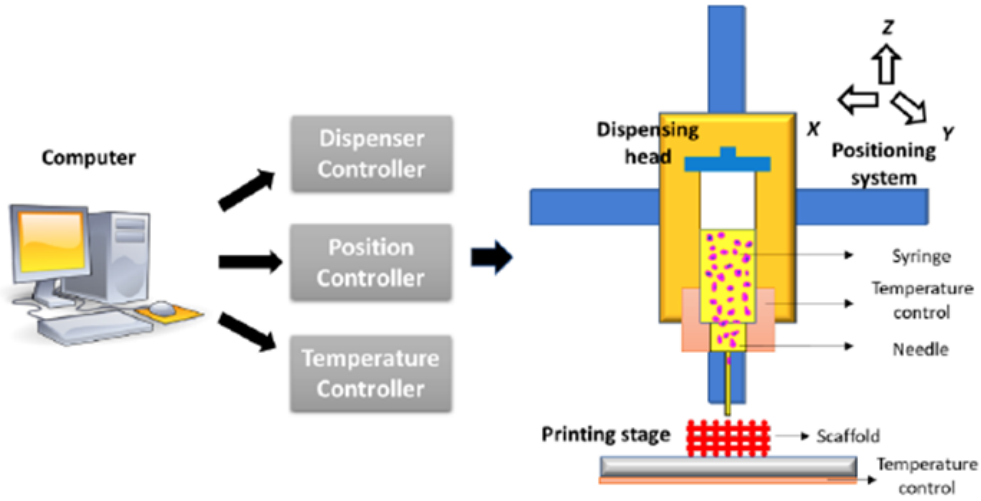

Figure 2.1: Schematic of the Extrusion Bioprinting System (Ning and Chen 2017)

The process begins by loading the prepared cell-laden biomaterial into the syringe, positioned inside the dispensing head. The dispensing head supplies force and heat into the syringe to drive the biomaterial out of the needle at a specified rate and temperature. The head is controlled in three axes to create the 3D scaffold layer-by-layer atop the printing stage (Ning and Chen 2017; Ozbolat and Hospodiuk 2016).

Typical extrusion bioprinting systems operate under pneumatic-, screw-, or piston-based mechanisms (Derakhshanfar et al. 2018). The pneumatic-based systems are preferred for their simplicity, but the printing characteristics are highly dependant on the viscosity of the material. The mechanical systems are attractive because of the precise control over the flow of the bioink; however, these systems generate high pressures and can damage cells if they are present in the bioink (Derakhshanfar et al. 2018; X. Chen 2018).

One of the most significant limitations is that many extrusion bioprinting constructs are made of only single bioinks (Malda et al. 2013; Ozbolat, Moncal, and Gudapati 2017; Choudhury, Anand,

and Naing 2018; Kačarević et al. 2018; Naghieh et al. 2018). Most native tissues/organs are both anisotropic and heterogeneous in composition and thus require many materials in a scaffold to make a suitable analog (Iatridis et al. 1998; Hollenstein et al. 2006; Annaidh et al. 2012; McCullen et al. 2012). There are various methods for multiple material extrusion bioprinting to create advanced tissue scaffolds, including side-by-side, core-and-shell, and other advanced approaches. The following section will briefly describe those methods and the fabrication methods needed to realize them.

2.2 Multi-material Bioprinting

The purpose of multi-material bioprinting in scaffold tissue engineering is to replicate the complex organization of native tissue and overcome the inability to include more than one biomaterial in scaffold construction (Ozbolat and Hospodiuk 2016; Kačarević et al. 2018; Choudhury, Anand, and Naing 2018). Practically, multi-material bioprinting allows researchers to combine biocompatible hydrogels with mechanically robust synthetic materials to harness the benefits of each material type (Xu et al. 2012; Malda et al. 2013; Z. Izadifar et al. 2016; J. M. Lee and Yeong 2016; M. Izadifar et al. 2017). Looking at data from the literature, Figure 2.2 breaks down the material usage, showing that alginate is by and large the favourite in multi-material bioprinting.

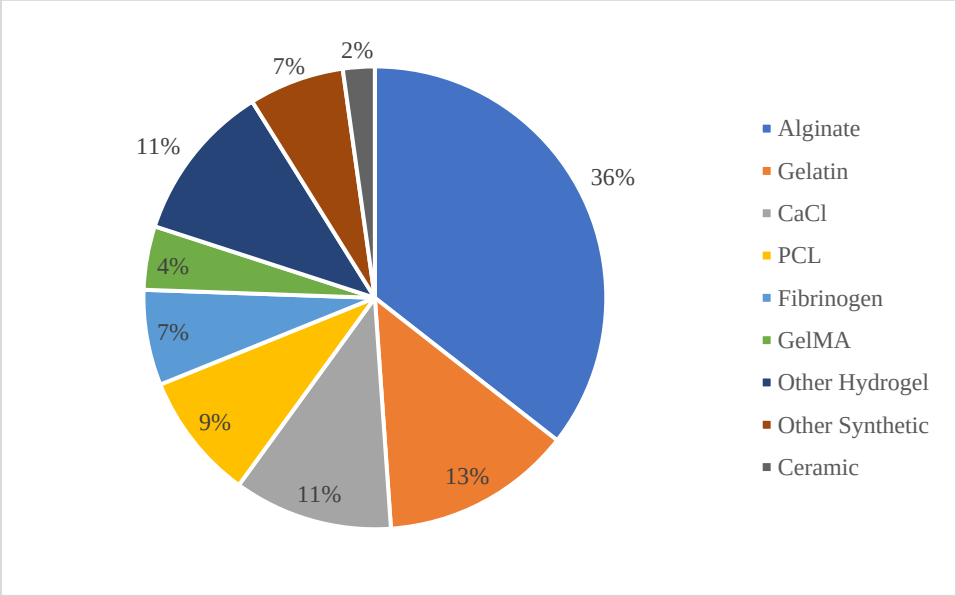

Figure 2.2: Material Usage in Multi-Material Bioprinting (Schuurman et al. 2011; Shim et al. 2012; H. Chen and Ozbolat 2013; Duan et al. 2013; Y. S. E. Tan and Yeong 2014; Cornock et al. 2014; Zhao et al. 2014; Z. Izadifar et

al. 2016; Gao et al. 2015; Raja and Yun 2016; Jia et al. 2016; J. Lee et al. 2017; Dai et al. 2017; Mistry et al. 2017; W. Liu et al. 2018)

Multi-material bioprinting can be divided into different categories, depending on how the fibres are assembled or their placement in the scaffold; the names are self-explanatory. The most common method is side-by-side printing, which, as it sounds, has each material deposited beside the next one in the same layer (Klein et al. 2009; Schuurman et al. 2011; Shim et al. 2012; Malda et al. 2013; Loh and Choong 2013; Z. Izadifar et al. 2016; J. Lee et al. 2017; Rocca et al. 2018). Next is core-and-shell printing, which is done by having to dispense two or more materials simultaneously and inside one another (Kim and Kim 2013; Cornock et al. 2014; Gao et al. 2015; E. Y. S. Tan and Yeong 2015; Raja and Yun 2016; Jia et al. 2016; Snyder et al. 2016; Dai et al. 2017; Mistry et al. 2017; W. Liu et al. 2018; Costantini et al. 2018). Core-and-shell printing is more commonly used for enhancing the crosslinking ability of hydrogels, however. Last of all are advanced methods that do not fit in the other groups. Table 2.2 shows a brief comparison of those three groups of techniques, stating their benefits and limitations.

Table 2.2: Brief Comparison of Multi-material Bioprinting Techniques

Technique	**Fabrication**	**Benefits**	**Limitations**	**Sources**
Side-by-Side	Multi-Head/Cartridge Multi-Arm	The simplest method Greatest ease-of-use Highest printing resolution Most commercially available technique Vast selection of compatible materials	Slow fabrication speed Lack of material control Homogenous, single-material fibres	(Schuurman et al. 2011; H. Chen and Ozbolat 2013; Duan et al. 2013; Y. S. E. Tan and Yeong 2014; Zhao et al. 2014; Z. Izadifar et al. 2016; J. Lee et al. 2017)

Core-and-Shell	Hydrogel + Crosslinker Hydrogel + Ceramic	The best method for creating vascularized fibres Ceramic reinforced hydrogel fibres benefit from the biological and mechanical features of respective materials.	Limited printing resolution. No spatial control of the core/shell organization	(Mistry et al. 2017; Gao et al. 2015; Dai et al. 2017; Raja and Yun 2016; Cornock et al. 2014; Jia et al. 2016; Gao et al. 2015; W. Liu et al. 2018)
Advanced	Embedded Continuous Pre-set Nozzle	"On-the-fly" swapping of materials. Ability to fabricate complex fibres with specific material placements/concentrations Fastest fabrication speed Promising approaches for recreating heterogeneous features of native tissues.	Only realized in the "proof-of-concept" stage Few materials are shown Complex mechanisms involved Larger resolutions	(W. Liu et al. 2017; Kang et al. 2018; Rocca et al. 2018)

Further categorizing multi-material bioprinting methods is their commercial availability; of the 27 listed commercially available extrusion-based printers in 2018, there are 21 that allow for multi-material methods, showing great interest in these techniques from industry (Choudhury, Anand, and Naing 2018). For commercially available multi-material bioprinting, the most common fabrication techniques are aligned with side-by-side bioprinting.

2.2.1 Side-by-side Bioprinting

Side-by-side bioprinting is the most common type of multi-material bioprinting method. This method involves depositing different materials, alternating at the same layer or alternating layer after layer. It is the most common method because it is the simplest and is the easiest to control. Side-by-side printing is a good "first step" for multi-material bioprinting, but the slow fabrication speeds limit the ceiling for efficiency. These methods usually have a single arm with multiple tools or multiple arms with single tools to achieve the desired scaffold shape. The main benefit of this technique is that maximum resolution is the same as single-material extrusion bioprinting. From the examined literature, the diameters of deposited materials ranged from 150 μm to 800 μm at an average of 300 μm.

The primary consideration of past work is the biological performance of the constructs, as mechanical and architectural characterization has either been ignored or done in a primitive way (Z. Izadifar et al. 2016; Schuurman et al. 2011; Shim et al. 2012; H. Chen and Ozbolat 2013). To investigate the architectural properties, most researchers imaged then measured the diameters and spacings of the filaments to compare with the CAD models – determining the printing efficacy and porosity. Mechanical properties of most constructs were obtained through uniaxial compression or compression. Side-by-side bioprinting has much potential to expand into a more feasible method for scaffold fabrication because of the low barrier to entry and ease-if use, from multi-arm/multi-tool in x-y-z to larger printers with more degrees of freedom. Typical scaffolds made from side-by-side bioprinting are produced with layers in an alternating zig-zag pattern; Figure 2.3 shows a few examples.

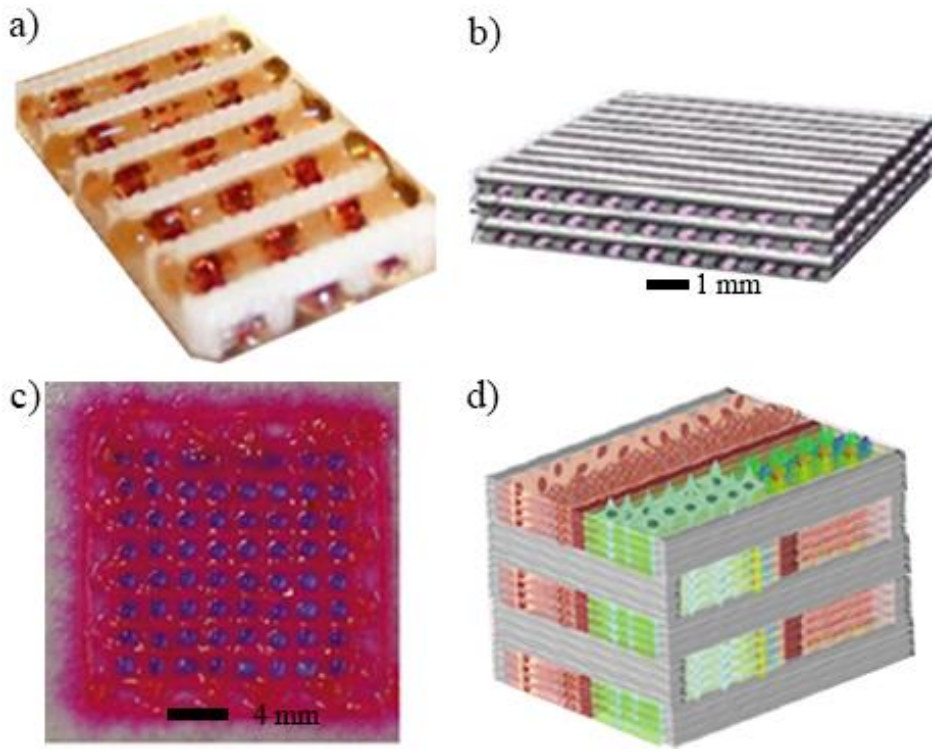

Figure 2.3: Examples of Side-by-side Constructs a)(Schuurman et al. 2011) b) (Z. Izadifar et al. 2016) c)(Ozbolat, Chen, and Yu 2014) d) (Shim et al. 2012)

The construct in Figure 2.3a was designed and constructed using extrusion bioprinting by Schuurman et al. in 2011 and is made of 2% w/v medium viscosity alginate and a 700000-90000 Da MW Polycaprolactone (PCL) to create a tissue scaffold that has fully tailorable mechanical properties (Schuurman et al. 2011). The method used here was an alternating approach using a single-arm multi-tool bioprinter that dispensed the two materials in an alternating fashion within the same layers, with the entire construct being crosslinked after construction. A significant limitation for this approach is the printing resolution – a 210 µm needle diameter for the alginate and a 23G needle diameter for the PCL.

Figure 2.3b shows a scaffold made with a similar approach to Figure 2.3a; a single-arm multi-tool extrusion bioprinting system with one tool housing PCL and the other tool housing alginate with both dispensed in an alternating pattern for layer-by-layer construction (Z. Izadifar et al. 2016). Here, the purpose was to illustrate the effects of the viability of the cells encapsulated in the alginate when exposed to the high-temperature melt-deposition of the adjacent PCL filaments to make tailorable scaffolds for cartilage tissue engineering in the future. The researchers, in this

case, showed favourable cell viability within the scaffold from day 0 to day 14-time steps and showed no correlation between dispensed PCL filaments and spatial cell damage post-fabrication (Z. Izadifar et al. 2016). Thus, this study emphasizes the feasibility of multi-material bioprinting that incorporates melt-dispensing of synthetic polymers without sacrificing one of the main requirements of scaffold fabrication – the biological requirement; however, the mechanical properties were not examined. Further, 200 µm and 230 µm needles were used for alginate and PCL, respectively, showing again that printing resolution is a limitation for these types of fabrication processes.

The scaffold in Figure 2.3c was constructed entirely differently from the last two examples; it was made using a multi-arm extrusion-based system with each arm housing tools with unique deposition characteristics (Ozbolat, Chen, and Yu 2014). One arm consists of a coaxial nozzle that simultaneously deposits a hydrogel and an ionic crosslinker for making tubular fibres, and the other arm deposits an aggregate of cell spheroids. Thus, this work was more of a proof-of-concept for the advanced printing process – using both multi-arm and simultaneous side-by-side printing. Ozbolat and their group performed cell viability and printability assays in the form of seven-day Calcein Acetoxymethyl (AM) staining and filament width/cell-spheroid diameter measurements, respectively. Major critiques of the work are the slow fabrication speed of the construct and the lack of mechanical analysis.

Last, Figure 2.3d shows a complex multi-material scaffold constructed using six different materials; four hydrogels and two synthetic materials (Shim et al. 2012). Each material was housed in its dispensing head and a single positioning system with the synthetic materials, PCL and Poly (Lactic-co-Glycolic Acid) (PLGA), including a temperature controller for molten deposition. In general, the synthetic materials were added to provide a framework for low concentration hydrogels and promote favourable cellular arrangement of the encapsulated bioink that mimics native tissue. The synthetic materials were first dispensed for Shim's scaffold on the outside and middle of a layer. The two hydrogels filled up the remaining space – this process is repeated for each subsequent layer, but the orientation of the filaments is rotated 90° on the new layer. This technique showed promise, as the viability of the cell-laden constructs was maintained for 7-days; however, a mechanical assay was not conducted here. Thus, while the construct has an exciting design, it is not sure if the added complexity is worth it- long

fabrication time, extra time for CAD design, and compounded errors like needle clogging during fabrication for all six needles. For an overview of other side-by-side bioprinting techniques, see Table 2.3.

Table 2.3: Summary of Side-by-side Bioprinting Methods

Needle 1	**Material 1**	**Needle 2**	**Material 2**	**Bioprinter**	**Pattern**	**Source**
23G	PCL Mw 70 000–90 000	210 µm Inner Diameter	2% w/v Alginate	BioScaffolder (SYS+ENG, Salzgitter-Bad, Germany)	Alginate between PCL	(Schuurman et al. 2011)
200 µm and 150 µm	PCL Mw 70 000-90 000	200 µm and 150 µm	4% w/v Alginate	Custom Multi-head Bioprinter	Alginate between PCL	(Shim et al. 2012)
250 µm	4% w/v Alginate	250 µm	Alginate /Cellular Spheroids	Custom Multi-arm Bioprinter	Spheroids between filaments	(H. Chen and Ozbolat 2013)
800 µm	0.06 g/mL Gelatin + 0.05 g/mL Alginate + Cell	800 µm	0.06 g/mL Gelatin + 0.05 g/mL Alginate + Cell	Standard Fab@Home Printhead adapted for dual syringes	Root region with Cell 1 and leaf region with cell 2	(Duan et al. 2013)

250 µm	0.06g/mL Alginate + 0.01-0.03 g/mL Xanthan gum + 0.022 g/mL CaCl	300 µm	500 mM CaCl Solution	Multi-nozzle extrusion-based technique from BioCad (RegenHu)	A circular shell of hydrogel with CaCl filling	(Y. S. E. Tan and Yeong 2014)
250 µm	10% w/v Gelatin + 1% w/v Alginate + 2% w/v Fibrinogen + Cells	250 µm	Hela/Hydrogel	Cell Assembly System 1	Cubic grid	(Zhao et al. 2014)
300 µm	PCL (Mw 48,000–90,000)	200 µm Inner Diameter	2% -5% Alginate + Cells	3D-Bioplotter system (EnvisionTec GmbH)	Alternating PCL and alginate	(Z. Izadifar et al. 2016)
200 µm	PLGA	250 µm Inner Diameter	5% w/v HA + Cells	Custom Carousel multi-channel dispensing system	Cylindrical PLGA cell with hydrogel filler	(J. Lee et al. 2017)

2.2.2 Core-and-shell Bioprinting

Core-and-shell bioprinting operates on the principle of having two different materials dispensed simultaneously with two concentric needles (Richards et al. 2017). The primary purpose of this method is to create fibres with vasculature, which facilitates a high transfer of nutrients and

movement of cellular waste within the scaffold (Kim and Kim 2013; Cornock et al. 2014; Gao et al. 2015; E. Y. S. Tan and Yeong 2015; Raja and Yun 2016; Jia et al. 2016; Snyder et al. 2016; Dai et al. 2017; Mistry et al. 2017; W. Liu et al. 2018; Costantini et al. 2018). The vasculature is created by depositing a crosslinkable hydrogel as the "shell" material and the crosslinker in the "core". Gelation occurs during deposition, and the user has hollow filaments. The lumen size is tailorable in size and shape depending on the organization of the needles; however, the adjustments can not be made on-the-fly. Typically, the resolution of core-and-shell constructs is relatively low, and the constructs are weak because of the hollow filaments. The average size of a "core" needle is about 300 µm, while the average "shell" needle is about 900 µm. With large needle sizes, the constructs made from this method do not resemble native tissue and are simple shapes. Another way that core-and-shell bioprinting is applied is by printing polymer-reinforced hydrogel fibres. Like hollow hydrogel filaments, the polymer is organized in the core or shell, depending on the application; filaments of polymer-polymer or hydrogel-hydrogel can be produced this way. Figure 2.4 shows four different scaffolds that were made using core-and-shell bioprinting methods.

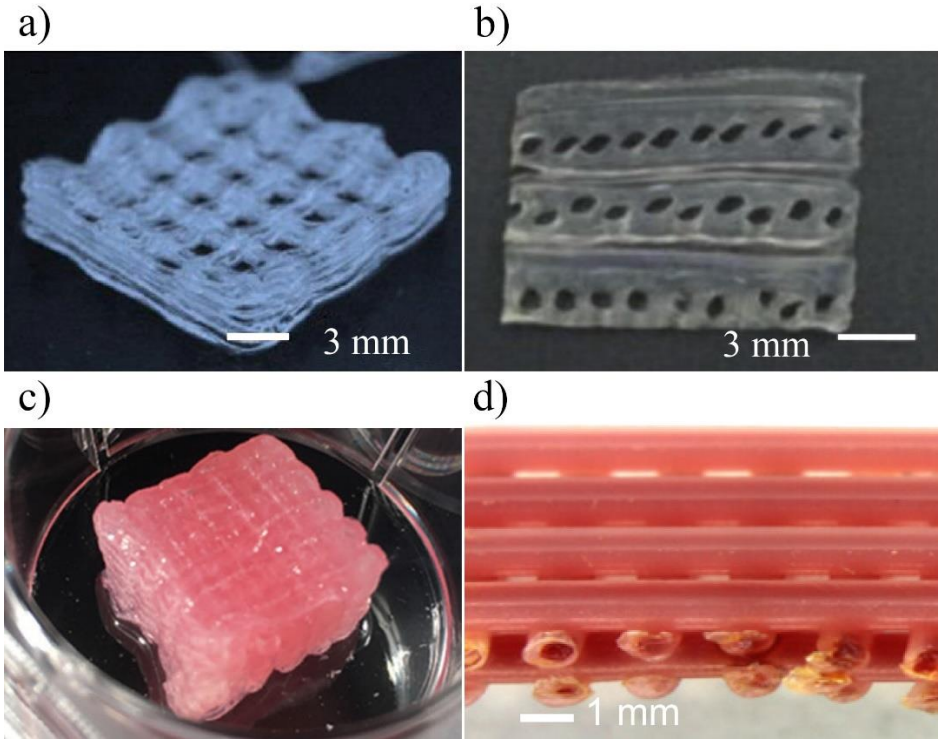

Figure 2.4: Examples of Core-and-shell Bioprinting Constructs a) (W. Liu et al. 2018) b) (Gao et al. 2015) c) (Mistry et al. 2017) d) (Cornock et al. 2014)

The scaffold in Figure 2.4a is made of 10 layers and was created using core-and-shell fibres with a crosslinker calcium dichloride ($CalCl_2$ of various concentrations), Gelatin Meth Acryloyl (GelMA) (1.0%, 1.5%, or 2.0% with 0.2% PI) and cells ($2x10^6$/mL) as the core, and alginate (1.0%) as the shell. A custom-made printhead for a commercial extrusion bioprinter connected two syringe pumps, one for each bioink, into a single coaxial needle using a pair of 23G and 28G needles. After deposition, the construct was crosslinked using Ultraviolet (UV) light before moving to a culture medium for maturation (W. Liu et al. 2018). Higher concentrations of GelMA increased the mechanical strength of the scaffolds under uniaxial compression while maintaining favourable printability and biological performance. The main limitation is that the pre-crosslinking mode, dispensing CaCl with cell-laden GelMA, may harm the cells. Also, there is a need for close control over the microenvironment of the scaffold to encapsulate the cells appropriately. However, the method of printing may be more viable in the future once iterated.

Like Figure 2.4a, the scaffold in Figure 2.4b is six layers of hollow cell-laden (10^6/mL) alginate (2-5%) filaments in alternating 90° orientation with the lumen created by dispensing CaCl (2-5%) in a coaxial needle organization(Gao et al. 2015). In this case, the inner needle diameter ranged from 21G to 23G, with the outer needle diameter being fixed at 1600 µm. The fabrication process used the coaxial needle moving in two dimensions depositing the filaments on a stage that moves down in "z" into a CaCl solution, further crosslinking the construct. These scaffolds were also tested mechanically, biologically, and architecturally. Mechanical testing was done through uniaxial compression, biological testing was done through live/dead assay, and architectural testing was done by examining the influence of printing parameters on the diameter of the hollow filaments (Gao et al. 2015). Another feature that Gao and their team wanted to investigate was the successful fusion of adjacent threads after fabrication. The fabricated scaffolds show great potential for higher nutrient transfer with microchannels in the alginate filaments; however, these designs are weaker than scaffolds with solid filaments. In the future, the material transfer within these scaffolds should be characterized to demonstrate the level of advantage.

Now for the scaffold in Figure 2.4c, a more straightforward approach was taken for its 20 layers – only cellular material ($4x10^6$/mL with 6% gelatin) in the core of the filament with a mechanically robust hydrogel (11% total concentration of Poly (Ethylene Glycol) Diacrylate

(PEGDA), alginate, or mixed with Lithium Phenyl-2,4,6-trimethyl-benzoyl Phosphinate (LAP) photoinitiator as the shell (Mistry et al. 2017). The inner and outer diameters of the coaxial needle were 27G and 18G, respectively, and the material was pushed through two separate syringes on a commercial extrusion 3D bioprinter. Out of all the other biological assays reported in this section, Mistry and their team conducted the most prolonged time scale tests, 28 days, with data collected at days 0, 1, 7, 14, and 28 after fabrication. Further making this study unique is the inclusion of tensile tests on the hydrogels. Tensile tests are difficult to conduct on tissue scaffolds because of their shape, and as such, they moulded dumbbell specimens for the testing (Mistry et al. 2017). While good for an estimation of the tensile mechanical properties, the internal and external structure of the fibres will influence the strength of the scaffold, and that influence was not characterized.

The last example of core-and-shell bioprinting, shown in Figure 2.4d, was created using a novel coaxial melt extrusion printed filaments with alginate (2%) as the core material, and PCL (80 kDa molecular weight) was used for the strengthening shell of the filaments (Cornock et al. 2014). The PCL nozzle diameter ranged from 900-1100 µm and was extruded at 90-140°C, and the alginate nozzle diameter ranged from 200-300 µm and was extruded at 23°C – both inks were also applied different pressures during the investigation. The cell-free alginate core was flushed out of the PCL using Milli-Q water to add cells to the scaffold post-fabrication safely. A cell-laden hydrogel was seeded with syringes, the purpose being to avoid high temperatures killing the cells. The mechanical characteristics, in this case, were evaluated solely on 20 mm lengths of the fibres tested in tension. As expected, the Alginate-PCL co-fibre had mechanical properties between pure alginate and pure PCL, showing the tailorable nature of multi-material bioprinting. Cellular and architectural studies showed favourable results as well. This system is uniquely adaptable as it can incorporate both synthetic and natural materials of differing viscosities simultaneously. The main drawback is having to seed cells after fabrication.

With the hydrogel/crosslinker deposition of hollow filaments, the opportunity for a higher nutrient transfer within the scaffolds is increased. More investigation needs to be done into the accurate characterization of the increased mass flow through hollow filaments. Further, the lumen can be tailorable in size and shape, depending on the organization of the needles. The main limitations for this process are the printing resolution and the mechanical strength, drawing

from the nature of the fabrication method. Nevertheless, like side-by-side, core-and-shell shows excellent potential for future bioprinting applications. Table 2.4 summarizes findings from the literature about core-and-shell bioprinting methods.

Table 2.4: Summary of Core-and-shell Bioprinting Methods

Core Needle	**Core Material**	**Shell Needle**	**Shell Material**	**Bioprinter**	**Pressure Source**	**Source**
200-300 µm	Alginate	900-1100 µm	PCL	Korean Institute for Machinery and Materials Scaffold Plotting System (SPS1000)	Unnamed pressure controller	(Cornock et al. 2014)
21G, 22G, 23G	2-5% w/v CaCl	14.5G	2-5% w/v Alginate Both cell-free and laden	n/a XYZ adjustable stage	Single four-channel pump	(Gao et al. 2015)
22-30G	Alpha-Tricalcium Phosphate (α-TCP) ceramic paste	18-20G	6 & 9% w/v Alginate	Screw-based core (400 rpm) and pneumatic shell	110-117 kPa via pump	(Raja and Yun 2016)
25-30G	GelMA (5&7%) + Alginate	20G	0.3M CaCl	Novogen MMX Bioprinter,	Microfluidic syringe pumps	(Jia et al. 2016)

	(1,2,3%), Pentaerythritol Triacrylate (PEGTA) (1,2,3%) Photo initiator			Organovo, San Diego, CA, USA	(Harvard Apparatus) 40 and 35 uL/min	
21G	Cell-laden Fibrinogen	16G	Alginate + Gelatin + Thrombin	XYZ adjustable stage	Pump core (3-6mL/h) shell (15-30mL/h)	(Dai et al. 2017)
27G	Cell-laden hydrogel. GelMA, Collagen, Matrigel	18G	Partial crosslink PEGDA (20 kDa) and/or Alginate Various concentrations	(RegenHU, Switzerland)	Two pumps 0.01 and 0.1 mL/min	(Mistry et al. 2017)
28G	CaCl (1%) + GelMA (1.5%) + Cells (2x10^6/mL)	23G	Alginate 1%	(Luzbolt TAZ 4, Aleph Objects, Loveland, CO, USA)	Two syringe pumps	(W. Liu et al. 2018)

2.2.3 Advanced Bioprinting Methods

The next group of multi-material bioprinting methods is characterized by their ability to change the extruded material “on-the-fly” through the same nozzle; without swapping the existing tools.

Since the printed material can be changed quickly, the user could transition from one material to another, creating a material gradient. This gradient could be helpful in selectively placing cells or growth factors in specific regions of a scaffold to mimic native tissue. This group of techniques is the most complex and has had little exposure because they are in the "proof-of-concept" phase. Figure 2.5 shows two constructs that are made from this type of bioprinting method.

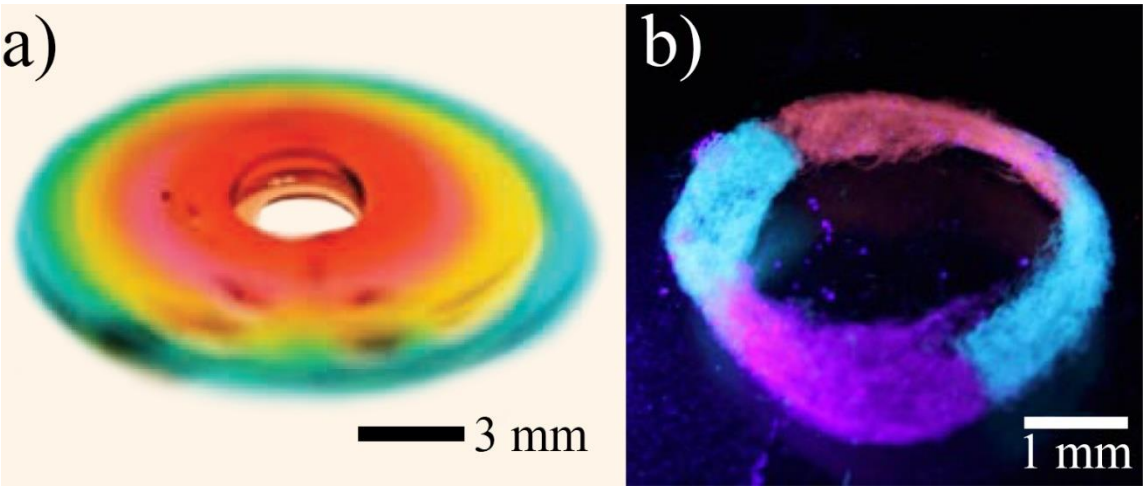

Figure 2.5: Example of Continuous Extrusion Bioprinting Methods a) Rapid Continuous (W. Liu et al. 2017) b) Embedded Bioprinting (Rocca et al. 2018)

The method used to fabricate the structure in Figure 2.5a is a rapid continuous extrusion method that adopted a mixture of GelMA and alginate as the bioink; dyed seven colours to emphasize the material switch (W. Liu et al. 2017). This method utilizes seven nozzles attached to a single nozzle in a non-concentric organization with a maximum printing resolution of ~800 μm for a multi-material fibre. The fibres created with this method can combine the seven materials simultaneously, and the mixture can be adjusted to predetermined conditions. Liu demonstrated that this method could combine cell-laden material with four different cell types. The viability of the cells can be maintained after day seven (around 90-60% depending on the cell type). Cells were placed in different regions within a construct and then tracked to observe the movement of the cells within the desired regions; this method seems viable. As far as characterizing the scaffolds goes, the work was preliminary and limited to the biological requirements. The focus here is to show off the prototype for this fabrication method that can work up to 15 times faster than existing nozzle-based printing techniques (Rocca et al. 2018). For limitations, the use of

only one material type, the large printing resolution, and the absence of characterization methods shows much advancement is needed for widespread adoption of this device.

The last advanced biofabrication technique is pre-set nozzle printing, created by Kang and their team in 2018. They added a custom-made cartridge preloaded with a second (or more) material to the working end of the syringe to form a type of core-and-shell filament with the core material's structure formed to the cartridge shape; the schematic shown in Figure 2.6c (Kang et al. 2018).

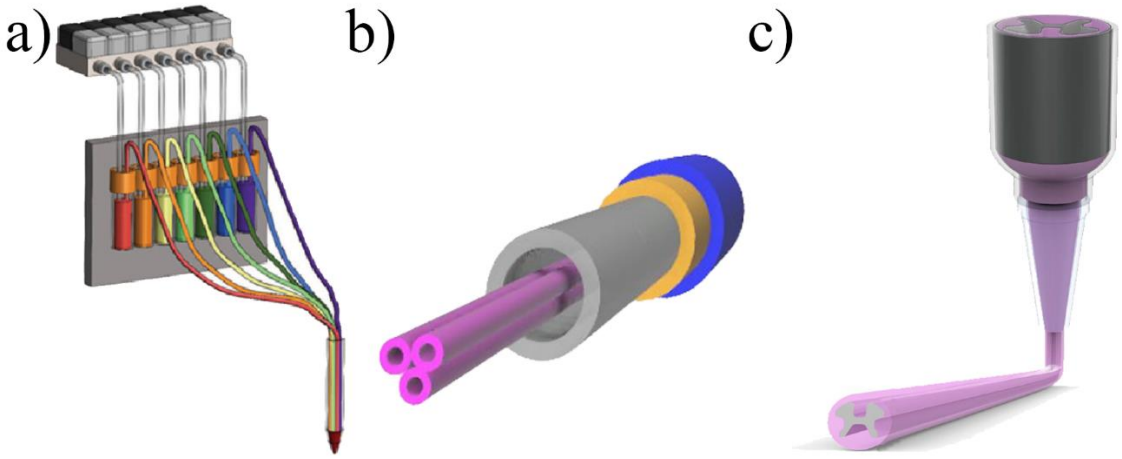

Figure 2.6: Advanced Bioprinting Mechanisms a) Rapid Continuous (W. Liu et al. 2017) b) Embedded (Rocca et al. 2018) c) Pre-set Extrusion (Kang et al. 2018)

The advantages of this method over traditional core-and-shell bioprinting are greater resolution, defined material separation, and adjustability of the core shape. In addition, scaffolds made from this new method were with cell-laden alginate and had better or equal cell viability than homogenous cell printing (Kang et al. 2018).

2.3 Closing Remarks

Homogenous bioprinting, or single-material bioprinting, has made strives in tissue engineering in the development of scaffolds. Like those previously mentioned, multi-material bioprinting methods show high potential for recreating the complex structures and patterns present in native tissue. However, many challenges need to be addressed for the realization of fully functional scaffolds or organs. The following section will bring up those specific challenges and present suggestions for multi-material bioprinting strategies.

2.3.1 General Suggestions for Multi-material Bioprinting

Since multi-material bioprinting is relatively new, there is room for many approaches to be taken to improve the method holistically. These approaches include developing better machinery/techniques, materials selection/design, and testing/characterization methods.

First, material selection and design are integral for the realization of fibres that make up the scaffolds. The accuracy of the bio-ink to the target tissue/organ in terms of biological, mechanical, and architectural properties is imperative for a functioning construct. Utilizing multiple materials with multiple cell types is why multi-material bioprinting is attractive; however, most current methods use alginate for its favourable printability. Possibly, the creation of new biomaterials or the mixing of hybrid materials by researchers is the next step to address this issue. Further, the encapsulation of cells within the biomaterial instead of seeding the cells after deposition will help the cellular material and nutrients within the scaffold. Cell-seeded material also allows the user to precisely place-specific cells at desired locations.

Next, the deposition techniques for multi-material bioprinting should be addressed, primarily concerning resolution. Native tissues and organs have intricate details which can not currently be realized with the techniques above. Decreasing needle sizes, changing needle shape, improved tool-pathing, or changing the deposition mode may increase the resolution. Once the resolution issue is resolved, more important constructs for repairing more significant defects can be done. They combine fabrication techniques, such as electrospinning of micro/nanofibres to mimic fibrous zones or hard extracellular matrix (ECM). Also, to do with fabrication is ensuring that the constructs are consistent and repeatable.

Testing and characterization of multi-material printed scaffolds are essential in understanding the flaws and strengths of each construct (and of native tissue) for creating a better product. In the future sophisticated imaging techniques, like synchrotron imaging, can better characterize mechanical and architectural properties *in vivo* and *in vitro*. However, current mechanical characterization methods are limited to uniaxial compression/tension/torsion, which does not accurately represent the complex stress environments of articular cartilage, for example. The development of testing machines that can mimic the target's body stresses (for evaluating both native tissue and scaffolds) can potentially address this issue.

2.3.2 Suggestions for Depositing Bioink in a Controllable Manner

Looking at the four main fabrication methods introduced in this review, the most attractive of them are core-and-shell bioprinting and continuous bioprinting. Coaxial bioprinting is attractive because of its ability to facilitate the fabrication of tubular filaments, which overcome the major challenge of vascularization in tissue engineering. Meanwhile, continuous bioprinting allows researchers to adjust concentrations of the deposited materials during the fabrication process, again leading to unique filament structures with material gradients or clear separation between different biomaterials and cells. What has not yet been addressed in the literature is that current biofabrication methods lack the spatial control of the multi-material filaments in both the longitudinal and circumferential directions. A comparison between spatially controllable fibres and current core-and-shell fibres is shown in Figure 2.7.

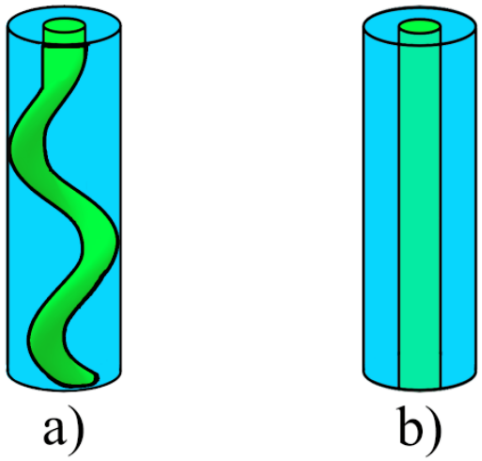

Figure 2.7: a) Fibres with Materials Controllable in Both Circumferential and Longitudinal Directions b) Typical Fibre from Coaxial Bioprinting

Another limitation for current core-and-shell bioprinting is that the printing resolution is limited because of the need to organize the needles in a coaxial fashion, as in Figure 2.7b. For single-material extrusion bioprinting, the resolution can reach levels around 150 µm, but most core-and-shell approaches are 300 µm or larger. Thus, it is difficult for constructs made with the method to resemble native tissue and are usually very simple in design. The ability to control the spatial organization of the core material of a multi-material fibre (Figure 2.7a) in combination with an on-the-fly material switching can allow for the realization of innovative scaffold designs that resemble native tissues. Advanced methods and tools for adjusting the composition and

organization of filaments in the manner described (circumferential, longitudinal, material concentration) may unlock limitations for biofabrication.

2.4 Conclusions

The purpose of this review was to briefly report on current fabrication methods in the development of multi-material tissue scaffolds. Scaffold-based tissue engineering is most important to minimize the need for organ donors by providing patients with a permanent solution to damaged organs and tissue, especially dire as global organ donor rates are not significantly increasing. All suitable scaffolds must satisfy and balance biological, architectural, and mechanical requirements. Multi-material bioprinting is essential to accurately reproduce the heterogeneous and anisotropic behaviour typical of native tissues.

Extrusion-based bioprinting is the basis of the multi-material bioprinting methods, primarily based on the pneumatic mechanism to print materials. On this basis, side-by-side bioprinting is characterized by having two or more different materials deposited sequentially within the same layer or in alternating layers. This method is the simplest and has the best resolution but has the longest fabrication time. Next, core-and-shell bioprinting employs coaxial needle systems to deposit two different materials simultaneously: typically, an ionically cross-linkable hydrogel as the shell and the crosslinker in the core. Coaxial fibres made in this way are hollow and are better for transferring materials through the scaffold but are weaker than robust fibres. These fibres are much more substantial than traditional ones, so their scaffolds do not resemble native tissues; there is no spatial control of the core within the shell. Last is advanced bioprinting methods that allow for on-the-fly adjustment of materials during deposition to directly place the material in a specific spot and concentration. This method has the shortest fabrication time but is limited because the devices are in a proof-of-concept phase.

For the future of tissue engineering, the focus should be on making a quickly produced product in a repeatable way. For that reason, rapid prototyping methods like extrusion-based bioprinting, modified inkjet printing, and three-dimensional electrospinning may prove to be the most beneficial for tissue engineering. However, the formation of scaffolds that mimic native tissue is a complex issue. Innovative fabrication methods, novel scaffold design, original composite materials, and spatially controllable fibres will give the best result.

3.0 DESIGN OF A NOVEL MULTI-MATERIAL BIOPRINTING SYSTEM

This chapter presents the design process of a novel multi-material bioprinting system from the technical specification to the detailed design stage. Each step of the design process is explained and applied to the printhead and the carriage. Also, the function, context, behaviour, principle, structure (FCBPSS) framework is demonstrated in conjunction with the design process to understand engineering design within bioprinting and the appeal of a methodical approach. These systematic advanced engineering design methodologies help to strengthen and justify the decision making, as each section has a distinct role. Advanced design methods have are not widely used in bioprinting systems, thus, this section offers a fresh look within the tissue engineering and bioprinting space.

3.1 Problem Definition and Overview of Proposed Bioprinting System

There is a gap for controllable material deposition within existing multi-material bioprinting systems in longitudinal and circumferential directions. Among the side-by-side bioprinting, core-and-shell bioprinting, and other advanced bioprinting methods, one can find the material deposition or distribution can be controlled in either the circumferential direction or the longitudinal direction, but not both. For example, core-and-shell bioprinting with coaxial fibres has control of material in the circumferential direction, and advanced rapid continuous bioprinting has control in the longitudinal direction. With the knowledge of the limitations of existing multi-material bioprinting systems, and the research objective is defined as "*to creatively design a multi-material extrusion-based bioprinting system with longitudinal and circumferential control of the printed filament."* More specifically, the system is designed with a printhead of modular configurations for printing multi-material filaments, as shown in Figure 3.1, which shows the visualization of circumferential and longitude-controlled fibres compared with current coaxial printed filaments.

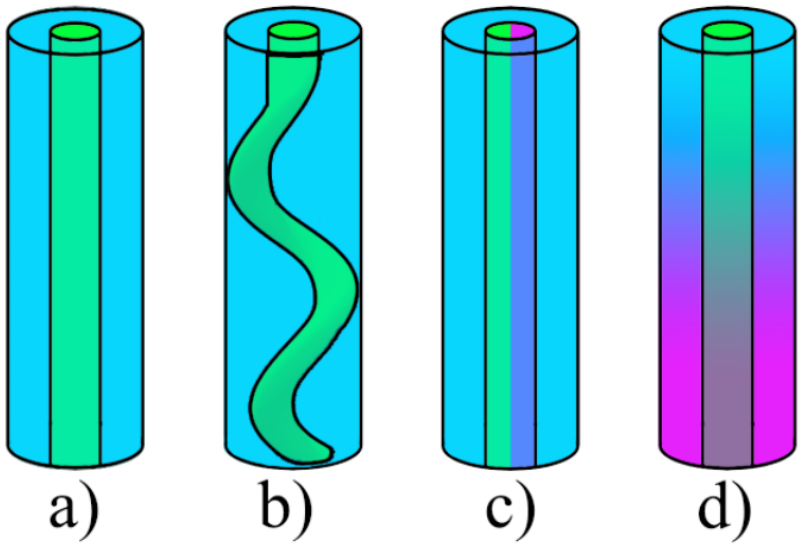

Figure 3.1: a) Typical Coaxial Fibre b) Longitudinal and Circumferential Controlled Fibre c) Split Core-and-shell d) Gradient-shell

For this proof-of-concept design, three different filament configurations will be demonstrated. The first configuration is shown in Figure 3.1b – a spiral organization of the core with a supportive shell. Second, Figure 10c shows a split vasculature with two core materials. Last in Figure 3.1d is similar in appearance to Figure 3.1a, but with a material gradient of the shell longitudinally.

Engineering design methods were applied to solve the problem, resulting in a novel, modular bioprinting system design, as shown in Figure 3.2. The main features of this design are one inlet in the first stage with a smooth channel, two inlets in the second stage with a mixing channel, and a single outlet to facilitate the multi-material deposition of the three materials.

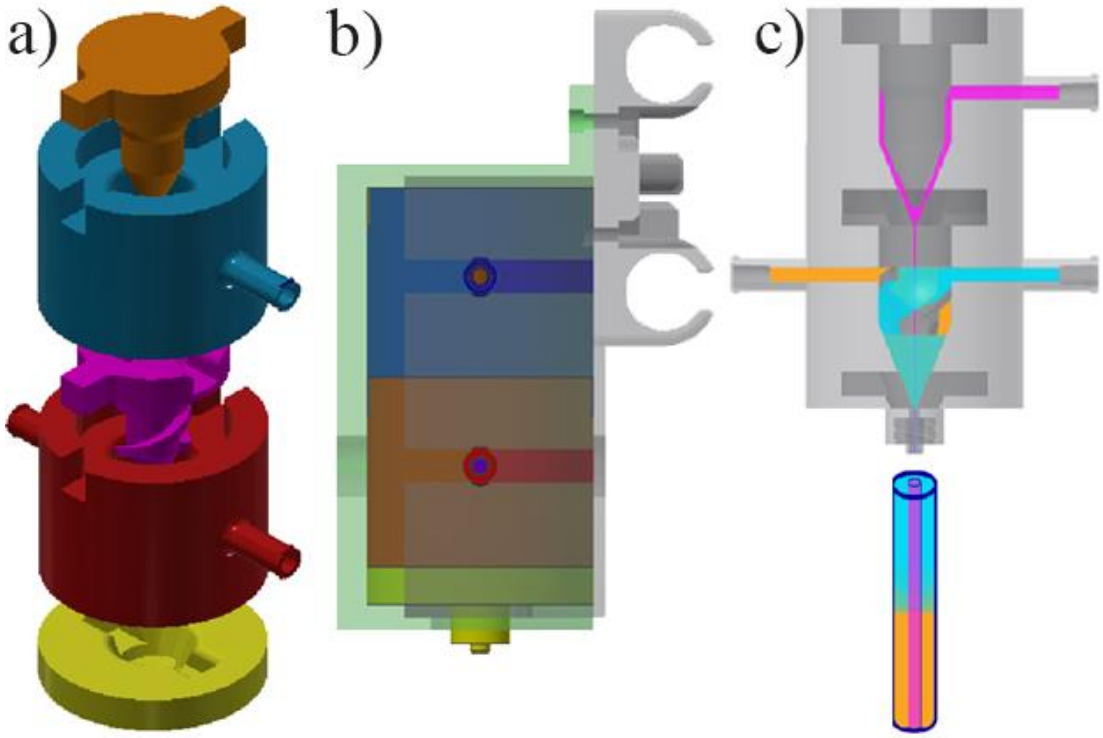

Figure 3.2: Printhead Overview a) Exploded View b) Side View with the Carriage c) Bio-ink Path

The rest of this chapter is to illustrate the designed process by

1) Applying the function, context, behaviour, principle, structure framework to this problem
2) Developing a technical specification for this problem
3) Developing the concept design, embodiment, and detail design of printhead
4) Assembling the novel system from the printhead and a multi-channel flow controller for precise deposition of bio-ink

3.2 Design Process

3.2.1 Brief introduction to the FCBPSS framework

There are notions of function, context, behaviour, principle, state, and structure within the engineering design domain to describe aspects of a designed system's need. A system is, in this case, a collection of objects that collectively work together to complete a set of tasks or objectives.

The notions have a slew of meanings within the space depending on specific usages or stages of design. However, the FCBPSS framework defined by Zhang et al. in 2011 introduced generalized definitions that can be easily adapted (Zhang, Lin, and Sinha 2011). The definitions of the notions are as follows:

Function: Two-part definition starts with the system's generic role and then moves to a specialized role

Context: The pre-condition, the post-condition, and the environment that must be connected through a specific system's behaviour

Behaviour: how the system responses are given a particular stimulus

Principle: Governs the relationships between the structure and its state and behaviour.

Structure: A set of entities that are connected in a meaningful way

State: The perceived entities of a structure of either physical or chemical domains that may change with time (Zhang, Lin, and Sinha 2011)

The FCBPSS framework's simplification allows it to be moulded to different design problems as a model for understanding candidate systems holistically in the conceptual stage. The framework is established through relationships in the emerging and governing dimensions (Zhang, Lin, and Sinha 2011). Now, applying this framework to the printhead in Figure 3.2 is shown in the following Table 3.1.

Table 3.1: FCBPSS Summary for the Printhead and Carriage System

Notion	In Bioprinting Printhead and Carriage System
Function	Facilitate the movement, deposition, and mixing of three bioinks to a single outlet
Context	Pre-condition is a collection of three individual bioinks, post-condition is a single filament, the environment is on an x-y-z controller
Behaviour	Dynamic
Principle	Facilitate the movement and mixing of bioink
State	Printhead full of bioink or void of bioink
Structure	Smooth core, single inlet head, static mixing core, dual inlet head, outlet adapter

Applying the FCBPSS framework to this design gives the user and designer, and the user a better understanding of the basics of the system. More detail of the functional requirements and constraints that were applied to the system will be described in the next section, the design process section

The design process that was taken for this system has four main sections: the technical specification that breaks down functional requirements (FR), performance requirements (PR), and constraint requirements (CR); conceptual design stage that deals with assigning design parameters (DP) to the functional requirements, specifically delated to finding general functions in solving the principle of the system; embodiment design stage determines the material and decides the volume of the system; last, the detail design stage determines the surface features.

3.2.2 Technical Specification

The technical specification is a designer-oriented description that breaks down the functional requirements, performance requirement, and constraint requirements. Each functional requirement may have several performance requirements associated with it, as well as several constraint requirements. Within this context, functions are defined as the structure's usefulness concerning the human, ecological, and technical system. Performance is defined as an assessment of how well the function performs by quantity, quality, coverage, timeliness, or

readiness; then, a constraint is defined as a condition or context under which a device plays its function. As described in Table 3.1, the overall function of the printhead is to facilitate the movement, deposition, and mixing of three bioinks to a single outlet. This prominent functional requirement is composed of sub-functions:

- FR1: Accommodate connection to three separate bioink reservoirs
- FR2: Facilitate the mixing of two bioinks
- FR3: Combine the mixed bioink with an unmixed bioink in a core-and-shell organization
- FR4: Be compatible with standard Leur Lock needle tips for single outlet deposition
- FR5: Compatibility for fitting the parts in several organizations and future modularity

For the three functional requirements, there are several performance requirement and constraint requirements to categorize the system's design. In functional requirement one, there constraint requirements is that the inlets have a standard male Luer Lock barb for connecting to the three fluid reservoirs and that there is one inlet in the first stage of the system and two inlets to the second stage of the system. For functional requirement two, mixing should occur in the system's second stage and dimensions of the mixing core such that the pressure buildup propels the mixed fluid to the outlet of the head. Further, at the end of stage two, the two bioinks should be thoroughly mixed and ready to be incorporated into the third stage governed by functional requirement three and functional requirement four. In functional requirement three, the fluids should be combined to accommodate the core-and-shell organization with the core size of 600 μm and the shell size of 800 μm. For functional requirement four, the system should accept male Luer Lock syringe tips for custom filament size depending on the user's need. Last, the system should have sectional type modularity to accept the exchange and different orders of components of similar type.

In summary, for the printhead:

- CR1 (FR1): Total three horizontal inlets with one in the first stage and two in the second with a standard male Luer lock barb
- CR2 (FR2): Two bioinks are thoroughly mixed by the end of stage two
- CR3 (FR3): Concentric organization of the interface between stage one and two
- CR4 (FR4): The single outlet is outfitted with a standard female Luer lock interface for multiple sizes of syringe tips

- CR5 (FR5): All interfaces between parts have sectional type modularity for adjustable filament organization in the future
- CR6 (FR1-5): Material is biocompatible and non-toxic for cellular study
- FR1-5 {PR-1| Core size is ~600 µm, and shell size is ~800 µm

Next, focusing on the functional requirements for the printhead carriage:

- FR1: Temporarily affix the printhead assembly
- FR2: Provide adequate access to the inlets and the outlet
- FR3: Connect with a controller to give the printhead movement in the x-y-z directions

Compared to the printhead assembly, the carriage is very simple for performance requirement and constraint requirements. For functional requirement one, the printhead assembly should be removable but not move during printing. The assembly should be removable so that the head parts can be cleaned in between jobs, or the configuration can be changed. For functional requirement two, there should be enough space between the inlets of the printhead and the carriage such that the user can easily connect the plumping to the bioink reservoirs. Further, the carriage should not block the outlet of the printhead assembly nor restrict material deposition in any way. Then for functional requirement three, the carriage should be stable and not impose undesired movement to the printhead; the movement of the printhead should move directly dictated by the x-y-z controller.

The description of functional requirements, constraint requirements, and performance requirement is the first part of the design process in the technical specification. With the technical specification finished for the multi-material bioprinting system, next is the conceptual design.

3.3 Conceptual Design

The goal of the conceptual design is to make sense of the design at the logical level, as is that there is a system proposed which can fulfill the technical specification. The conceptual design phase oversees the principle of the solution and excludes any notion of dimension or scale, which are tackled in the following design stages. Further, the conceptual design stage assigns design parameters the functional requirements from the previous section. There will have to be a conceptual design of the printhead assembly, which governs the flow of bio-ink, the carriage,

which governs the connection between the printhead assembly and an x-y-z controller, and the entire multi-material bioprinting system.

3.3.1 Conceptual Design of the Printhead Assembly

Looking at the overview of the printhead in Figure 3.2, the governing principles for fluid deposition are air pressure and gravity. The principle of fluid movement through the printhead is shown in Figure 3.3; note the bioink pathway and the difference between the smooth plug in the first stage and the mixing core in the second stage. There are five components: smooth plug, single-inlet head, dual-inlet head, mixing core, and the adapter.

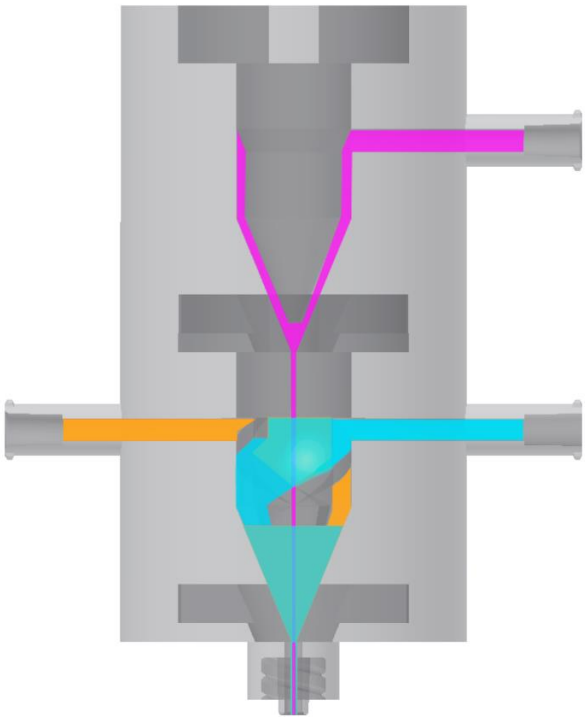

Figure 3.3: Principle of Printhead

Next is to assign design parameters for each of the functional requirements of the system. If the design concepts are not appropriate, then the functional requirements would need to be adjusted. As per the axiomatic design principle, a better design has independent functional requirements, and its design parameters should maintain the independence of the functional requirements (Suh 2001). Following this, the design parameters for the system are:

- DP1: Cylindrical chambers with some Luer inlets
- DP2: Mixing core for combining two bioinks
- DP3: Smooth plug for moving the unmixed bioink
- DP4: Adapter to organize bioink and move to Luer syringe
- DP5: Channel throughout the second stage for core-shell organization

To assess if this design meets Axiom 1, the independence of the functional requirements should be maintained by the design parameters. The following figure, Figure 3.4, shows the relationship between the design parameters and the functional requirements.

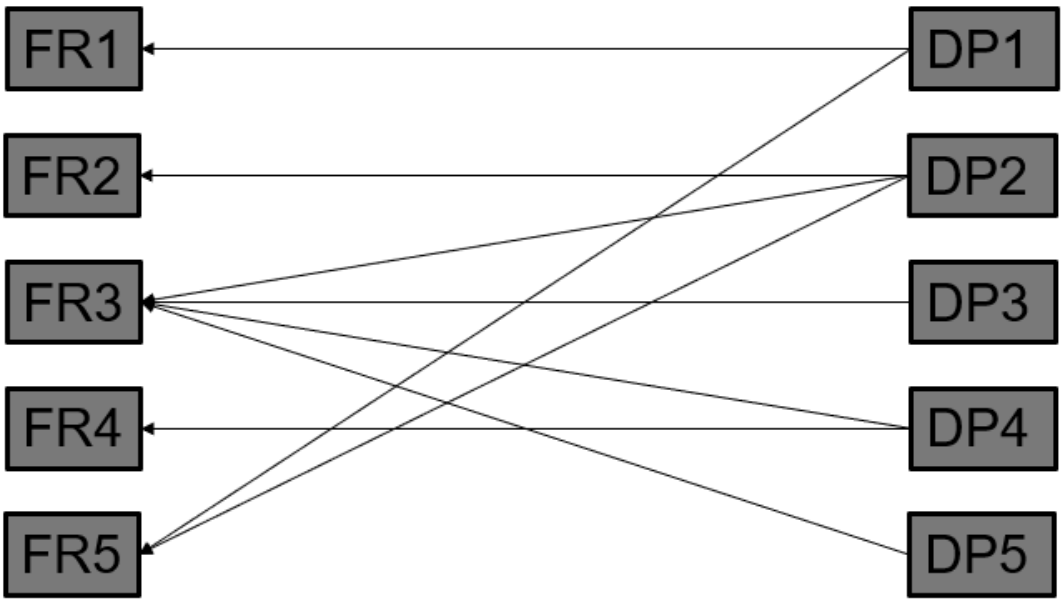

Figure 3.4: Functional Requirement and Design Parameter Relationship for Printhead Assembly

Here, the design parameters interact with multiple functional requirements and form a design matrix that is neither diagonal nor triangular, which is an example of a coupled design and fails to meet Axiom 1. The way the functional requirements and Design parameters are outlined makes it nearly impossible to have anything but a coupled design, but this does not pose a problem to the solution – a new set of functional requirements and design parameters can be introduced.

3.3.2 Conceptual Design of the Carriage

Before introducing a new set of functional requirements and design parameters for the printhead system, the design parameters for the carriage in Figure 3.3 should be built. Based on the list of functional requirements from the section, the design parameters are:

- DP1: Section that 'holds' the printhead
- DP2: Section that 'connects' to the x-y-z controller

Again, the design parameters are assigned to functional requirements for the carriage – this is shown in Figure 3.5.

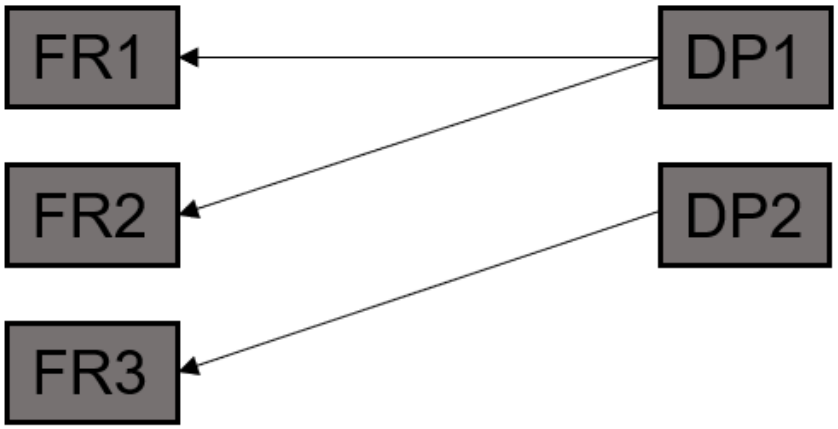

Figure 3.5: Functional Requirement and Design Parameter Relationship for Carriage

Again, the design matrix is neither triangular nor diagonal, so this set of functional requirements and design parameters fails Axiom 1. Now move to examine the multi-material bioprinting system to build a new set of design parameters and functional requirements that can pass Axiom 1 and display functional independence.

3.3.3 Conceptual Design of the Multi-material Bioprinting System

For the sake of simplicity, look at the system from a surface level; a multi-material bioprinting system consisting of a pressure controller for material deposition, a controller for x-y-z movement, and a printhead to facilitate the flow of the bioink. Figure 3.6 gives an overview of the system. This system will employ a combination of a desktop fused deposition modelling (FDM) 3D printer for x-y-z control, a multi-channel pressure controller for facilitating on-the-fly

adjustments of the biomaterial inlets, a custom printhead for organizing the multiple inlets to a single outlet, and a PC to control the relevant software for the hardware.

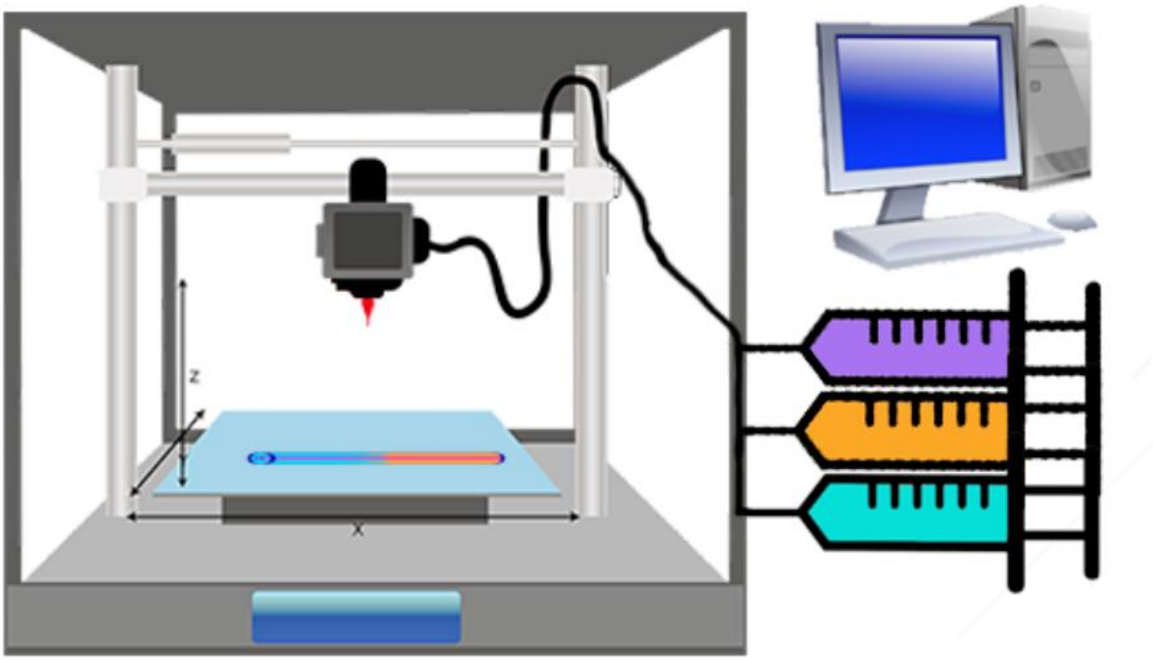

Figure 3.6: System Overview

Now, for the system, the functional requirements to meaningfully evaluate the conceptual design are:

- FR1: Dispense multi-material bioink with control of the material composition in the circumferential direction
- FR2: Dispense multi-material bioink with control of the material composition in the longitudinal direction. (% range from 0 % to 100%)
- FR3: The system is easily reconfigurable to dispense multi-material fibres in a different longitudinal and circumferential organization.

Meanwhile, the design parameters to satisfy the functional requirements are:

- DP1: Hardware
- DP2: Software
- DP3: Process control

The general terms of hardware, software, and process control relate to the nozzle assembly, the PC, and pressure controller of the system. Again, match the functional requirements to design parameters to check if the functional independence of the system, shown in Figure 3.7.

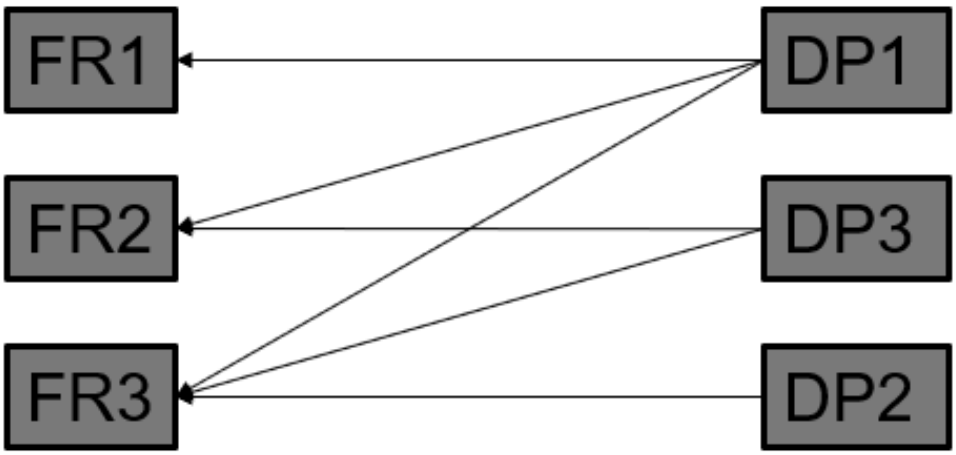

Figure 3.7: Relationship of General functional requirements and Design Parameters for the Multi-material Bioprinting System

With the updated general functional requirements and design parameters, the design matrix for the multi-material bioprinting system is triangular. A triangular design matrix means that functional independence is satisfied if the design parameters are applied in a particular order (Suh 2001).

With the conceptual design passing Axiom 1, the next step is to add volume and material in the embodiment design.

3.4 Embodiment Design

Here, the goal is to add volume and material to the system based on the design parameters from the conceptual design stage. Lending from the design parameters of the conceptual design stage, a physical representation of the system that can achieve the main principle with temporal and spatial characterization will be devolved. This stage of the design process is meant for initial dimensions to create space, starting with the embodiment of the printhead assembly.

3.4.1 Embodiment of the Printhead Assembly

As mentioned previously, there are five components in this system: smooth plug, single inlet head, mixing core, dual inlet head, and syringe adapter, shown in Figure 3.2a. This embodiment process started with deciding the total diameter of the cylindrical chamber. The design was based on a 30 mL syringe, a typical size for bioprinting purposes – equalling a 45 mm diameter. Next, there was a concern for having sharp corners for the transition between stages, leading to more considerable cell damage, so a 60-degree angle was added, as per standard bioprinting tapered needles (Ning et al. 2018). Further, following ISO 80369-7:2016 for the Luer connections, the proper dimensions were used for compatibility in the inlets and the adapter (International Organization for Standardization [ISO] 2016). This feature is for compatibility with piping connections from the bioink reservoirs and with custom-sized syringe tips. Figure 3.8 shows the embodiment of the system.

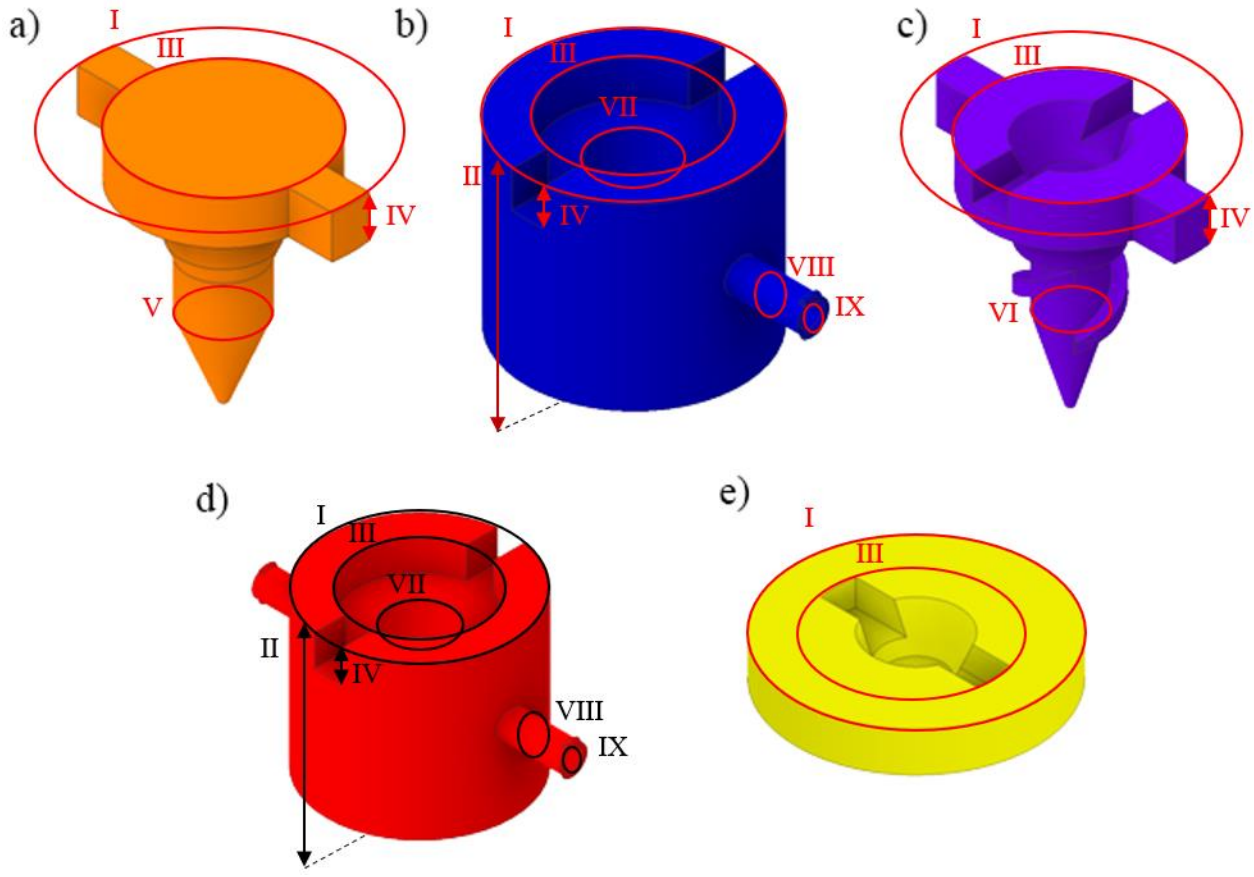

Figure 3.8: Embodiment of the Printhead Assembly a) Plug b) Head 1 c) Core d) Head 2 e) Adapter

In Figure 3.8, we have the smooth plug, single-channel head, mixing core, dual-channel head, and the adapter from left to right and top to bottom. A summary of the key dimensions of the embodiment of the printhead assembly is shown below in Table 3.2.

Table 3.2: Key Embodiment Dimensions of Printhead Assembly

Parameter	**Label from Figure 3.8**	**Measurement (mm)**
Base Diameter	I	45
Base Length	II	45
Plug/Core Base Diameter	III	30
Plug/Core Head Height	IV	8.5
Plug Shaft Smallest Diameter	V	12.5
Core Shaft Smallest Diameter	VI	10.5
Head Hole Diameter	VII	16
Inlet Inner Diameter	VIII	3
Inlet Outer Diameter	IX	6.73
Stage 1 Outlet Outer Diameter	N/A	0.4
Stage 2 Outlet Outer Diameter	N/A	0.6
Adapter Outer Diameter	N/A	0.8

A 68-degree chamfer was added to create the tapered end of the core and plug and the matching shape for the head, making a 2 mm gap between the pieces for fluid to move. For the mixing core, a 0.5 rotation of a 1 mm tall rectangle in the straight region of the core was added to each side – one half rotation thread for each inlet. The last feature for the embodiment stage is the sectional modularity for pushing together the different parts. Figure 3.9d shows the interface between the parts. The top row shows the top of the parts, and the bottom row is the bottom of the parts.

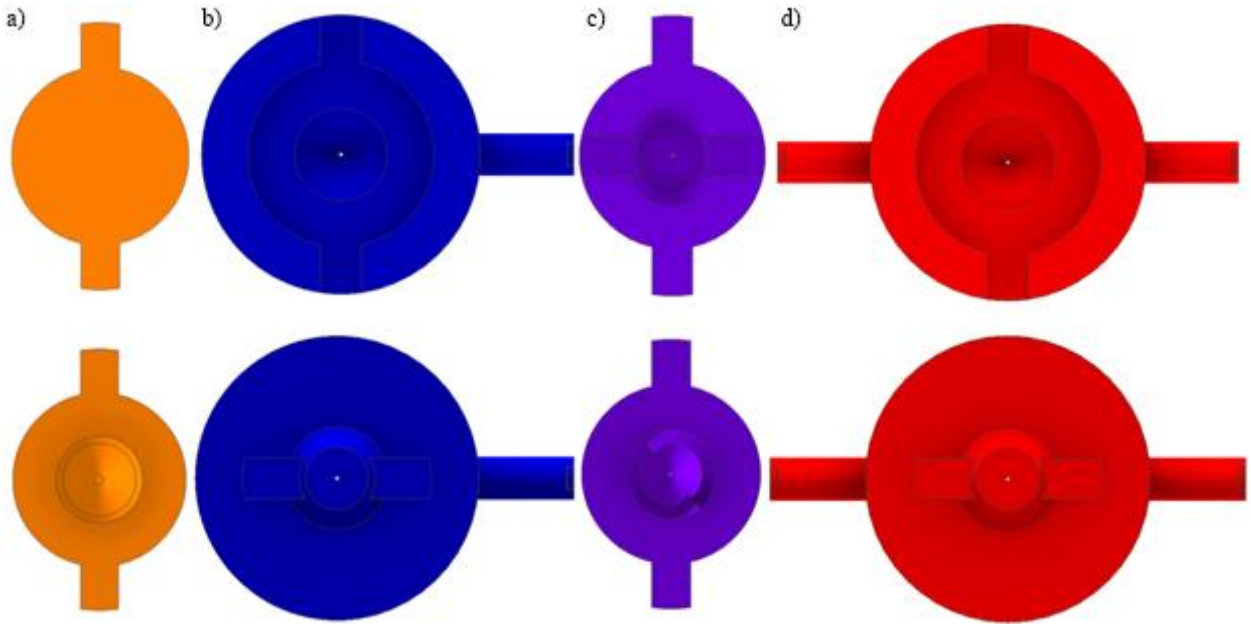

Figure 3.9: Modular Interface Between Parts a) Plug b) Head 1 c) Core d) Head 2

The way that the parts fit together aids in the future modularity of the printhead system. All parts in this configuration were designed to produce filaments as in Figure 3.1d, or the core-and-shell organization with a longitudinal control of material concentrations. The user could switch the single and dual inlet heads for a different filament organization within the current configuration. Further, the parts only fit together in the order of plug, head, core, head, and adapter, with the rotation fixed to ensure the mixing core's threads align with the inlets of the relevant head. At this point, the initial geometry of the printhead assembly is complete. However, the geometry is likely to change in the detail design phase, where the design for manufacturing is done.

3.4.2 Embodiment of the Carriage

Connection of the printhead assembly to the x-y-z controller is necessary for the system to deposit material in a meaningful manner. A carriage to fix the printhead components in place and hold the assembly to driving components is needed. The main features of this carriage are that it fixes the printhead in any of the printhead's configurations, does not impede the movement x-y-z controller in any direction, and has access to the inlets and outlets. Figure 3.10 shows the embodiment of the carriage and labels key measurements, which are detailed in Table 3.3.

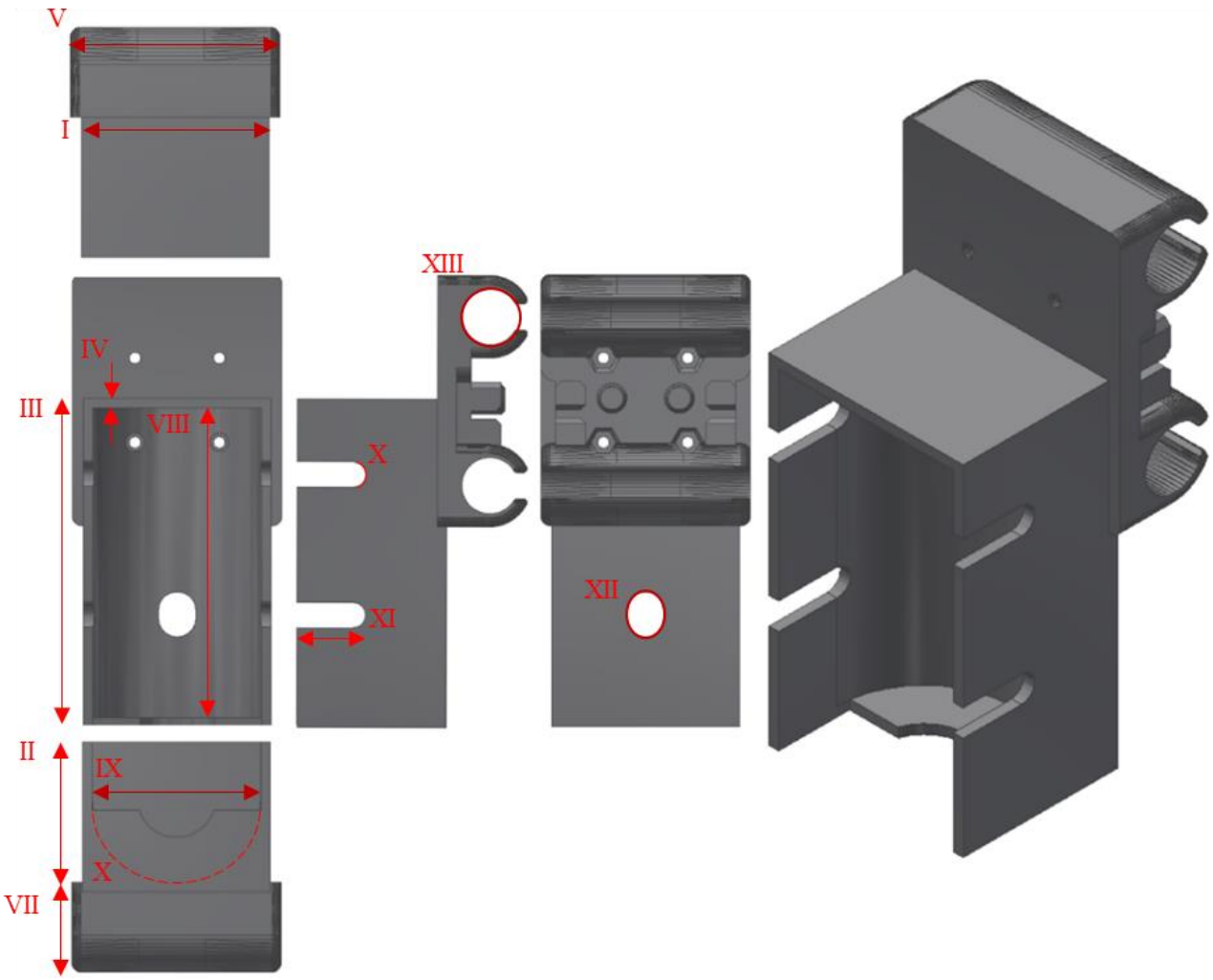

Figure 3.10: Embodiment of the Carriage

The dimensions of the carriage are dependent on the dimensions of the printhead assembly. For example, the inner column of the carriage box is shaped with a height to match the tip and tail edges of the plug and adapter, respectively; the radius of the column is the same as the printhead. Further, the “connectors” on the rear plate of the carriage are dependent on the specific x-y-z controller being used, as different controllers would require different elements. The embodiment of the connectors shows space for bearings and smooth rods attached to the frame of the x-y-z controller. Then, the four slots on the upper and lower ends of the carriage box are for securing the inlet arms, the hole at the back of the box is clearance for inlets of future parts, and the inner circular cut through the bottom of the box is to make space for the adapter. Table 3.3 shows a summary of the key dimensions for the embodiment of the carriage.

Table 3.3: Key Embodiment Dimensions of Carriage

Parameter	Label from Figure 3.10	Measurement (mm)
Box Width	I	50.5
Box Depth	II	40.5
Box Height	III	87.5
Box Thickness	IV	2.25
Plate Width	V	56
Plate Depth	VI	24
Plate Height	VII	67
Column Height	VIII	83
Column Radius	IX	23
Inlet Slot Radius	X	3.625
Inlet Slot Depth	XI	18.625
Back Hole Diameter	XII	10
Connector Diameter	XIII	15

With the initial geometry of the carriage complete, the next step of the embodiment design stage is to add material.

3.4.3 Material Selection

The last activity in the embodiment design stage is to determine the material for the device. We know from the technical specification that the material should be biocompatible, non-cytotoxic, and suitable for sterilization in use with cellular material (International Organization for Standardization [ISO] 2009). Another consideration is that the material is easily manufacturable and can accurately reproduce the necessary features to satisfy the functional requirements. With

these factors in mind, the candidate materials for the printhead assembly are from rapid prototyping methods shown in Table 3.4 (Espalin et al. 2015) (Belloncle et al. 2012).

Table 3.4: Candidate Rapid Prototyping Materials

Material	Technique	Biocompatible	Sterilization	Melting Point	Glass Transition, Tg	Tensile Strength	Tensile Elongation	Flexural Strength	Izod Impact, Notched	ASTM D648 (A)	Resolution
PC	FDM	No	EtO or Gamma	N/A	161°C	57 MPa	4.80%	89 MPa	73 J/m	138°C (0.45 MPa)	127 µm max
ABS-M30i	FDM	ISO 10993 USP Class V	EtO or Gamma	N/A	108°C	36 MPa	4%	61 MPa	139 J/m	96°C (0.45 MPa)	5 mm layer
HP PA12 Nylon	HP MJF	Yes (ISO 10993-5)	Autoclave	186°C (Powder)	N/A	48 MPa	20%	70 MPa	3.5 kJ/m^2	173°C (0.45 MPa)	80 µm
HP PA12 Nylon	HP MJF	Yes (ISO 10993-5)	Autoclave	186°C (Powder)	N/A	48 MPa	20%	70 MPa	3.5 kJ/m2	173°C (0.45 MPa)	80 µm
HP Nylon PA 12	HP MJF	Yes (ISO 10993-5)	Autoclave	186°C (Powder)	N/A	48 MPa	20%	70 MPa	3.5 kJ/m^2	173°C (0.45 MPa)	80 µm
MED-WHT 10	Figure 4 Standalone	Yes (ISO 10993-5)	Autoclave	N/A	102°C	60 MPa	3%	112 MPa	17 J/m	102°C (0.45 MPa)	30 µm layer
MED-WHT 10	Figure 4 Standalone	Yes (ISO 10993-5)	Autoclave	N/A	102°C	60 MPa	3%	112 MPa	17 J/m	102°C (0.45 MPa)	50 µm layer
ULTEM 9085	FDM	N/A	Autoclave	N/A	186°C	69 MPa	5.80%	112 MPa	120 J/m	153°C (264 PSI)	254 µm max
ULTEM 1010	FDM	Yes (ISO 10993)	Autoclave	N/A	215°C	81 MPa	3.30%	144 MPa	41 J/m	216°C (0.45 MPa)	254 µm layer
PC-ISO	FDM	Yes (ISO 10993)	EtO or Gamma	N/A	161°C	57 MPa	4.00%	90 MPa	86 J/m	133°C (0.45 MPa)	7 µm layer

From the materials list, the top two candidates are the MED-WHT 10 with either the 30 µm or 50 µm layer height and the HP PA12 Nylon. The materials were initially selected for sterilization methods, biocompatibility, rapid prototyping compatibility, quick availability from Canadian companies and rapid prototyping services.

However, rapid prototyping is not the most available method for the USask Biofabrication Lab. The USask Biofabrication Lab has quick and easy access to the manufacturing of anodized aluminum for the printhead assembly and the carriage; as such, anodized aluminum is the material for the prototype. This aluminum prototype can be used for acellular studies to demonstrate the dispensed biomaterial's longitudinal and circumferential control. The simplicity, here, is in ignoring the biocompatibility and sterilization factors for the flow control

demonstration. A decision between MED-WHT 10 and HP PA12 Nylon can be made in the future, after testing of the aluminum printhead and carriage.

With the design parameters from the conceptual design stage realized and the design brought to "life", the next step is to refine the system by adding surface features and making it ready for manufacturing.

3.5 Detail Design

The goal of the detailed design stage is to develop complete specifications for the system to be ready for manufacturing. This stage is a natural progression from the embodiment design stage, which includes adding geometry and selecting a material. It considers the fine geometrical details covering the ease of manufacturing and assembly. For example, where embodiment is to determine the layout, volume, material, and distribution of the material, then the detail stage is to determine the surface quality, fillets, chamfers, and adjusting geometry in favour of a particular manufacturing method, machining of anodized aluminum, in this case.

3.5.1 Detail Design of the Printhead Assembly

The main goal of the printhead prototype's detailed design is to simplify the prototype's features. This simplification of the assembly includes and is shown in Figure 3.11 with key measurements labelled and detailed in Table 3.5:

1. Removing the "tabs" and matching recesses and adding through-holes to the assembly to fix the components with metallic fasteners.
2. Remove the Luer connection of the inlets and use standard-sized tubes to hold plumbing for the biomaterial.
3. Use standard dimensions for available aluminum pieces as the base of the components.
4. Remove the adapter for a Luer locking needle and deposit material from the head 2.

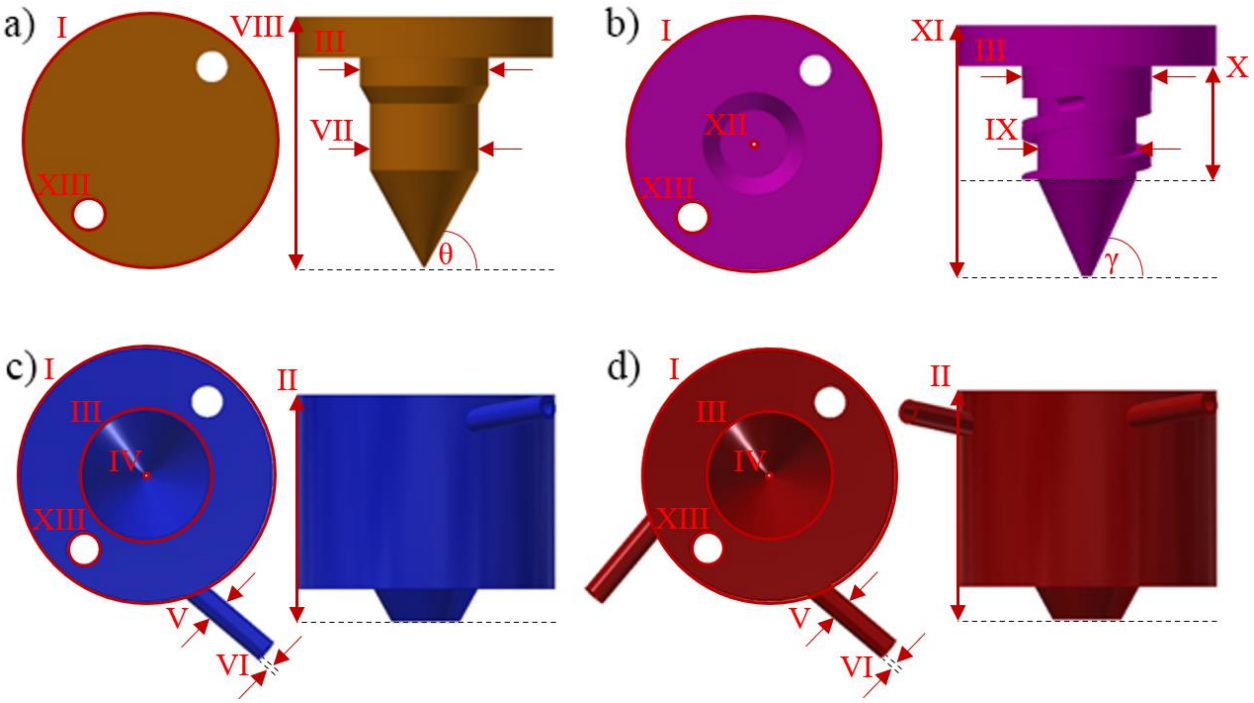

Figure 3.11: Detailed Design of Aluminum Prototype Components a) Plug b) Core c) Head 1 d) Head 2

For example, the outer diameter of the components is 2 inches (50.8 mm), the diameter of the hole in Head 1 and Head 2 for the shafts are 1 inch, and the through-holes are 0.25 inch (6.35 mm). The outer diameter of the inlet pipes is 0.1875 inches (4.7625 mm), and its walls are 0.035 inches (0.889 mm) thick, from readily available stock parts from an online vendor (McMaster-Carr 2021a). For more information on the key dimensions of the prototype components, see Table 3.5.

Table 0.5: Aluminum Prototype Detail Design Key Component Measurements

Parameter	**Label in Figure 3.11**	**Measurement**
Outer Diameter	I	2 (50.8 mm)
Head 1/Head 2 Height	II	1.75 inches (44.45 mm)
Head 1/Head 2 Hole Diameter Plug/Core Outer Shaft Diameter	III	1 inch (35.4 mm)
Head 1/Head 2 Fluid Hole Diameter	IV	0.031 inches (0.7874 mm)

Inlet Pipe Outer Diameter	V	0.1875 inches (4.7625 mm)
Inlet Pipe Wall Thickness	VI	0.035 inches (0.889 mm)
Plug Inner Shaft Diameter	VII	0.848 inches (21.5392 mm)
Plug Height	VIII	1.938 inches (49.2252 mm)
Core Inner Shaft Diameter	IX	0.768 inches (19.5072 mm)
Core Coil Height	X	0.625 inches (15.875 mm)
Core Height	XI	1.938 inches (49.2252 mm)
Core Centre Through-Hole Diameter	XII	0.031 inches (0.7874 mm)
Fastener Through-Hole Diameter	XIII	0.25 inches (6.35 mm)
Taper Angle of Plug Tip	θ	60°
Taper Angle of Core Tip	γ	65°

Several other features were changed from the embodiment of the pieces to the detailed design of the prototype. One, the angle of the taper at the tip of the plug and core is 60 degrees and 65 degrees, respectively. Two, the mixing core was changed from a double-helix with a 0.5 revolution to a single-helix with a 1.5 revolution along the shaft's height. Three, the inlets were changed from co-linear to the centre plane of Head 1 and Head 2 to tangent to the coil of the mixing core. Four, the coil's end was extended to be cut by the horizontal plane of the cylindrical part of the core. Five, the transition area between the first inlet of Head 2 and the core was filled to remove any trapped volume of fluid to lead the flow path around the core. These changes were done to simplify the components for manufacturing and increase the means of combining the biomaterials between entering the core from the dual-inlet head 2. The consideration for Head 2 and the mixing core is shown in Figure 13.12; 13.12a shows that the inlets are parallel to the helical core, 13.12b shows that the helical rib is cut by the horizontal plane of the head, and 13..2c shows the lack of dead volume at the entrance of the upper inlet. See Appendix A for detailed renders of the components for the printhead assembly.

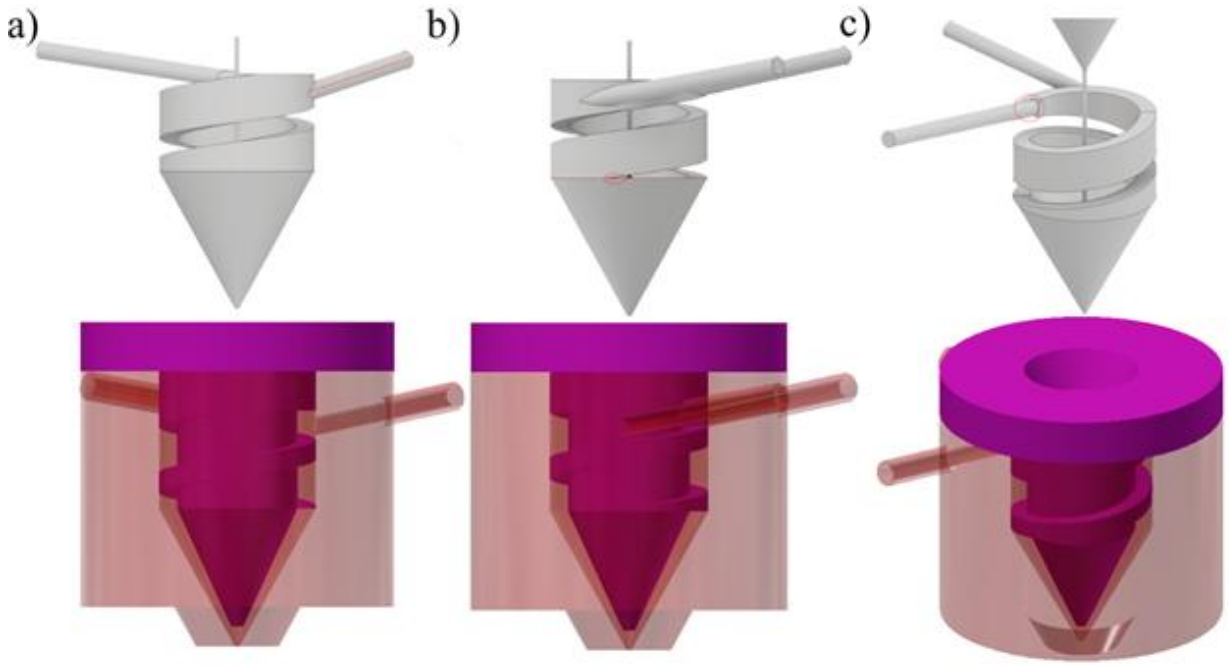

Figure 3.12: Detail Design Consideration of Head 2 and Core a) Inlets Parallel to Helical Rib b) Terminus of Helical Rib is the Horizontal Plane of the Shaft c) Removing Dead Volume at the Inlet

The next part of the detail design is not visible. However, it adds space for clearance between the fitted parts and accounting for tolerance, depending on the manufacturing method and the purchased base. For the aluminum prototype, the components have an included tolerance of -+ -0.024 inches in the diameter, the inlet tubes have a tolerance of -+0.01 inches in the outer diameter and -+ 0.006 inches tolerance in the wall thickness (McMaster-Carr 2021a). In designing the components to fit together, a decision for what kind of fit must be made – clearance or interference. A clearance fit is a fit in which the smallest diameter of the hole is larger or equal to the largest diameter of the shaft. In contrast, an interference fit has an overlap between the largest diameter of the hole with the smallest diameter of the shaft (International Organization for Standardization [ISO] 2010). Here, a clearance fit between the printhead components and the metallic fasteners aid in keeping a tight fit to ensure no fluid leaks the printhead during deposition. As this detail design is for a prototype, all parameters' nuanced considerations were ignored and can be addressed after fabrication and assessment of the physical representation. However, some consideration was taken to the mixing capabilities of the printhead assembly.

3.5.2 Mixing Consideration of Printhead Assembly

Mentioned in Chapter 2, biocompatible hydrogels, like alginate and gelatin, are among the most popular medium for multi-material bioprinting; however, these materials are typically shear-thinning, or pseudo-plastic fluids that flow with low Reynolds numbers (Drury, Dennis, and Mooney 2004; Hozumi, Ohta, and Ito 2015; Ma et al. 2014; J. R. Mitchell and Blanshard 1974; Ma et al. 2014; Colosi et al. 2016; Schwab et al. 2020). Flow with low Reynolds numbers is difficult for mixing, so the printhead's geometry and design and the method for introducing the biomaterial to the dual-inlet head must encourage mixing (C.-Y. Lee et al. 2011; Gan et al. 2006). Here, the approach is to design the helical ribs of the core like a static mixer, which has been used to improve the mixing capability between hydrogels (Hozumi, Ohta, and Ito 2015; Meng et al. 2017; Szalai and Muzzio 2003). Further, mixing of the biomaterials due to primarily angular momentum, like the two-channel helix of the embodiment design, is ignored. The printhead assembly's primary mixing mechanism is an alternating time-dependent pulsatile flow of the two inlets along a single-channel helix. Pulsatile flow along the helical path of the mixing core may increase the mixing capability of the two inlets, but it may not mix them thoroughly (Afzal and Kim 2015; Gan et al. 2006; 2006). Although complete and precise mixing of the two inlet materials is not a priority, the goal of the printhead is to facilitate the deposition of material for broad control in the longitudinal and circumferential direction. A representation of the flow path of the three biomaterials through the printhead assembly is shown in Figure 3.13.

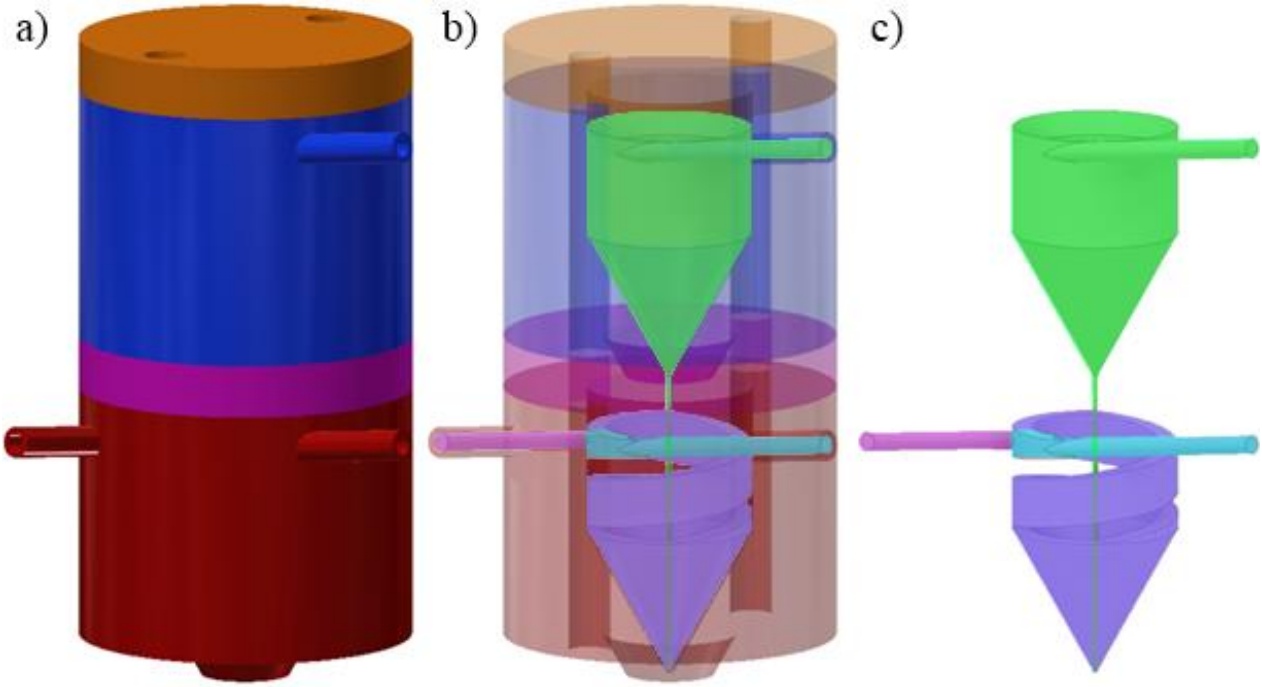

Figure 3.13: Flow Path Through Printhead Assembly a) Printhead Assembly b) Flow Path Through Assembly c) Flow Path

With detailed specifications added to the general geometry added to the system, the models adjusted for ease of manufacturability with the selected technique, and the manufacturing conditions selected, the component's prototype is ready for fabrication. Those three tasks make up the detail design stage and complete the design of the multi-material bioprinting head. This bioprinting head prototype is meant to demonstrate the feasibility of controlling acellular material in the circumferential and longitudinal direction. Further, detailed optimization of the diameter, angle, or position of the inlets, height, and pitch of the core coil, or the outlet's position and diameter is out of scope. The next part of the detail design of the bioprinting system is for the further specification of the carriage.

3.5.2 Detail Design of the Carriage

Like the detail design of the printhead assembly, care needs to be taken for the printhead carriage to express the fine details of the carriage, select a manufacturing method, and make the carriage easily manufacturable with the selected method. Here, The Original Prusa i3 MK3S 3D printer with a 0.2 mm diameter nozzle would manufacture the carriage with spools of 1.75 mm - Polyethylene Terephthalate Glycol (PETG) filament. PETG is a favourable material to use

because of its good printability, durability, and good layer adhesion (Prusa Research a.s. 2021b; Szykiedans, Credo, and Osiński 2017).

The changes made between the detail and the embodiment of the carriage were primarily adding fillets to the harsh corners of the components and matching the features of the updated printhead components. Mainly the fillets were added to the pieces of geometry which are interfacing with other components – all fillets are 2 mm in diameter. Next, space was added for the printer's tolerance and the manufacturing of the printhead components. As a start, there is a 0.5 mm clearance for the fitted parts, but that will be adjusted after fine-tuning the printer settings and consideration of resolution of the printer, consistency of the PETG filament, calibration of the printer, and printing parameters such as head speed of the 3D printer and the extruder temperature.

The "connectors" on the back of the carriage were updated to account for fitting LM8UU bearings for smooth movement along 8 mm smooth rods and space for affixing a 2GT timing belt to drive the carriage in the x-direction; all for The Original Prusa i3 MK3S 3D printer. Then, through-holes for the carriage column were added to match the holes in the printhead assembly for metallic fasteners – ¼ inch bolts and appropriate nuts and washers (McMaster-Carr 2021b). The last feature of the carriage is a holder for a P.I.N.D.A (Prusa INDuction Autoleveling) probe as part of The Original Prusa i3 MK3S 3D printer to facilitate the calibration of the nozzle in the z-direction, which can be used in calibrating the multi-material bioprinting system as well. Figure 3.14 shows the detail design of the carriage and the printhead assembly. A render of the carriage is in Appendix A.

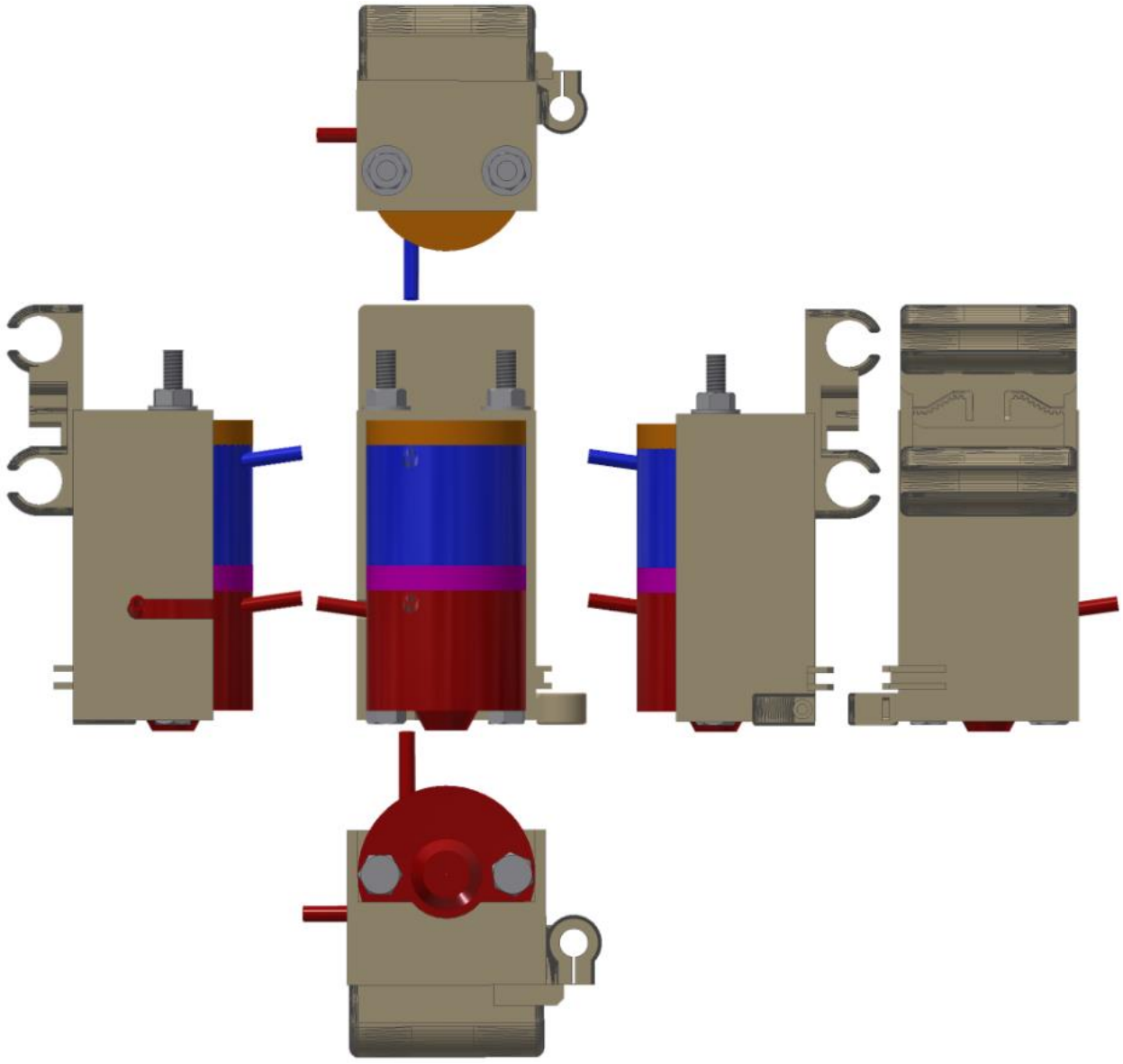

Figure 3.14: Detailed Design of Printhead and Carriage Overview

The 3D model of the carriage needs to be translated to G-Code from the CAD software's format from the CAD software for 3D printing through the slicing process. In slicing the 3D models for FDM, the parts were laid in orientation to minimize "overhang" for fabrication. A general rule of thumb for FDM is to minimize the overhang to 45 degrees to print without supports (Torres et al. 2015). Therefore, in slicing, the carriage will be placed to limit features over 45 degrees from the print bed, and that supports are holding the exterior of the part only. Next in the slicing is to determine the infill percentage and infill pattern. Typically as the infill percentage of an FDM printed part increases, so do the mechanical properties and the effective printing time – a balance

between time and properties needs to be made (Alvarez C, Lagos C, and Aizpun 2016). As mechanical robustness is not a concern in the proof-of-concept phase, the infill percentage is set to a lower-end value of 15% in a zig-zag pattern. As with the clearance of the fitted parts, this value will change with the feasibility test of the printer.

The updated carriage, adding manufacturing considerations, detailed geometry, and features for deposition, is complete and ready for prototyping. Along with the printhead assembly, the carriage will facilitate material deposition through connection with a flow and x-y-z controller. The flow controller will govern the pressure and, thus, the flow rate of the inlet materials, while the x-y-z controller governs the layer-by-layer deposition of the materials.

3.5.3 Selection of the Elveflow OB1 MK3+ Controller and the Prusa i3 MK3S 3D Printer

A flow controller is needed to work with the multi-material bioprinting tool head to dispense various cell-laden biomaterials simultaneously. As mentioned in Chapter 2, common extrusion bioprinting systems are driven by pneumatic-, screw-, or piston-based mechanisms, with the pneumatic being favoured for their simplicity and for limiting cell damage (Derakhshanfar et al. 2018; X. Chen 2018). As such, a pneumatic mechanism is a favourite for the proposed multi-material bioprinting system. The pneumatic controller should have the capability for precise, independent control of three fluid channels with the possibility of expansion to a fourth channel, lending to the system's modularity. Next, the controller should have "on-the-fly" control of the inlets to accommodate the longitudinal organization of the deposited material, shown in Figure 3.15. Throughout the filament, the core material is fully present, while at P1 there is 100% of shell material 1 and 0% percent of shell material 2; P3 is the opposite; P2 is a mixture of material 1 and 2 due to the alternating pulsatile flow described in Section 3.5.2.

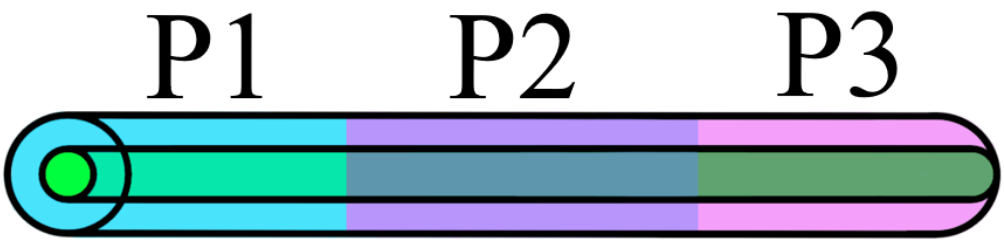

Figure 3.15: Longitudinal Control of Material

The selected flow controller is the OB1 MK3+ Microfluidic Flow Controller from Elveflow to facilitate the deposition of the fluids (for the prototype, an acellular 2% w/v medium viscosity sodium alginate solution, dyed for clarity) through the printing head. In this case, the fluids would be housed in syringes and then fed to the head for continuous layer-by-layer deposition of the solutions with a total filament diameter of ~0.6 mm to eventually create tissue scaffolds of about 20x20x20 mm in size. A photo of the flow controller is below, in Figure 3.16 (Elveflow 2021)

Figure 3.16: Elveflow OB1 MK3+ Microfluidic Flow Controller (Elveflow 2021)

The main features of the Elveflow controller are that it can accurately control up to four inlets independently from five pressure ranges, using an external pressure source, and a response time as low as 9 ms with customizable profiles in proprietary software (Elveflow 2021). Visit Appendix B for technical specifications of the Elveflow OB1 MK3+ Microfluidic Flow Controller. Here, the pressure-driven flow controller has a pressure range of 0 to 8000 mbar with

an accuracy of 0.5 mbar feeding three 50 mL high-pressure reservoirs of biomaterial to the printhead assembly for layer-by-layer deposition with the help of an x-y-z controller.

Selecting an x-y-z controller, on the other hand, was simple. In a previous section, The Original Prusa i3 MK3S 3D printer was selected to make the carriage using a 1.75 mm spool of PETG (Prusa Research a.s. 2021a). It follows, then, that the Prusa Printer can also be used as the x-y-z controller for the multi-material bioprinting system. After the carriage is made, the x-carriage and the FDM extruder system of the Prusa printer can be removed and replaced with the printhead assembly and carriage for bioprinting, shown in Figure 3.17.

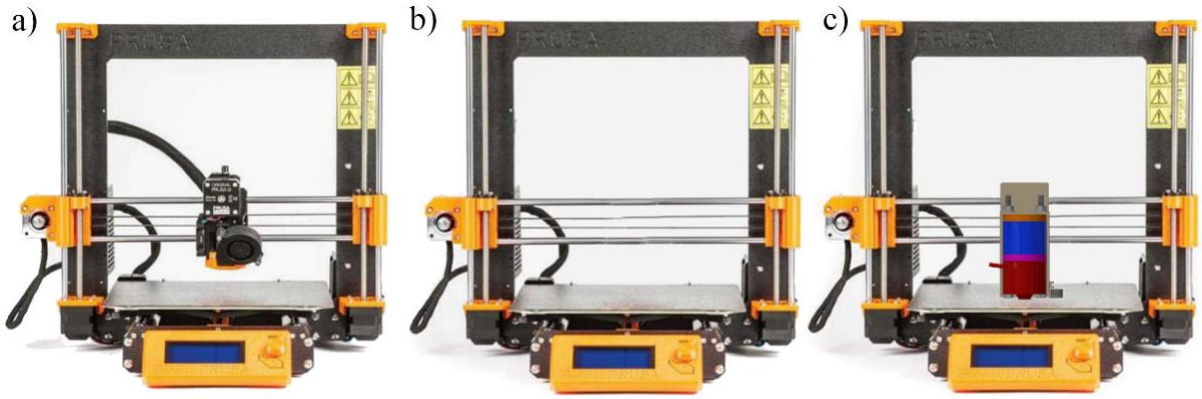

Figure 3.17: Prusa i3 MK3S 3D Printer for x-y-z Controller a) Stock Printer b) FDM Printhead Assembly Removed c) Modular Bioprinting Assembly Attached (Prusa Research a.s. 2021a)

The Original Prusa i3 MK3S 3D printer uses many 1.8-degree NEMA 17 stepper motors to control the x-y-z movement of the extruded material. Two motors for the z-direction, one for the y-direction, and one for the x-directions; the motors have a maximum travel speed of 200+ mm/s (Prusa Research a.s. 2021a). In the x-direction, the carriage is fixed to LM8UU bearings on 8 mm smooth rods, and a 2GT timing belt, also connected to the carriage, drives it. The same LM8UU bearings are fixed to the stage, and a 2GT timing belt connected to a motor under the stage drives it in the y-direction. For the z-direction, a pair of threaded rods on trapezoidal nuts drive the x-axis assembly with vertically oriented LM8UU bearings along matching smooth rods. G-code controls the x-y-z movement of the Prusa printer loaded via an SD Card to its EINSY RAMbo motherboard or via Universal Serial Bus (USB) connection to a personal computer running the PrusaSlicer program (Prusa Research a.s. 2021a). For bioprinting, the Prusa printer

will be loaded with instructions solely for x-y-z movement, similar to a previous study (Bessler et al. 2019). Combing the Prusa Printer and the Elveflow Controller with the printhead assembly and carriage completes the detail design of the multi-material bioprinting system.

3.6 Conclusions

The novel design of the multi-material bioprinting system is to provide a solution for "on-the-fly" adjustment of material concentrations between its inlets (longitudinal control) and circumferential control of the material organization within the filament through changing head configurations. This system addresses the significant issue of conventional bioprinting techniques. They cannot deposit multiple materials simultaneously, missing out on replicating the sophisticated anisotropic and heterogeneous features of native tissue and the organization of native biomaterials and cell types. Altogether, the bioprinting system consists of a Prusa i3 MK3S 3D Printer for x-y-z control, an Elveflow OB1 MK3+ Microfluidic Flow Controller for pressure-driven control of the inlets, an aluminum bioprinting head for facilitating mixing and deposition, and a carriage made of PETG for fixing the head assembly to the x-y-z controller.

This completed bioprinting head prototype design consists of four parts, made from anodized aluminum: a plug, a single-inlet head, a mixing core, and a dual-inlet head. The components may be assembled in different configurations for future modularity and adjustment, although this thesis focuses on a "gradient core" configuration. A significant consideration in the "gradient core" configuration is on mixing materials in the dual-inlet head. Design features in the helical rib of the mixing core were added and adjusted to improve mixing. A future version of the bioprinting head components may be made from biocompatible and sterilizable materials such as MED-WHT 10 or HP PA12 Nylon from rapid prototyping methods. The carriage will be made from 1.75 mm PETG using a Prusa i3 MK3S 3D printer, later adapted as the x-y-z controller for the bioprinting system. A flow controller with control of up to four independent channels will be used to deliver material through the head. The controller will provide alternating pulsatile flow for the material feeding to the dual-inlet head to improve mixing when needed and deliver a constant pressure to the material in the single-inlet head.

This chapter outlines the design processes of the multi-material bioprinting system through the lens of advanced engineering design methodology, axiomatic design and the FCBPSS framework in a systematic approach. The motivation for such design work is to understand further the

methodology of engineering design and how to apply the four general stages to the research objectives of the thesis. Those four design stages are the technical specification where the functional, constraint, and performance requirements are defined. Two, the conceptual design stage identifies the general logic behind the solution and assigns design parameters to the functional requirements (maintaining independence between functional requirements and design parameters). Three, embodiment adds volume and material to the system. Finally, four, the detail design completes the process with surface details like fillets and chamfers and adjusted geometry for ease of manufacturing. The outlining of the design process proved to be a valuable exercise in the importance of the distinct stages of engineering design and applying traditional engineering design methodology to bioprinting. Advanced engineering design methodologies are not widely used in bioprinting and tissue engineering applications, and this chapter offers a fresh look at bioprinters through that lens.

4.0 CONCEPTUAL EVALUATION AND COMPARISON OF BIOPRINTING SYSTEMS

This chapter presents the application of Axiomatic Evaluation to multi-material bioprinting systems to help refine the proposed modular design and give insight into selecting the best system based on the desired material control. Here, the evaluation and comparison offer a meaningful method that does not exist in the bioprinting space, which then highlights the strengths and weaknesses of existing systems versus the proposed modular system.

4.1 Proposed Method

The proposed method is a multi-material bioprinting system with a modular printhead coordinated with a four-channel regulated pressure source to precisely deposit multiple materials simultaneously or sequentially, with a controllable organization in circumferential or longitudinal directions adjustable material composition. Depending on the configuration of the head parts, the filament organization can change. For visualization of circumferential and longitude-controlled fibres with the modular bioprinting head's configurations, see Figure 4.1.

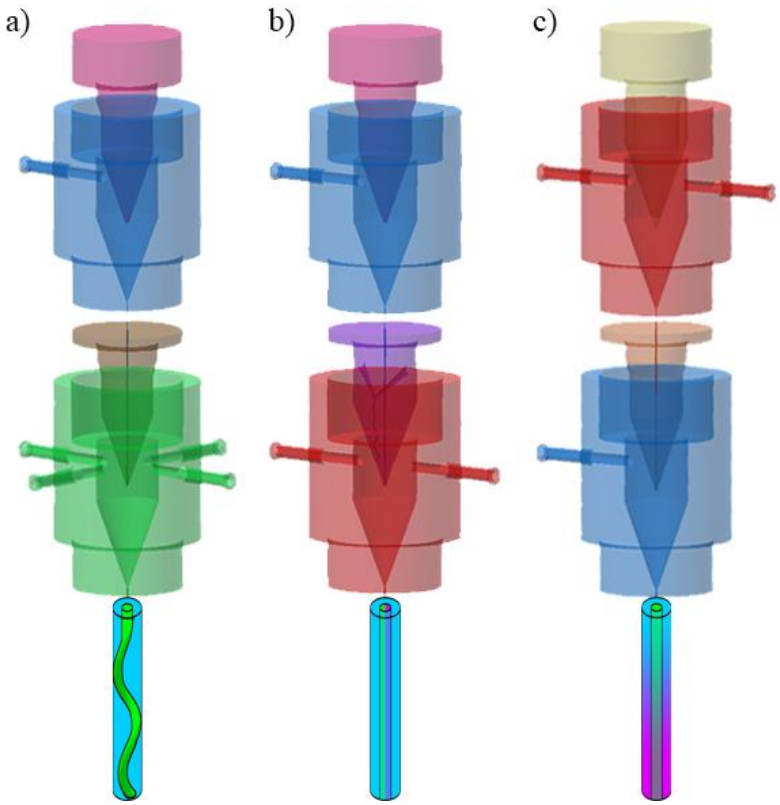

Figure 4.1: Conceptual Design of a Modular Bioprinting Head a) Spiral-Core b) Split-Core c) Gradient-Shell

The first configuration is shown in Figure 4.1a – a spiral organization of the core with a supportive shell. Second, Figure 4.1b shows a split vasculature with two core materials. Last in Figure 4.1c is similar in appearance to Figure 4.1a, but with a material gradient of the shell longitudinally. This system takes the benefits of the existing design groups and reduces the limitations. The ability to control the internal material of a multi-material fibre in combination with an on-the-fly material switching can allow for the realization of innovative scaffold designs, limited only by the user's creativity.

Given the design for an original multi-material bioprinting system, there exists a need for an evaluation and comparison method with existing multi-material bioprinting systems. Comparing a proposed design against existing designs under a common goal can help designers in their efforts to produce the best system, and two, users select the best system for their application. The principles of Axiomatic Design provide an evaluation method for functional independence between a set of functional requirements and design parameters in a system, and a comparison of the probabilities for a group of systems completing specific functional requirements, resulting in the single-best system (X. B. Chen, Kai, and Hashemi 2007). This chapter aims to build a similar evaluation and comparison model for existing multi-material bioprinting systems against the proposed modular bioprinting system through the lens of Axiomatic Design.

4.2 Axiomatic Design

Axiomatic Design is a systematic approach to design developed to make the field "academic" by building mathematical relationships between functional requirements and design parameters (design parameters) of a given system (Suh 1995). Here, N. P. Suh introduced two "axioms" or general principles that govern the design process in the equation,

$$\{FR\} = [A]\{DP\} \quad \text{.....(4.1)}$$

where [A] is the design matrix given by elements *Aij,* representing the change in functional requirements by the change in design parameters of the system

$$A_{ij} = \frac{\partial FR}{\partial DP} \quad \text{.....(4.2)}$$

The first axiom is the Independence Axiom, which categorizes the independence of the functions from the design parameters. A system satisfies the Independence Axiom when its design matrix is

either diagonal or triangular (Suh 1995). Systems with diagonal design matrices are considered *uncoupled* designs. In an uncoupled design, each of the functional requirements can be independently satisfied through a single design parameter.

$$[A] = \begin{bmatrix} A_{11} & 0 & 0 \\ 0 & A_{22} & 0 \\ 0 & 0 & A_{33} \end{bmatrix} \text{.....(4.3)}$$

If a system has a triangular design matrix, then it is considered a *decoupled* design. A decoupled design may satisfy each functional requirement independently only if the design parameters are applied in a particular order. If the design parameters are applied in any other order, the system fails to satisfy the Independence Axiom, and the design is *coupled*.

$$[A] = \begin{bmatrix} A_{11} & 0 & 0 \\ A_{21} & A_{22} & 0 \\ A_{31} & A_{32} & A_{33} \end{bmatrix} \text{.....(4.4)}$$

A system with any other design matrix is also considered a *coupled* design and does not satisfy the Independence Axiom. If a system has fewer design parameters than the number of functional requirements, it will always be a coupled design and can not satisfy Axiom 1; there must be at least the same number of design parameters as functional requirements for a system to satisfy Axiom 1. However, Axiom 1 is either pass or fail; there is not a single-best design. With the same set of functional requirements, to meaningfully evaluate a group of designs, there may be a vast number and variety, of designs that can satisfy the Independence Axiom. When the goal is to determine the single-best design from a group, Axiom 1 is not enough, and we must move to Axiom 2.

Axiom 1 is the "qualitative" axiom; then Axiom 2 is the "quantitative" axiom. Axiom 2 serves to determine, among the designs that satisfy Axiom 1, the superior design via the minimum *information content*; the probability of a given design satisfying its functional requirements with the simplest solution. The information content of a design for a given functional requirement is defined by

$$I_i = log_2 \frac{1}{P_i} = -log_2 P_i \text{.....(4.5)}$$

where P_i is the probability of success for functional requirement *i*, with *I* having the unit of "bits: (Suh 1995). Practically, the probability of success is the overlap between the *design range* of a functional requirement specified by the designer and the *system range*; this overlap is called the *common range*. A visual representation of the design range, system range, and common range for a functional requirement is shown in Figure 4.2 (Suh 2001).

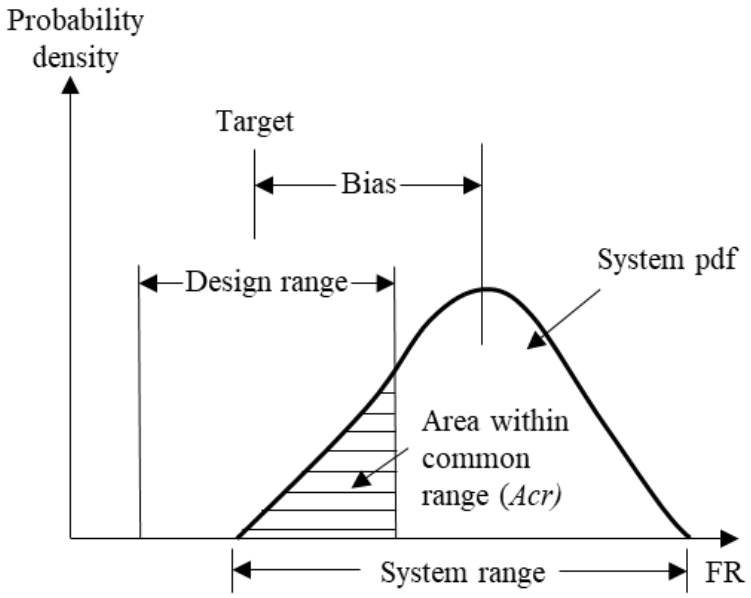

Figure 4.2: Defining Design Range, System Range, and Common Range for a Functional Requirement (Suh 2001)

Using this definition of common range, the expression for information content is

$$I_i = log_2 \frac{1}{A_{CRi}} = -log_2 A_{CRi} \quad \text{.....(4.6)}$$

where A_{CR} is the area within the common range for *FRi* being satisfied by *DPi.* Thus, a system with *n* functional requirements may have its information content expressed as

$$I = \sum_{i=1}^{n} \left[log_2 \frac{1}{A_{CRi}} \right] = \sum_{i=1}^{n} [-log_2 A_{CRi}] \quad \text{.....(4.7)}$$

Finally, the system with the lowest information content is deemed the best design. When the information content is 'zero,' all probabilities of success must be 'one,' and the design must be simple. Conversely, when the probability of success of one or more functional requirements is 'zero,' then the information content is 'infinite,' and the design must be complex (Suh 1995). To calculate the information content between a group of designs, one must have either experimental

data from the systems or a great deal of knowledge of their operation. Between the determination of functional independence using Axiom 1 and the information content using Axiom 2, the evaluation and comparison of the multi-material bioprinting systems will use existing data (Cornock et al. 2014; Gao et al. 2015; Jia et al. 2016; Dai et al. 2017; Mistry et al. 2017; W. Liu et al. 2018; Schuurman et al. 2011; Shim et al. 2012; H. Chen and Ozbolat 2013; Duan et al. 2013; Y. S. E. Tan and Yeong 2014; Zhao et al. 2014; Z. Izadifar et al. 2016; J. Lee et al. 2017; W. Liu et al. 2017; Kang et al. 2018; Rocca et al. 2018). The table of values used in the following sections is in Appendix C. Through the lens of Axiomatic Design, the proposed design of a multi-material bioprinting system will be compared and evaluated with existing designs to meaningfully show the single-best design for a given set of functional requirements.

4.3 Axiomatic Evaluation of Multi-material Bioprinting Systems

The first step of any evaluation under the lens of Axiomatic Design is to impose common functional requirements that meaningfully evaluate the multi-material bioprinting systems for their application (Suh 1995). Depending on the application, the evaluation may change, and the single-best design may be different. Since the improvement of the design of the proposed modular bioprinting system is the aim of this study, the application for evaluation and comparison is related to its main features; reconfigurability and control of materials during deposition. The chosen application for this study is circumferential and longitudinal control of deposited material and how easily a system can be reconfigured to control the material. The functional requirements follow:

Functional Requirement 1: Dispense multi-material bioink with control of the material composition in the circumferential direction, shown in Figure 4.3.

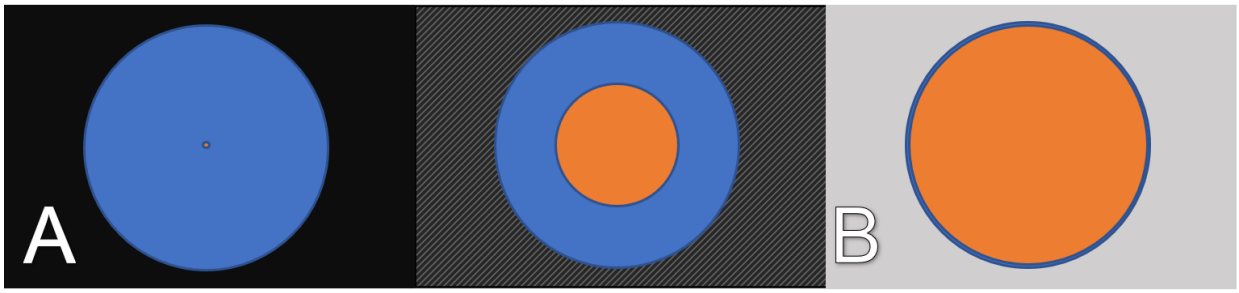

Figure 4.3: Visual Representation of Functional Requirement 1

Functional Requirement 2: Dispense multi-material bioink with control of the material composition in the longitudinal direction, shown in Figure 4.4.

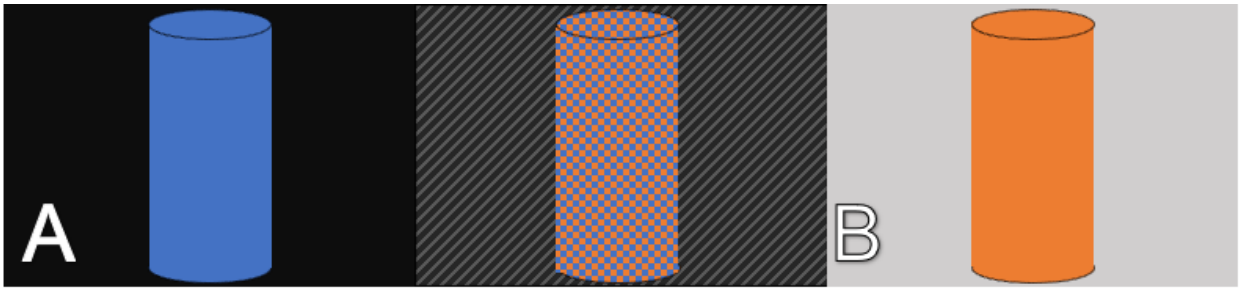

Figure 4.4: Visual Representation of Functional Requirement 2

Functional Requirement 3: The system is easily reconfigurable to dispense multi-material fibres in a different longitudinal and circumferential organization, shown in Figure 4.5.

Figure 4.5: Visual Representation of Functional Requirement 3

The purpose of these three functional requirements is to quantify specific aspects of multi-material bioprinting that have not previously been investigated. In the physical domain, no such system can fully achieve the three functional requirements to the highest level; however, understanding the strengths and weaknesses of the bioprinting systems for these functional requirements will improve the design of the proposed system. For the comparison and evaluation, the bioprinting systems are grouped by 1. Side-by-side 2. Core-and-shell 3. Advanced (Rapid Continuous) 4. Advanced (Pre-set Extrusion) 5. Advanced (Embedded) and 6. Modular (Proposed).

4.3.1 Independence Axiom

Next is to assign design parameters for the systems groups that achieve the functional requirements, build the design matrices, and then categorize the designs per the Independence

Axiom. To generalize, the design parameters for the multi-material bioprinting systems chosen to achieve the three functional requirements are:

Design Parameter 1: Hardware

Design Parameter 2: Software

Design Parameter 3: Process control

Design Parameter 4: Hardware and software.

These design parameters apply to the six groups of bioprinting systems and may achieve the functional requirements with some combination of the four design parameters. The Independence Axiom states that a system may only be functionally independent if its design matrix is diagonal or triangular (Suh 1995). Systems with any other design matrices fail to satisfy the Independence Axiom. Using the data from Appendix C and the previously stated functional requirements and design parameters, the design matrices are built as (Cornock et al. 2014; Gao et al. 2015; Jia et al. 2016; Dai et al. 2017; Mistry et al. 2017; W. Liu et al. 2018; Schuurman et al. 2011; Shim et al. 2012; H. Chen and Ozbolat 2013; Duan et al. 2013; Y. S. E. Tan and Yeong 2014; Zhao et al. 2014; Z. Izadifar et al. 2016; J. Lee et al. 2017; W. Liu et al. 2017; Kang et al. 2018; Rocca et al. 2018):

Table 4.1: Design Matrices of Multi-material Bioprinting Systems

System	Design Matrix
Side-by-side	$\begin{Bmatrix} FR_1 \\ FR_2 \\ FR_3 \end{Bmatrix} = \begin{bmatrix} 0 & 0 & 0 \\ 0 & 0 & 0 \\ 0 & 0 & A_{33} \end{bmatrix} \begin{Bmatrix} N/A \\ N/A \\ DP_4 \end{Bmatrix}$
Core-and-shell	$\begin{Bmatrix} FR_1 \\ FR_2 \\ FR_3 \end{Bmatrix} = \begin{bmatrix} A_{11} & 0 & 0 \\ 0 & 0 & 0 \\ 0 & 0 & A_{33} \end{bmatrix} \begin{Bmatrix} DP_1 \\ N/A \\ DP_3 \end{Bmatrix}$
Advanced (Embedded)	$\begin{Bmatrix} FR_1 \\ FR_2 \\ FR_3 \end{Bmatrix} = \begin{bmatrix} 0 & 0 & 0 \\ 0 & A_{22} & 0 \\ 0 & A_{32} & A_{33} \end{bmatrix} \begin{Bmatrix} N/A \\ DP_1 \\ DP_1 \end{Bmatrix}$

Advanced (Rapid Continuous)	$\begin{Bmatrix} FR_1 \\ FR_2 \\ FR_3 \end{Bmatrix} = \begin{bmatrix} 0 & 0 & 0 \\ 0 & A_{22} & 0 \\ 0 & A_{32} & A_{33} \end{bmatrix} \begin{Bmatrix} N/A \\ DP_3 \\ DP_1 \end{Bmatrix}$
Advanced (Pre-set Extrusion)	$\begin{Bmatrix} FR_1 \\ FR_2 \\ FR_3 \end{Bmatrix} = \begin{bmatrix} A_{11} & 0 & 0 \\ 0 & 0 & 0 \\ 0 & 0 & A_{33} \end{bmatrix} \begin{Bmatrix} DP_1 \\ N/A \\ DP_3 \end{Bmatrix}$
Advanced (Proposed)	$\begin{Bmatrix} FR_1 \\ FR_2 \\ FR_3 \end{Bmatrix} = \begin{bmatrix} A_{11} & 0 & 0 \\ A_{21} & A_{22} & 0 \\ A_{31} & A_{32} & A_{33} \end{bmatrix} \begin{Bmatrix} DP_1 \\ DP_2 \\ DP_3 \end{Bmatrix}$

Here, most of the bioprinting systems fail to satisfy Axiom 1. The side-by-side, embedded, and rapid continuous systems fail to achieve the first functional requirement. Meanwhile, the side-by-side, core-and-shell, and pre-set extrusion systems fail to satisfy the second functional requirement. The modular bioprinting system has a triangular design matrix, meaning that the design parameters must be applied in a specific order to satisfy functional independence. Although the modular system is the only one that passes Axiom 1, it is still worth comparing the systems using Axiom 2. Axiom 2, the information axiom, shows the single-best design by calculating the probability of achieving specified functional requirements to the desired level, the design range. The probability of success, or the information content of a given functional requirement, will provide designs, and users, a systematic ranking of the systems' performance either as a whole or by functional requirements.

4.3.2 Information Axiom

The first step in comparing a group of systems with the Information Axiom is defining the functional requirements' design range. From the previous section, the three functional requirements are: one, dispense multi-material bioink with control of the material composition in the circumferential direction; two, dispense multi-material bioink with control of the material composition in the longitudinal direction; three, easily reconfigurable to dispense multi-material fibres in a different longitudinal and circumferential organization. The design ranges are specified to compare the group of systems meaningfully, and the system range is the outputs to satisfy the functional requirements; Table 4.2 shows the design ranges.

Table 4.2: Design Range of the Functional Requirements

Functional Requirement	Design Range
FR1: Dispense multi-material bioink with control of the material composition in the circumferential direction	0% to 100% The theoretical limit for a group of bioprinting systems is 100%, but the physical limitations of an infinitely small inner nozzle, an infinitely thin wall, or an infinitely high pressure
FR2: Dispense multi-material bioink with control of the material composition in the longitudinal direction	0% to 100%
FR3: The system is easily reconfigurable to dispense multi-material fibres in a different longitudinal and circumferential organization	(Score from 1 to 4 with a score of 4 meaning no reconfiguration is needed to adjust the fibre control, and a score of 0 is a system that needs to reconfigure hardware and software to adjust the fibre control) (no reconfiguration needed = 4, reconfigure the software = 3, reconfigure the hardware = 2, reconfigure the hardware and the software = 1)

Next, the system ranges for each of the multi-material bioprinting systems of the functional requirements must be determined. Building the system ranges of the bioprinting systems was done using the experimental data in Appendix C; the system ranges are shown in Table 4.3.

Table 4.3: System Range of the Multi-material Bioprinting Systems

System	FR1: Circumferential Control of Materials [%]	FR2: Longitudinal Control of Materials (%)	FR3: System is Reconfigurable (1-4)
Side-by-side	0 range. Current side-by-side systems can not control the	0 range. Current side-by-side systems can not	1. A hardware and software change is needed to make it able to

	materials in the circumferential direction	control the materials in the longitudinal direction	control materials in longitudinal and circumferential directions
Core-and-shell	18.2 to 80.8; 62.6 range. The smallest difference between the pair of nozzles was 50 µm (80.8% of the larger nozzle), and the largest difference between nozzles was 1260 µm (18.2% of the larger nozzle)	0 range. Current core-and-shell bioprinting systems can not control the materials in the longitudinal direction	2. A hardware change is needed to change the organization of the extruded materials in the longitudinal and circumferential direction
Advanced (Rapid Continuous)	0 range. This system can not control the materials in the circumferential direction	100 range. This system can go from 100% material A and 0% material B to 100% material B and 0% material A	2. A hardware change is needed to make the system reconfigurable for circumferential control of extruded materials)
Advanced (Embedded)	0 range. This system can not control the materials in the circumferential direction	100 range. This system can go from 100% material A and 0% material B to 100% material B and 0% material A	1. A hardware and software change is needed to make the system configurable for longitudinal and circumferential control of the extruded materials
Advanced (Pre-set Extrusion)	18.5 to 71.2; 52.7 range. This range was determined by the relative sizes of cartridges	0 range. This system can not control the materials in the	1 (hardware and software changes are needed to make the system configurable for

	from figures in the published paper	longitudinal direction	longitudinal and circumferential control of the extruded materials)
Modular (Proposed)	25 to 66.6; 41.6 range. The smallest inner diameter for the shell-gradient configuration is 400 µm and an upper limit of 1600 µm. The lower limit of the outer diameter is 600 µm, again	100 range. This system can go from 100% material A and 0% material B to 100% material B and 0% material A	3. A software change is needed to change the organization of the extruded materials in circumferential and longitudinal directions

The system range for functional requirement two and functional requirement three is self-explanatory, but the calculations for functional requirement one are not as straightforward. Comparing the smallest and largest difference between sizes of nozzles between the groups, the configuration with the thinnest ‘wall’ and the thickest wall was determined. These geometries were found from data in the literature, found in Appendix C, or by taking measurements from published figures. The percentage of the inner nozzles to the outer nozzles are the upper and lower limits of the system range. Figures 4.6, 4.7, and 4.8 are visual representations of the system range for the core-and-shell, pre-set extrusion, and modular systems, respectively.

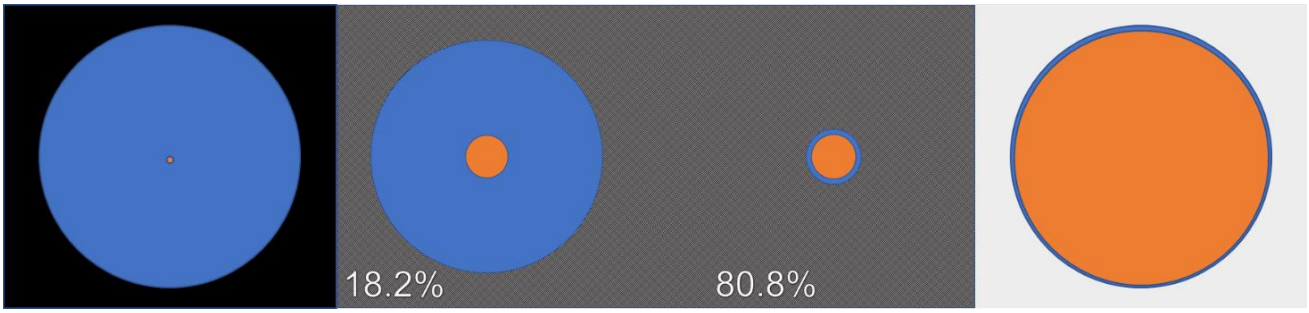

Figure 4.6: System Range of Functional Requirement One for Core-and-shell Systems

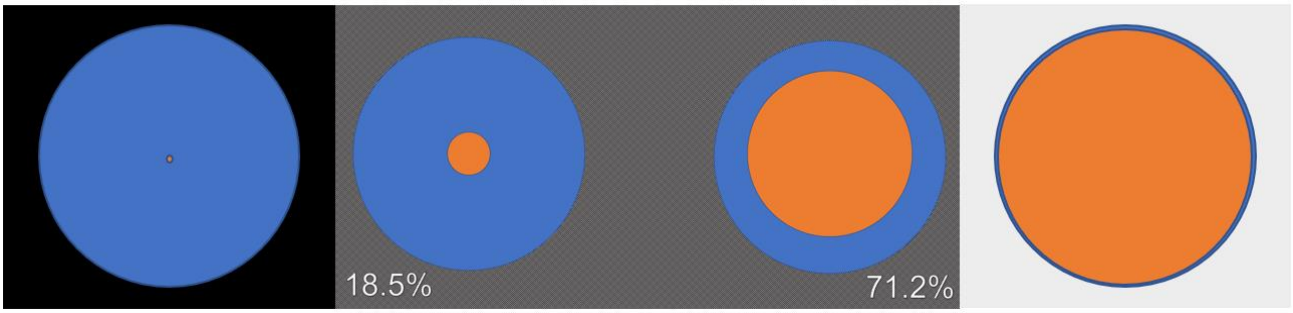

Figure 4.7: System Range of Functional Requirement One for the Pre-set Extrusion System

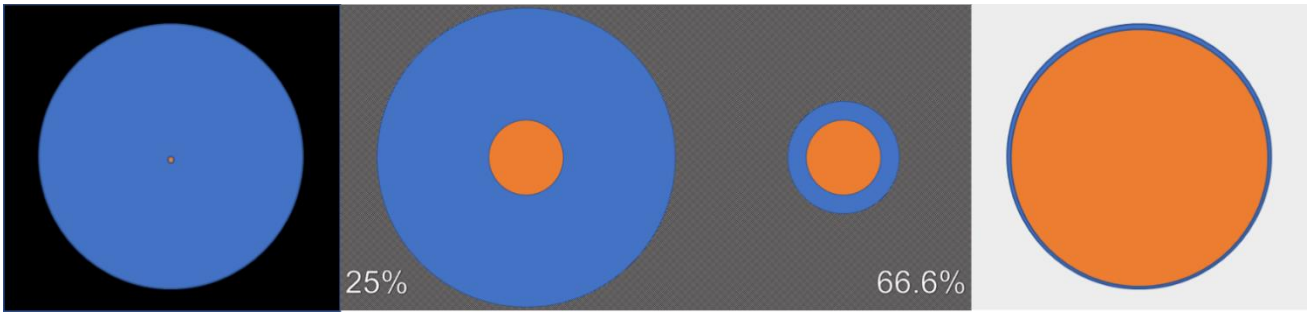

Figure 4.8: System Range of Functional Requirement One for the Modular System

The common range for the three functional requirements is determined using the overlap of the specified design range and the system range from the literature. Quantifying these ranges is imperative for evaluating and comparing Axiom 2; Table 4.4 shows the common range for the multi-material bioprinting systems.

Table 4.4: Common Range of the Multi-material Bioprinting Systems

System	FR1: Circumferential Control of Materials [%]	FR2: Longitudinal Control of Materials [%]	FR3: System is Reconfigurable [x/4]
Side-by-side	0	0	1
Coaxial	62.6	0	0.5
Rapid Continuous	0	100	0.5
Embedded	0	100	0.25
Pre-set Extrusion	52.7	0	0.25
Modular	41.6	100	0.75

Applying Equation 4.6 and Equation 4.7 to the values in Table 4.4 yields the information content for the six systems from the three functional requirements and the system. Table 4.5 shows the results of the information content.

Table 4.5: Information Content of the Multi-material Bioprinting Systems

System	I_1	I_2	I_3	ΣI
Side-by-side	Infinite	Infinite	2.00	Infinite
Core-and-shell	0.68	Infinite	1.00	Infinite
Rapid Continuous	Infinite	0.00	1.00	Infinite
Embedded	Infinite	0.00	2.00	Infinite
Pre-set Extrusion	0.92	Infinite	2.00	Infinite
Modular	1.27	0.00	0.42	1.68

Here, the core-and-shell systems are favourable for achieving functional requirement one. Then the rapid continuous, embedded, and modular systems are equally favourable for achieving functional requirement two. Last, the modular design is the most favourable for functional requirement three. The modular design is the only group of systems that can satisfy all functional requirements; thus, it has the lowest total information content. Though the existing systems fail Axiom 2, some aspects can help improve the proposed modular design. For example, we can look at core-and-shell systems to improve the circumferential control, and we can look at the other systems for aspects to avoid. From Axiom 1 and Axiom 2, the modular system is the single-best design to achieve the specified functional requirements.

4.4 Conclusions

The present state of multi-material bioprinting is limited in that most systems are slow, have low resolution, or have no longitudinal and circumferential control of the printed filament. A proposed modular design aims to cover these pitfalls. Specifically, the proposed design expects to be easily configurable within three arrangements to deposit bioink in controllable organizations. However, there are no systematic methods for evaluating and comparing designs in bioprinting while in the conceptual stage. Through Axiomatic Design principles, this work helps refine the current design and determine which of the present multi-material bioprinting systems is the single-best and top performer for a specified set of functional requirements. Expressly, the functional requirements were set to evaluate the existing systems based on the key

features of the modular system. Either great knowledge of the systems or experimental data is needed to evaluate systems using Axiom Design principles; here, data from literature was used.

Axiom 1, the Independence Axiom, is more qualitative as it does not show the single-best design but categorizes a design's functional independence as either coupled, decoupled, or uncoupled. Here, the proposed design is decoupled in that its design parameters must be applied in a specific order to satisfy Axiom 1; all other designs fail to satisfy Axiom 1. Axiom 2 is more quantitative as it shows the probability of a given design satisfying all its functional requirements at a specified range, resulting in the single-best design. Coaxial bioprinting systems ranked highest for circumferential control of deposited material. Rapid continuous, embedded, and modular bioprinting systems were the best for longitudinal control of deposited material. The modular system is the best for easy reconfiguration. Overall, the modular system had the lowest information content and, thus, is the single-best design per Axiom 2.

Although the proposed modular system was ranked as the single-best design, this work has many limitations. First, the chosen functional requirements heavily favour the modular design. Next, the modular system is missing a physical representation, and the system ranges in the information content calculation were taken from the conceptual design. Last, a small number of papers were included (eight for side-by-side, six for core-and-shell, and three for the advanced) for the comparison, and the data was inconsistent across the papers. The inconsistency is that not all the studies used the same materials, nozzle sizes/shapes, deposition temperatures, or flow rate for developing system ranges. A complete Axiomatic Evaluation would include experimental data from studies with common parameters and data from a physical representation for the modular system.

The framework for this Axiomatic Evaluation can be used for other types of multi-material bioprinting systems. Such a comparison and evaluation method does not exist in this space, and this work contributes a new approach to view bioprinting systems. Of specific note is quantifying circumferential and longitudinal control on a scale from 0% to 100% instead of passing or failing. Future studies could include expanding the Axiomatic Evaluation to other applications, repeating the Axiomatic Evaluation with the physical modular system, or expanding the Axiomatic Evaluation to single-material bioprinting systems.

5.0 CONCLUSIONS

Extrusion-based bioprinting is an emerging and promising technology for addressing a massive healthcare issue; organ and tissue need continuing to surpass donor rates. While single-material bioprinting systems allow for creating analogue for simple tissue and organs, multiple materials are needed to embody native features. Notably, existing multi-material bioprinting systems lack control over depositing material in both the circumferential and longitudinal directions. The thesis garners a thorough recounting of the research, design, and evaluation of a multi-material bioprinting system through the previous four chapters. This chapter summarizes the work presented in this thesis, along with the main conclusions of Chapters 2, 3, and 4.

5.1 Summary of Presented Work and Conclusions

The first research objective of designing a multi-material extrusion-based printing system with longitudinal and circumferential filament control yields a custom modular printhead and carriage design to be used with a flow controller and tabletop 3D printer, shown below.

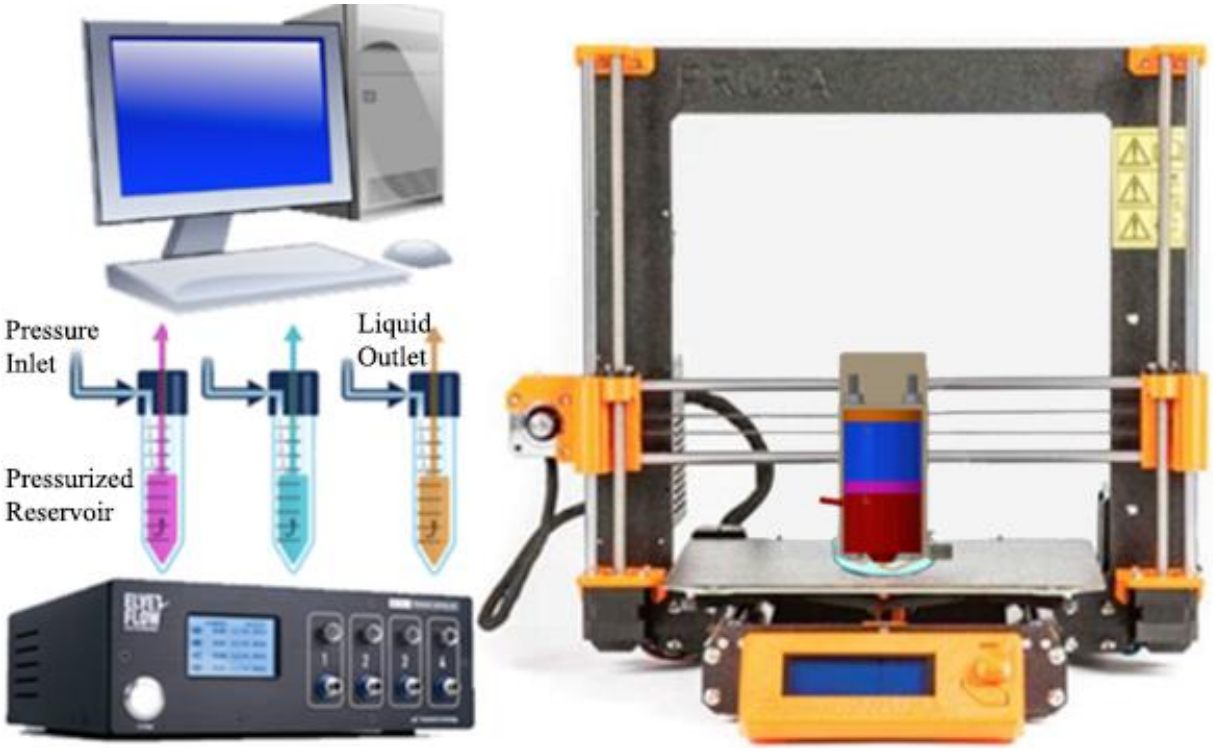

Figure 5.1: Multi-material Bioprinting System (Elveflow 2021; Prusa Research a.s. 2021a)

Chapter 2 briefly presents current fabrication methods in the development of multi-material tissue scaffolds. The idea of multi-material bioprinting and its applications in tissue engineering is recent and promising. As such, this review is beneficial to the bioprinting community. A prominent contribution of the review is categorizing multi-material bioprinting systems and highlighting their distinct benefits and limitations. First, side-by-side is shown as the most straightforward method with the highest resolution but the longest time fabricating scaffolds. Next, core-and-shell bioprinting is favourable for introducing vasculature to scaffolds, but the fibres are not as strong as robust fibres. The coaxial fibres have low resolution and resemble native tissues; there is no spatial control of the core within the shell. Advanced bioprinting methods such as rapid continuous, embedded, and pre-set extrusion allow for on-the-fly adjustment of materials during deposition to place the material in a specific spot and concentration directly. This review identified gaps in current research within multi-material bioprinting systems and gathered data for future analyses. An overarching limitation of existing multi-material bioprinting systems is the lack of control in deposited material along longitudinal and circumferential directions; this is a primary research gap on which the first research objective is built.

Chapter 3 starts with the definition of this design problem with the function, context, behaviour, principle, state, and structure framework within the engineering design domain. The design process has four stages: technical specification in which the problem is broken down, the conceptual design where the general logic of the solution is identified, the embodiment to add volume and material to the system, and the detail design where surface details, manufacturing, and procurement was considered. A systematic design process is used to clearly achieve the research objective of a system with spatial control. Also, the advanced engineering design methodologies add merit and justification to the design process by having deep documentation and directly focusing on solving the problem. Here, the printhead assembly with a carriage, flow controller, and the x-y-z controller is presented. The custom printhead assembly consists of four pieces: a plug, a single-inlet head, a mixing core, and a dual-inlet head. Together this printhead aims to facilitate the movement of three inlet materials to create a filament with a gradient-shell organization; an unmixed core with a shell that can have its ratio of material A and material B adjusted during deposition. Further, considerations for mixing are taken, such as making the inlets dual-inlet head parallel to the helical rib in the mixing core, terminating the helical rib of

the core at the end of the shaft, and removing dead volume at inlet junctions of the core. An Elveflow OB1 MK3+ pressure-driver controller governs the flow through the printhead because of its precise and independent control of up to four pressure channels. Independent control of the inlet channels allows for an alternating sinusoidal pulsatile flow of the inlets to encourage mixing. Future configurations of the printhead may allow for spiral-core or split-core filament organizations for more options in spatial control. The carriage is then designed to affix the printhead assembly to an x-y-z controller for eventual layer-by-layer construction of scaffolds. A Prusa i3 MK3S 3D printer is the selected x-y-z controller and is the tool for creating the carriage, using 1.75 mm PETG for its printability and strength. The prototype for the printhead assembly will be made of anodized aluminum as it is easily accessible for the USask Biofabrication group and can be used for acellular testing of the material control. Biological studies may use a biocompatible and sterilizable material for the printhead assembly, namely MED-WHT 10 or HP Nylon 12. A bioprinting system such as this opens researchers to create multi-material tissue scaffolds that better match native tissue as spatial control of extruded material is not limited.

Meanwhile, the second research objective was evaluating and comparing the proposed design against existing multi-material bioprinting systems. Using Axiomatic Design principles shows that the proposed design is favourable for material control and configurability. Chapter 4 presents a systematic method for evaluation and comparison based on principles of Axiomatic Design for a specified set of functional requirements: is the system easily configurable, and can the system control deposited material in the circumferential and longitudinal direction. In specifying the functional requirements, the spatial control had to be quantified – from 0% to 100% in the circumferential and longitudinal directions. Configurability was also quantified in that a higher score was given to the most easily reconfigurable designs. The Independence Axiom categorizes the proposed design as decoupled in that its design parameters must be applied in a specified order to pass; all other designs fail. Axiom 2, the information axiom, results in a single-best design. To appropriately apply Axiomatic Design principles to a group of designs, either physical experiments or deep knowledge of the designs are needed. Here, data and knowledge of the systems are from the literature in the review from Chapter 2. Core-and-shell bioprinting systems rank highest for circumferential control of deposited material. Rapid continuous, embedded, and modular bioprinting systems are the best for longitudinal control of deposited material. The modular system is the best for easy reconfiguration. Overall, the modular

system has the lowest information content and, thus, is the single-best design per Axiom 2. Although the evaluation and comparison method shows that the proposed method is the single-best, the contribution of this approach comes from quantifying spatial control and gaining a deeper understanding of existing multi-material bioprinting systems. Axiomatic Design has not been applied to bioprinting, and the analysis in Chapter 4 shows the value of such an application. Future designs of multi-material bioprinting systems may use a similar evaluation and comparison method under Axiomatic Design principles to meaningfully assess performance against existing systems. This work satisfies the second research objective and reaches the end of the tasks for the M.Sc. project.

5.2 Suggestions of Future Work

Although a prototype has not been created and physical testing has not been completed as planned due to the COVID-19 pandemic, this work would form the basis for a multi-material bioprinting system with circumferential and longitudinal material control. Thus, prototyping and testing are the focus in suggestions for future work. The prototype of the printhead assembly is to be made of aluminum and the carriage of PETG, using the drawings from Chapter 3 for part specifications. Testing the system should start with tuning the printing parameters such as applied pressure and nozzle speed for depositing continuous filaments in the gradient-shell configuration. Again, specifically to demonstrate the feasibility of this system to have spatial control of the material before biological testing, with fluorescence microscopy or other means. Other parameters that could be adjusted are the concentrations of the biomaterial, the crosslinking mode, or timings of the alternating pulsatile flow for mixing considerations. Further, biological testing should occur to examine the effects on cell damage through deposition of the bioink within the head. The last of the future work should be to expand the system to include printhead configurations to create the split-core and spiral-core filaments and any other organizations needed to represent features of native tissues and organs.

REFERENCES

Afzal, Arshad, and Kwang-Yong Kim. 2015. “Convergent–Divergent Micromixer Coupled with Pulsatile Flow.” *Sensors and Actuators B: Chemical* 211 (May): 198–205. https://doi.org/10.1016/j.snb.2015.01.062.

Alvarez C, Kenny L., Rodrigo F. Lagos C, and Miguel Aizpun. 2016. “Investigating the Influence of Infill Percentage on the Mechanical Properties of Fused Deposition Modelled ABS Parts.” *Ingeniería e Investigación* 36 (3): 110–16. https://doi.org/10.15446/ing.investig.v36n3.56610.

Annaidh, Aisling Ni, Karine Bruyere, Michel Destrade, Michael D. Gilchrist, and Melanie Ottenio. 2012. “Characterising the Anisotropic Mechanical Properties of Excised Human Skin.” *Journal of the Mechanical Behavior of Biomedical Materials* 5 (1): 139–48. https://doi.org/10.1016/j.jmbbm.2011.08.016.

Atala, Anthony. 2011. “Tissue Engineering of Human Bladder.” *British Medical Bulletin* 97 (1): 81–104. https://doi.org/10.1093/bmb/ldr003.

Atala, Anthony, and James J Yoo. 2015. *Essentials of 3D Biofabrication and Translation*. http://public.eblib.com/choice/publicfullrecord.aspx?p=2097726.

Autodesk. 2018. *Autodesk Inventor Professional*. San Rafael, CA: Autodesk.

Belloncle, Benjamine, Claude Bunel, Laurence Menu-Bouaouiche, Olivier Lesouhaitier, and Fabrice Burel. 2012. “Study of the Degradation of Poly(Ethyl Glyoxylate): Biodegradation, Toxicity and Ecotoxicity Assays.” *Journal of Polymers and the Environment* 20 (3): 726–31. https://doi.org/10.1007/s10924-012-0429-2.

Bessler, Nils, Dennis Ogiermann, Maj-Britt Buchholz, Alexander Santel, Jan Heidenreich, Rawas Ahmmed, Holm Zaehres, and Beate Brand-Saberi. 2019. “Nydus One Syringe Extruder (NOSE): A Prusa I3 3D Printer Conversion for Bioprinting Applications Utilizing the FRESH-Method.” *HardwareX* 6 (October): e00069. https://doi.org/10.1016/j.ohx.2019.e00069.

Canadian Blood Services. 2018. “Organ Donation and Transplantation in Canada - System Progress Report 2017 Update.” Canadian Blood Services. https://professionaleducation.blood.ca/sites/msi/files/system_progress_report_2017_update_final_en_8.pdf.

Chen, Howard, and Ibrahim T. Ozbolat. 2013. “A Multi-Material Bioprinting Platform towards Stratified Articular Cartilage Tissue Fabrication.” *IIE Annual Conference. Proceedings; Norcross*, 2246–52.

Chen, X. B., J. Kai, and M. Hashemi. 2007. “Evaluation of Fluid Dispensing Systems Using Axiomatic Design Principles.” *Journal of Mechanical Design* 129 (6): 640–48. https://doi.org/10.1115/1.2717233.

Chen, XB. 2018. *Extrusion Bioprinting of Scaffolds for Tissue Engineering*. Springer. https://bblearn.usask.ca/bbcswebdav/pid-2263799-dt-content-rid-11064680_2/courses/86714.201809/Chapter%201%20Introduction.pdf.

Choudhury, Deepak, Shivesh Anand, and May Win Naing. 2018. “The Arrival of Commercial Bioprinters - Towards 3D Bioprinting Revolution!” *International Journal of Bioprinting* 4 (2). https://doi.org/10.18063/ijb.v4i2.139.

Coburn, Jeannine, Matt Gibson, Pierre Alain Bandalini, Christopher Laird, Hai-Quan Mao, Lorenzo Moroni, Dror Seliktar, and Jennifer Elisseeff. 2011. “Biomimetics of the Extracellular Matrix: An Integrated Three-Dimensional Fiber-Hydrogel Composite for

Cartilage Tissue Engineering." *Smart Structures and Systems* 7 (3): 213–22. https://doi.org/10.12989/sss.2011.7.3.213.

Colosi, Cristina, Su Ryon Shin, Vijayan Manoharan, Solange Massa, Marco Costantini, Andrea Barbetta, Mehmet Remzi Dokmeci, Mariella Dentini, and Ali Khademhosseini. 2016. "Microfluidic Bioprinting of Heterogeneous 3D Tissue Constructs Using Low-Viscosity Bioink." *Advanced Materials* 28 (4): 677–84. https://doi.org/10.1002/adma.201503310.

Cornock, R, S Beirne, B Thompson, and G G Wallace. 2014. "Coaxial Additive Manufacture of Biomaterial Composite Scaffolds for Tissue Engineering." *Biofabrication* 6 (2): 025002. https://doi.org/10.1088/1758-5082/6/2/025002.

Costantini, Marco, Cristina Colosi, Wojciech Święszkowski, and Andrea Barbetta. 2018. "Co-Axial Wet-Spinning in 3D Bioprinting: State of the Art and Future Perspective of Microfluidic Integration." *Biofabrication* 11 (1): 012001. https://doi.org/10.1088/1758-5090/aae605.

Cui, Xiaofeng, Kurt Breitenkamp, M.G. Finn, Martin Lotz, and Darryl D. D'Lima. 2012. "Direct Human Cartilage Repair Using Three-Dimensional Bioprinting Technology." *Tissue Engineering Part A* 18 (11–12): 1304–12. https://doi.org/10.1089/ten.tea.2011.0543.

Dai, Xingliang, Libiao Liu, Jia Ouyang, Xinda Li, Xinzhi Zhang, Qing Lan, and Tao Xu. 2017. "Coaxial 3D Bioprinting of Self-Assembled Multicellular Heterogeneous Tumor Fibers." *Scientific Reports* 7 (1): 1457. https://doi.org/10.1038/s41598-017-01581-y.

Derakhshanfar, Soroosh, Rene Mbeleck, Kaige Xu, Xingying Zhang, Wen Zhong, and Malcolm Xing. 2018. "3D Bioprinting for Biomedical Devices and Tissue Engineering: A Review of Recent Trends and Advances." *Bioactive Materials* 3 (2): 144–56. https://doi.org/10.1016/j.bioactmat.2017.11.008.

Drury, Jeanie L., Robert G. Dennis, and David J. Mooney. 2004. "The Tensile Properties of Alginate Hydrogels." *Biomaterials* 25 (16): 3187–99. https://doi.org/10.1016/j.biomaterials.2003.10.002.

Drury, Jeanie L., and David J. Mooney. 2003. "Hydrogels for Tissue Engineering: Scaffold Design Variables and Applications." *Biomaterials* 24 (24): 4337–51. https://doi.org/10.1016/S0142-9612(03)00340-5.

Duan, Bin, Laura A. Hockaday, Kevin H. Kang, and Jonathan T. Butcher. 2013. "3D Bioprinting of Heterogeneous Aortic Valve Conduits with Alginate/Gelatin Hydrogels." *Journal of Biomedical Materials Research Part A* 101A (5): 1255–64. https://doi.org/10.1002/jbm.a.34420.

Elveflow. 2021. "OB1 - 4 Channel Microfluidic Flow Controller." *Elveflow* (blog). 2021. https://www.elveflow.com/microfluidic-products/microfluidics-flow-control-systems/ob1-pressure-controller/.

Espalin, David, Medina Francisco, Perez Mireya, Wicker Ryan, Hope Terry, and Winker Rob. 2015. "Sterilization of FDM-Manufactured Parts."

Freed, Lisa E., Gordana Vunjak-Novakovic, Robert J. Biron, Dana B. Eagles, Daniel C. Lesnoy, Sandra K. Barlow, and Robert Langer. 1994. "Biodegradable Polymer Scaffolds for Tissue Engineering." *Nature Biotechnology* 12 (7): 689–93. https://doi.org/10.1038/nbt0794-689.

Gan, Hiong Yap, Yee Cheong Lam, Nam Trung Nguyen, Kam Chiu Tam, and Chun Yang. 2006. "Efficient Mixing of Viscoelastic Fluids in a Microchannel at Low Reynolds Number." *Microfluidics and Nanofluidics* 3 (1): 101–8. https://doi.org/10.1007/s10404-006-0109-4.

Gao, Qing, Yong He, Jian-zhong Fu, An Liu, and Liang Ma. 2015. “Coaxial Nozzle-Assisted 3D Bioprinting with Built-in Microchannels for Nutrients Delivery.” *Biomaterials* 61 (August): 203–15. https://doi.org/10.1016/j.biomaterials.2015.05.031.

Ge, Zigang, Chao Li, Boon Chin Heng, Guoxin Cao, and Zheng Yang. 2012. “Functional Biomaterials for Cartilage Regeneration.” *Journal of Biomedical Materials Research Part A*, n/a-n/a. https://doi.org/10.1002/jbm.a.34147.

Hollenstein, Marc, Alessandro Nava, Davide Valtorta, Jess G. Snedeker, and Edoardo Mazza. 2006. “Mechanical Characterization of the Liver Capsule and Parenchyma.” In *Biomedical Simulation*, edited by Matthias Harders and Gábor Székely, 4072:150–58. Berlin, Heidelberg: Springer Berlin Heidelberg. https://doi.org/10.1007/11790273_17.

Hollister, Scott J. 2005. “Porous Scaffold Design for Tissue Engineering.” *Nature Materials* 4 (7): 518–24. https://doi.org/10.1038/nmat1421.

Hozumi, Takuro, Seiichi Ohta, and Taichi Ito. 2015. “Analysis of the Calcium Alginate Gelation Process Using a Kenics Static Mixer.” *Industrial & Engineering Chemistry Research* 54 (7): 2099–2107. https://doi.org/10.1021/ie5044693.

Iatridis, James C., Lori A. Setton, Robert J. Foster, Bernard A. Rawlins, Mark Weidenbaum, and Van C. Mow. 1998. “Degeneration Affects the Anisotropic and Nonlinear Behaviors of Human Anulus Fibrosus in Compression.” *Journal of Biomechanics* 31 (6): 535–44. https://doi.org/10.1016/S0021-9290(98)00046-3.

International Organization for Standardization [ISO]. 2009. “ISO 10993-5:2009(En), Biological Evaluation of Medical Devices — Part 5: Tests for in Vitro Cytotoxicity.” 2009. https://www.iso.org/obp/ui#iso:std:iso:10993:-5:ed-3:v1:en.

———. 2010. “ISO 286-1:2010(En), Geometrical Product Specifications (GPS) — ISO Code System for Tolerances on Linear Sizes — Part 1: Basis of Tolerances, Deviations and Fits.” 2010. https://www.iso.org/obp/ui/#iso:std:iso:286:-1:en.

———. 2016. “ISO 80369-7:2016(En), Small-Bore Connectors for Liquids and Gases in Healthcare Applications — Part 7: Connectors for Intravascular or Hypodermic Applications.” ISO. 2016. http://www.iso.org/cms/render/live/en/sites/isoorg/contents/data/standard/05/80/58011.html.

Izadifar, Mohammad, Paul Babyn, Michael E. Kelly, Dean Chapman, and Xiongbiao Chen. 2017. “Bioprinting Pattern-Dependent Electrical/Mechanical Behavior of Cardiac Alginate Implants: Characterization and *Ex Vivo* Phase-Contrast Microtomography Assessment.” *Tissue Engineering Part C: Methods* 23 (9): 548–64. https://doi.org/10.1089/ten.tec.2017.0222.

Izadifar, Zohreh, Tuanjie Chang, William Kulyk, Xiongbiao Chen, and B. Frank Eames. 2016. “Analyzing Biological Performance of 3D-Printed, Cell-Impregnated Hybrid Constructs for Cartilage Tissue Engineering.” *Tissue Engineering Part C: Methods* 22 (3): 173–88. https://doi.org/10.1089/ten.tec.2015.0307.

J. R. Mitchell, and J. M. V. Blanshard. 1974. “Viscoelastic Behaviour of Alginate Gels.” *Rheologica Acta* 13 (2): 5.

Jia, Weitao, P. Selcan Gungor-Ozkerim, Yu Shrike Zhang, Kan Yue, Kai Zhu, Wanjun Liu, Qingment Pi, et al. 2016. “Direct 3D Bioprinting of Perfusable Vascular Constructs Using a Blend Bioink.” *Biomaterials* 106 (November): 58–68. https://doi.org/10.1016/j.biomaterials.2016.07.038.

Kačarević, Željka, Patrick Rider, Said Alkildani, Sujith Retnasingh, Ralf Smeets, Ole Jung, Zrinka Ivanišević, and Mike Barbeck. 2018. "An Introduction to 3D Bioprinting: Possibilities, Challenges and Future Aspects." *Materials* 11 (11): 2199. https://doi.org/10.3390/ma11112199.

Kang, Donggu, Geunseon Ahn, Donghwan Kim, Hyun-Wook Kang, Seokhwan Yun, Won-Soo Yun, Jin-Hyung Shim, and Songwan Jin. 2018. "Pre-Set Extrusion Bioprinting for Multiscale Heterogeneous Tissue Structure Fabrication." *Biofabrication* 10 (3): 035008. https://doi.org/10.1088/1758-5090/aac70b.

Kim, YongBok, and GeunHyung Kim. 2013. "Collagen/Alginate Scaffolds Comprising Core (PCL)–Shell (Collagen/Alginate) Struts for Hard Tissue Regeneration: Fabrication, Characterisation, and Cellular Activities." *Journal of Materials Chemistry B* 1 (25): 3185–94. https://doi.org/10.1039/C3TB20485E.

Klein, Travis J., Jos Malda, Robert L. Sah, and Dietmar W. Hutmacher. 2009. "Tissue Engineering of Articular Cartilage with Biomimetic Zones." *Tissue Engineering Part B: Reviews* 15 (2): 143–57. https://doi.org/10.1089/ten.teb.2008.0563.

Lee, Chia-Yen, Chin-Lung Chang, Yao-Nan Wang, and Lung-Ming Fu. 2011. "Microfluidic Mixing: A Review." *International Journal of Molecular Sciences* 12 (5): 3263–87. https://doi.org/10.3390/ijms12053263.

Lee, Jaehoo, Kyu Eon Kim, Sumi Bang, Insup Noh, and Chibum Lee. 2017. "A Desktop Multi-Material 3D Bio-Printing System with Open-Source Hardware and Software." *International Journal of Precision Engineering and Manufacturing* 18 (4): 605–12. https://doi.org/10.1007/s12541-017-0072-x.

Lee, Jia Min, and Wai Yee Yeong. 2016. "Design and Printing Strategies in 3D Bioprinting of Cell-Hydrogels: A Review." *Advanced Healthcare Materials* 5 (22): 2856–65. https://doi.org/10.1002/adhm.201600435.

Liu, W., Z. Zhong, N. Hu, Y. Zhou, L. Maggio, A. K. Miri, A. Fragasso, X. Jin, A. Khademhosseini, and Y. S. Zhang. 2018. "Coaxial Extrusion Bioprinting of 3D Microfibrous Constructs with Cell-Favorable Gelatin Methacryloyl Microenvironments." *Biofabrication* 10 (2): 024102–024102. https://doi.org/10.1088/1758-5090/aa9d44.

Liu, Wanjun, Yu Shrike Zhang, Marcel A. Heinrich, Fabio De Ferrari, Hae Lin Jang, Syeda Mahwish Bakht, Mario Moisés Alvarez, et al. 2017. "Rapid Continuous Multimaterial Extrusion Bioprinting." *Advanced Materials* 29 (3): 1604630. https://doi.org/10.1002/adma.201604630.

Loh, Qiu Li, and Cleo Choong. 2013. "Three-Dimensional Scaffolds for Tissue Engineering Applications: Role of Porosity and Pore Size." *Tissue Engineering. Part B, Reviews* 19 (6): 485–502. https://doi.org/10.1089/ten.teb.2012.0437.

Ma, Junyi, Yanbin Lin, Xiangling Chen, Baotang Zhao, and Ji Zhang. 2014. "Flow Behavior, Thixotropy and Dynamical Viscoelasticity of Sodium Alginate Aqueous Solutions." *Food Hydrocolloids* 38 (July): 119–28. https://doi.org/10.1016/j.foodhyd.2013.11.016.

Malda, Jos, Jetze Visser, Ferry P. Melchels, Tomasz Jüngst, Wim E. Hennink, Wouter J. A. Dhert, Jürgen Groll, and Dietmar W. Hutmacher. 2013. "25th Anniversary Article: Engineering Hydrogels for Biofabrication." *Advanced Materials* 25 (36): 5011–28. https://doi.org/10.1002/adma.201302042.

McCullen, Seth D., Hélène Autefage, Anthony Callanan, Eileen Gentleman, and Molly M. Stevens. 2012. "Anisotropic Fibrous Scaffolds for Articular Cartilage Regeneration."

Tissue Engineering Part A 18 (19–20): 2073–83. https://doi.org/10.1089/ten.tea.2011.0606.
McMaster-Carr. 2021a. “Anodized Multipurpose 6061 Aluminum Rods.” 2021. https://www.mcmaster.com/.
———. 2021b. “High-Strength Grade 8 Steel Hex Head Screws.” 2021. https://www.mcmaster.com/.
Meng, Hui-Bo, Ming-Yuan Song, Yan-Fang Yu, Xiu-Hui Jiang, Zong-Yong Wang, and Jian-Hua Wu. 2017. “Enhancement of Laminar Flow and Mixing Performance in a Lightnin Static Mixer.” *International Journal of Chemical Reactor Engineering* 15 (3). https://doi.org/10.1515/ijcre-2016-0112.
Mistry, Pritesh, Ahmed Aied, Morgan Alexander, Kevin Shakesheff, Andrew Bennett, and Jing Yang. 2017. “Bioprinting Using Mechanically Robust Core–Shell Cell-Laden Hydrogel Strands.” *Macromolecular Bioscience* 17 (6): 1600472. https://doi.org/10.1002/mabi.201600472.
Murphy, Sean V, and Anthony Atala. 2014. “3D Bioprinting of Tissues and Organs.” *Nature Biotechnology* 32 (8): 773–85. https://doi.org/10.1038/nbt.2958.
Naghieh, Saman, Md. Sarker, Mohammad Izadifar, and Xiongbiao Chen. 2018. “Dispensing-Based Bioprinting of Mechanically-Functional Hybrid Scaffolds with Vessel-like Channels for Tissue Engineering Applications – A Brief Review.” *Journal of the Mechanical Behavior of Biomedical Materials* 78 (February): 298–314. https://doi.org/10.1016/j.jmbbm.2017.11.037.
Ning, Liqun, Nicholas Betancourt, David J. Schreyer, and Xiongbiao Chen. 2018. “Characterization of Cell Damage and Proliferative Ability during and after Bioprinting.” *ACS Biomaterials Science & Engineering* 4 (11): 3906–18. https://doi.org/10.1021/acsbiomaterials.8b00714.
Ning, Liqun, and Xiongbiao Chen. 2017. “A Brief Review of Extrusion-Based Tissue Scaffold Bio-Printing.” *Biotechnology Journal* 12 (8): 1600671. https://doi.org/10.1002/biot.201600671.
Ozbolat, Ibrahim T., Howard Chen, and Yin Yu. 2014. “Development of ‘Multi-Arm Bioprinter’ for Hybrid Biofabrication of Tissue Engineering Constructs.” *Robotics and Computer-Integrated Manufacturing* 30 (3): 295–304. https://doi.org/10.1016/j.rcim.2013.10.005.
Ozbolat, Ibrahim T., and Monika Hospodiuk. 2016. “Current Advances and Future Perspectives in Extrusion-Based Bioprinting.” *Biomaterials* 76 (January): 321–43. https://doi.org/10.1016/j.biomaterials.2015.10.076.
Ozbolat, Ibrahim T., Kazim K. Moncal, and Hemanth Gudapati. 2017. “Evaluation of Bioprinter Technologies.” *Additive Manufacturing* 13 (January): 179–200. https://doi.org/10.1016/j.addma.2016.10.003.
Prusa Research a.s. 2021a. “Original Prusa I3 MK3S+.” *Prusa3D - 3D Printers from Josef Průša* (blog). 2021. https://www.prusa3d.com/original-prusa-i3-mk3/.
———. 2021b. “PETG.” Prusa Knowledgebase. 2021. https://help.prusa3d.com/en/article/petg_2059/.
Raja, Naren, and Hui-suk Yun. 2016. “A Simultaneous 3D Printing Process for the Fabrication of Bioceramic and Cell-Laden Hydrogel Core/Shell Scaffolds with Potential Application in Bone Tissue Regeneration.” *Journal of Materials Chemistry B* 4 (27): 4707–16. https://doi.org/10.1039/C6TB00849F.

Richards, Dylan, Jia Jia, Michael Yost, Roger Markwald, and Ying Mei. 2017. “3D Bioprinting for Vascularized Tissue Fabrication.” *Annals of Biomedical Engineering* 45 (1): 132–47. https://doi.org/10.1007/s10439-016-1653-z.

Rocca, Marco, Alessio Fragasso, Wanjun Liu, Marcel A. Heinrich, and Yu Shrike Zhang. 2018. “Embedded Multimaterial Extrusion Bioprinting.” *SLAS TECHNOLOGY: Translating Life Sciences Innovation* 23 (2): 154–63. https://doi.org/10.1177/2472630317742071.

Schuurman, W, V Khristov, M W Pot, P R van Weeren, W J A Dhert, and J Malda. 2011. “Bioprinting of Hybrid Tissue Constructs with Tailorable Mechanical Properties.” *Biofabrication* 3 (2): 021001. https://doi.org/10.1088/1758-5082/3/2/021001.

Schwab, Andrea, Riccardo Levato, Matteo D’Este, Susanna Piluso, David Eglin, and Jos Malda. 2020. “Printability and Shape Fidelity of Bioinks in 3D Bioprinting.” *Chemical Reviews* 120 (19): 11028–55. https://doi.org/10.1021/acs.chemrev.0c00084.

Shim, Jin-Hyung, Jung-Seob Lee, Jong Young Kim, and Dong-Woo Cho. 2012. “Bioprinting of a Mechanically Enhanced Three-Dimensional Dual Cell-Laden Construct for Osteochondral Tissue Engineering Using a Multi-Head Tissue/Organ Building System.” *Journal of Micromechanics and Microengineering* 22 (8): 085014. https://doi.org/10.1088/0960-1317/22/8/085014.

Snyder, Jessica, Ae Rin Son, Qudus Hamid, Honglu Wu, and Wei Sun. 2016. “Hetero-Cellular Prototyping by Synchronized Multi-Material Bioprinting for Rotary Cell Culture System.” *Biofabrication* 8 (1): 015002. https://doi.org/10.1088/1758-5090/8/1/015002.

Sobral, Jorge M., Sofia G. Caridade, Rui A. Sousa, João F. Mano, and Rui L. Reis. 2011. “Three-Dimensional Plotted Scaffolds with Controlled Pore Size Gradients: Effect of Scaffold Geometry on Mechanical Performance and Cell Seeding Efficiency.” *Acta Biomaterialia* 7 (3): 1009–18. https://doi.org/10.1016/j.actbio.2010.11.003.

Stoddart, Martin J, Sibylle Grad, David Eglin, and Mauro Alini. 2009. “Cells and Biomaterials in Cartilage Tissue Engineering.” *Regenerative Medicine* 4 (1): 81–98. https://doi.org/10.2217/17460751.4.1.81.

Suh, N. P. 1995. “Axiomatic Design of Mechanical Systems.” *Journal of Mechanical Design* 117 (B): 2–10. https://doi.org/10.1115/1.2836467.

———. 2001. *Axiomatic Design Advances and Applications*. New York: Oxford University Press.

Szalai, E. S., and F. J. Muzzio. 2003. “Fundamental Approach to the Design and Optimization of Static Mixers.” *AIChE Journal* 49 (11): 2687–99. https://doi.org/10.1002/aic.690491103.

Szykiedans, Ksawery, Wojciech Credo, and Dymitr Osiński. 2017. “Selected Mechanical Properties of PETG 3-D Prints.” *Procedia Engineering* 177: 455–61. https://doi.org/10.1016/j.proeng.2017.02.245.

Tan, Edgar Yong Sheng, and Wai Yee Yeong. 2015. “Concentric Bioprinting Of Alginate-Based Tubular Constructs Using Multi-Nozzle Extrusion-Based Technique.” *International Journal of Bioprinting*, July. https://doi.org/10.18063/IJB.2015.01.003.

Tan, Y. S. E., and W. Y. Yeong. 2014. “Direct Bioprinting of Alginate-Based Tubular Constructs Using Multi-Nozzle Extrusion-Based Technique.” In *Proceedings of the 1st International Conference on Progress in Additive Manufacturing*, 423–27. Research Publishing Services. https://doi.org/10.3850/978-981-09-0446-3_093.

Torres, Jonathan, José Cotelo, Justin Karl, and Ali P. Gordon. 2015. “Mechanical Property Optimization of FDM PLA in Shear with Multiple Objectives.” *JOM* 67 (5): 1183–93. https://doi.org/10.1007/s11837-015-1367-y.

Van Blitterswijk, Clemens. 2014. *Tissue Engineering*. Boston, MA: Elsevier.
Xu, Tao, Kyle W Binder, Mohammad Z Albanna, Dennis Dice, Weixin Zhao, James J Yoo, and Anthony Atala. 2012. "Hybrid Printing of Mechanically and Biologically Improved Constructs for Cartilage Tissue Engineering Applications." *Biofabrication* 5 (1): 015001. https://doi.org/10.1088/1758-5082/5/1/015001.
Zhang, W. J., Y. Lin, and Niraj Sinha. 2011. "ON THE FUNCTION-BEHAVIOR-STRUCTURE MODEL FOR DESIGN." *Proceedings of the Canadian Engineering Education Association*, August. https://doi.org/10.24908/pceea.v0i0.3884.
Zhao, Yu, Rui Yao, Liliang Ouyang, Hongxu Ding, Ting Zhang, Kaitai Zhang, Shujun Cheng, and Wei Sun. 2014. "Three-Dimensional Printing of Hela Cells for Cervical Tumor Model *in Vitro*." *Biofabrication* 6 (3): 035001. https://doi.org/10.1088/1758-5082/6/3/035001.

APPENDIX A - DETAIL RENDERS OF PRINTHEAD ASSEMBLY AND CARRIAGE

This appendix includes renders of the printhead components and the carriage from the detail design of the multi-material bioprinting system. All of the renders were made using Inventor® 2018 (Autodesk 2018). Figure A.1 shows the plug, Figure A.2 shows the single-inlet head, Figure A.3 shows the mixing core, Figure A.4 shows the dual-inlet head, and Figure A.5 shows the carriage.

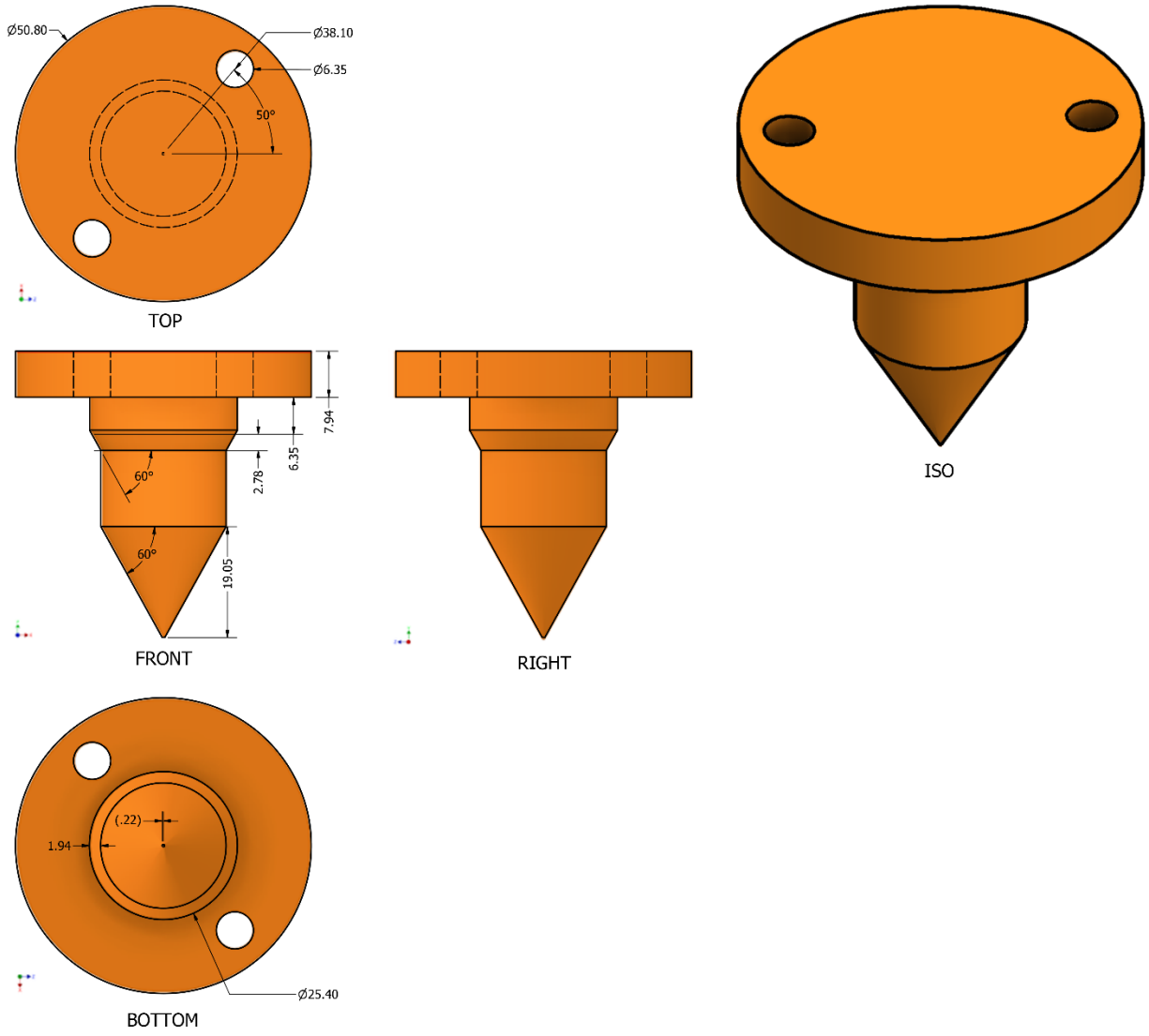

Figure A.1: Detail Render of Plug

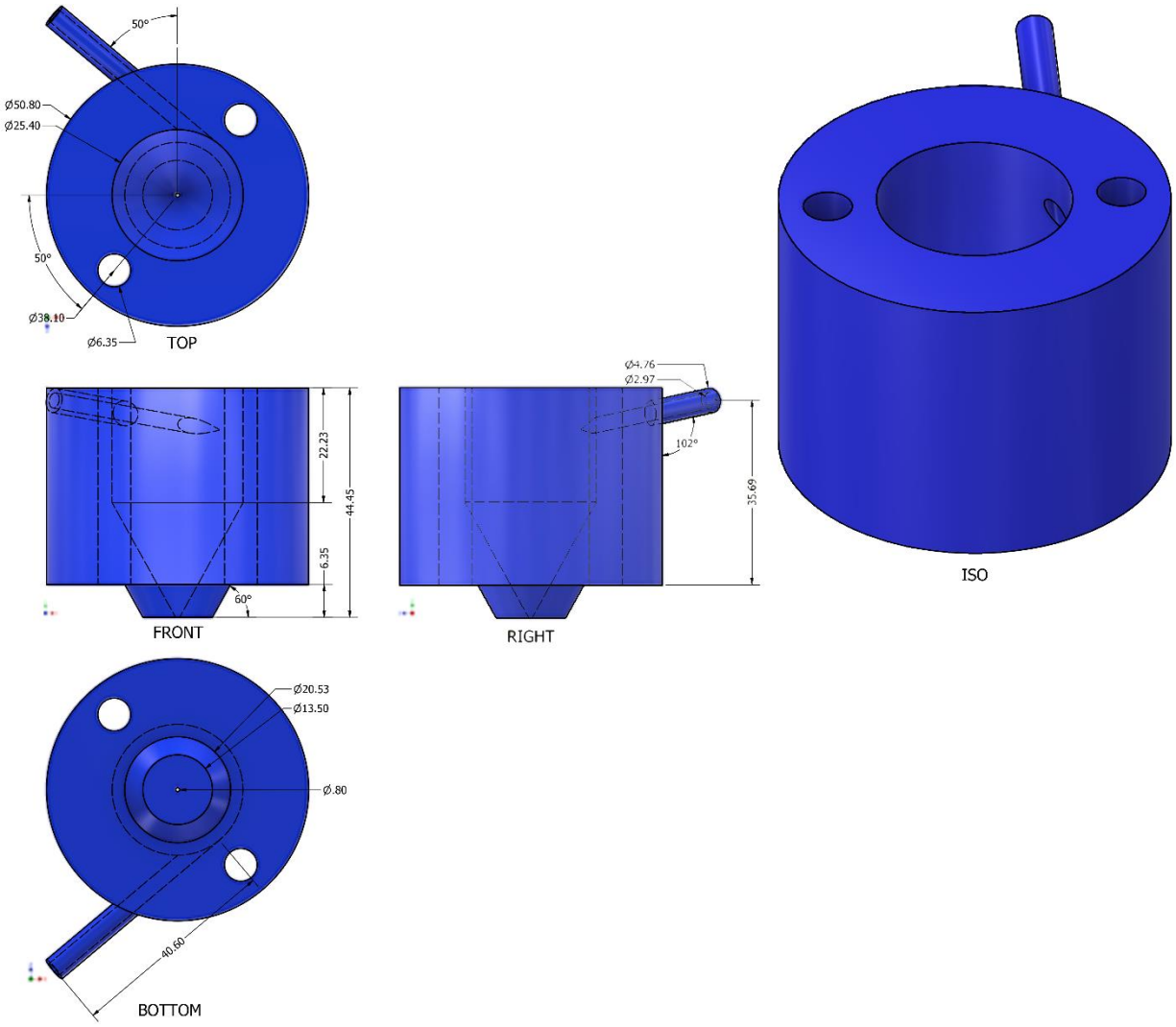

Figure A.2: Detail Render of Head 1

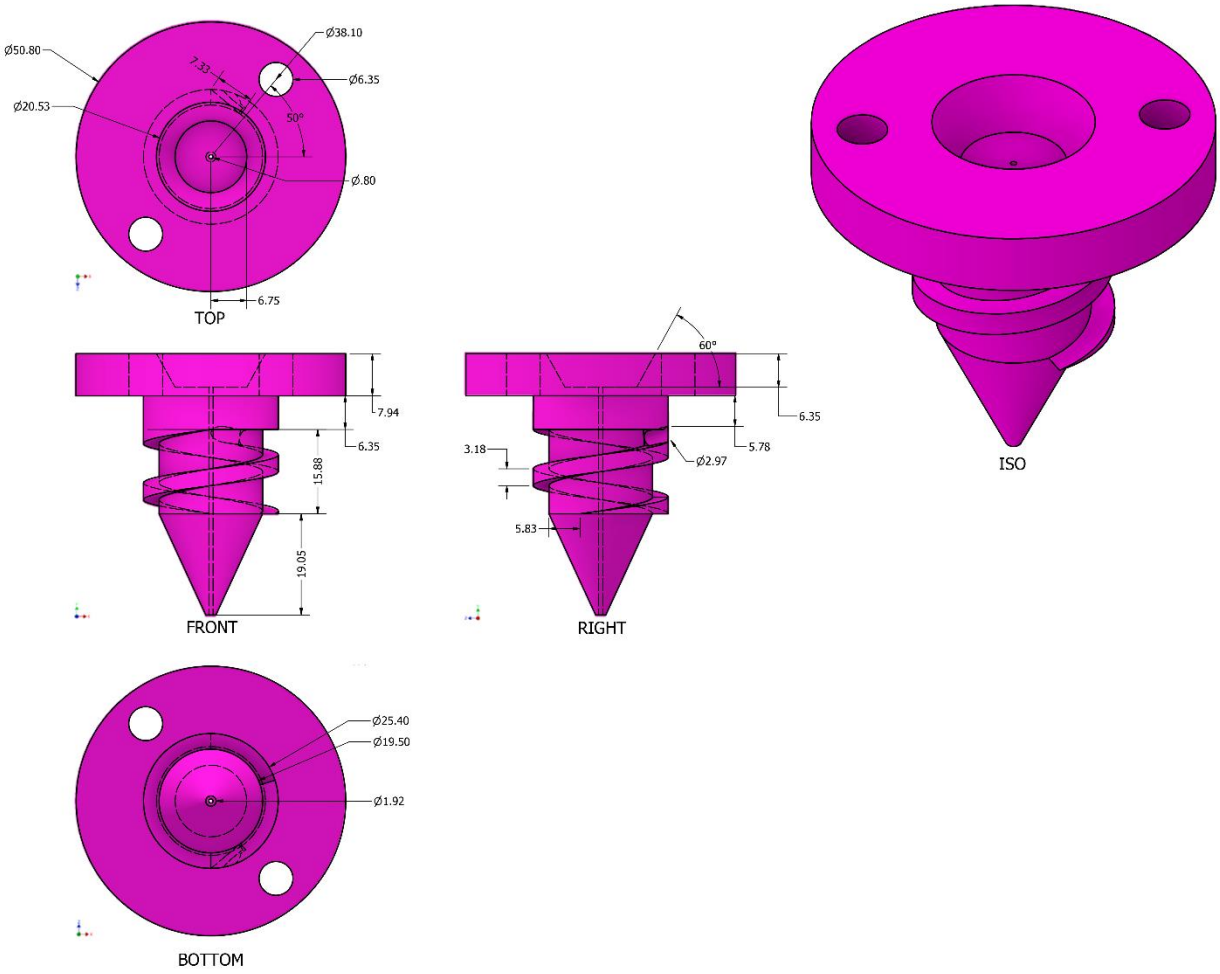

Figure A.3: Detail Render of Core

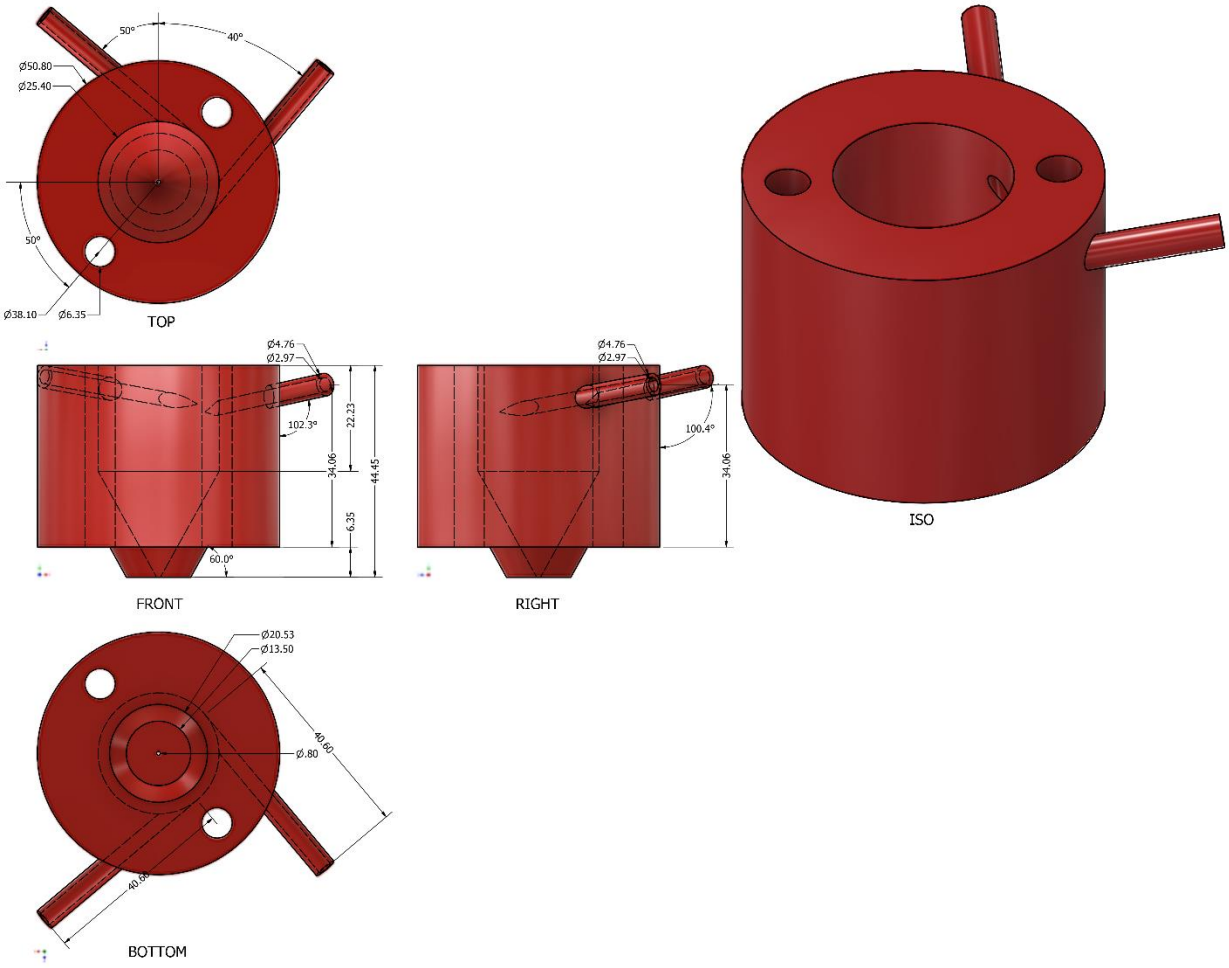

Figure A.4: Detail Render of Head 2

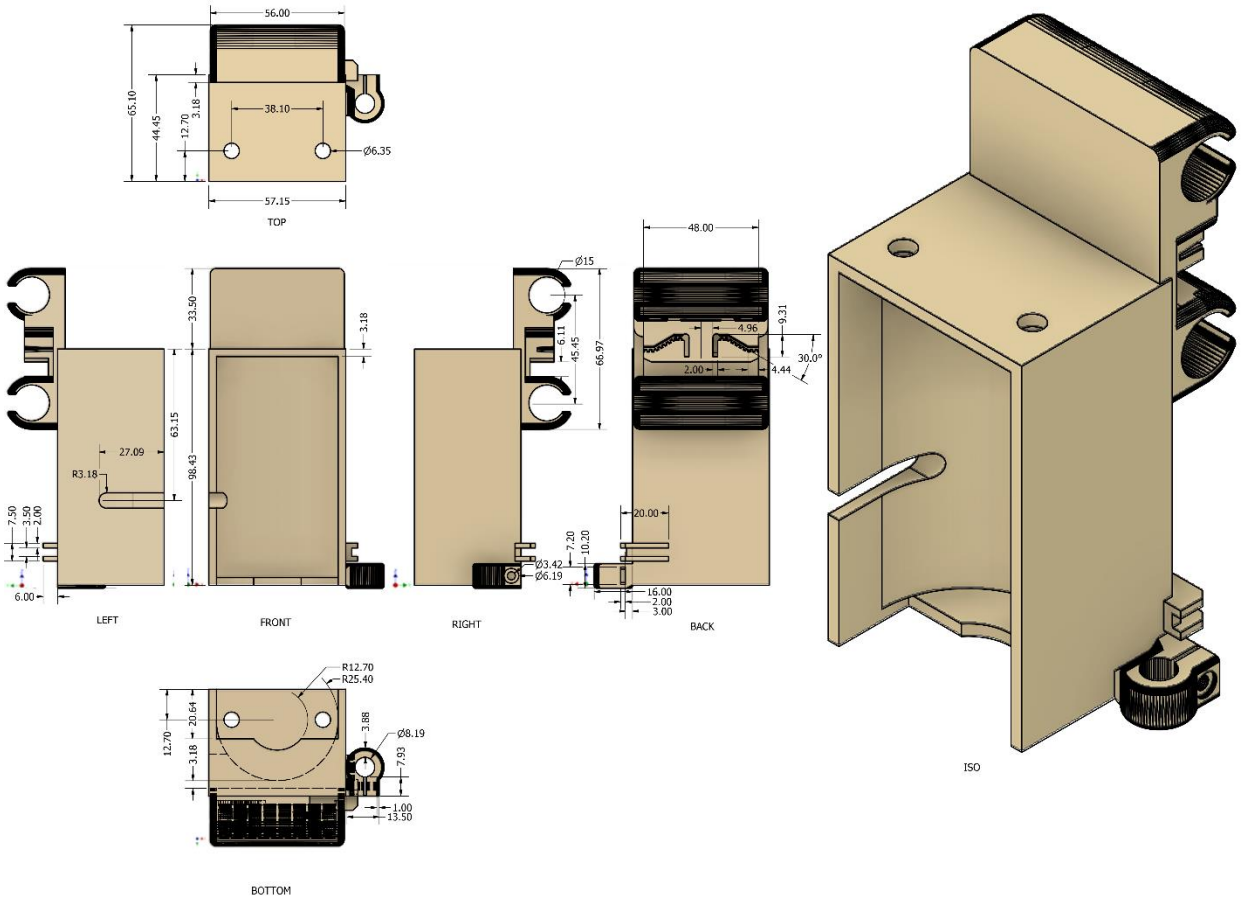

Figure A.5: Detail Render of Carriage

APPENDIX B - SPECIFICATIONS OF ELVEFLOW OB1 MK3+ MICROFLUIDIC FLOW CONTROLLER

This appendix holds the technical specifications of the selected pressure-driven controller to drive the material through the printhead assembly – the Elveflow OB1 MK3+ Microfluidic controller. Figure B.1 shows a table of the technical specifications (Elveflow 2021).

TECHNICAL SPECIFICATIONS OB1 MK3+

OB1 MK3+ CHANNEL PRESSURE RANGE	0 to 200 mbar[1] (0 to 2.9 psi)	0 to 2,000 mbar[1] (0 to 29 psi)	0 to 8,000 mbar[1] (0 to 116 psi)	-900 to 1,000 mbar[1] (-13 to 14.5 psi)	-900 to 6,000 mbar[1] (-13 to 87 psi)
Pressure stability [2]	**0.005 % FS** 10 µbar (0.00014 psi)	**0.005 % FS** 100 µbar (0.0014 psi)	**0.006% FS** 500 µbar (0.007 psi)	-900 to 500 mbar: **0.005 % FS** 100 µbar (0.0014 psi) 500 to 1,000 mbar: **0.007 % FS** 150 µbar (0.0021 psi)	-900 to 2,000 mbar: **0.005 % FS** 350 µbar (0.05 psi) 2,000 to 6,000 mbar: **0.007 % FS** 525 µbar (0.076 psi)
Response time [3]	down to 9 ms				
Settling time [4]	down to 35 ms				
Minimum pressure increment	**0.003 % FS** 6.1 µbar - 0,000085 ps	**0.003 % FS** 56 µbar - 0,00085 psi	**0.003 % FS** 240 µbar - 0,0035 psi	**0.0032 % FS** 61 µbar - 0,00085 psi	**0.003 % FS** 210 µbar - 0.003 psi
Input pressure	**1.5 bar - 10 bar** non corrosive, non explosive, dry and oil-free gases, e.g. air, argon, N2, CO2, ...				
Input vacuum [5]	/			any value from 0 to -1 bar	
Liquid compatibility	no liquid should enter the OB1 any aqueous or organic solvent, oil or biological sample solution can be propelled				

Non-contractual information, may be changed without notice.

POWER CONSUMPTION (maximum): 12 W **CASE DIMENSIONS** (length x width x height): 240 x 223 x 80 mm **WEIGHT:** 1.7 kg to 3.04 kg (3.1 Kg) **TTL TRIGGER:** input 5V / output 3,3V

(1) Max pressure value might vary by +/- 2.5% (2) Pressure stability (standard deviation) measured over the full pressure range with an external high accuracy pressure sensor (Paroscientific MODEL 745) (3) Depending on your computer's operating system (4) Volume dependent – Measurement done on 12 mL reservoir for a set point from 100 to 200 mbar (5) The vaccum channels can be used without vacuum source if only positive pressures are desired.

Figure B.1: Elveflow OB1 MK3+ Technical Specifications (Elveflow 2021)

APPENDIX C - DATA FROM AXIOMATIC EVALUATION OF MULTI-MATERIAL BIOPRINTING SYSTEMS

This appendix includes the raw data used to determine the system range in the information content calculations for the multi-material bioprinting systems. Table C.1 shows data for the core-and-shell systems, Table C.2 shows data from the side-by-side systems, and Table C.3 shows data from the advanced systems. Last, Table C.4 summarizes the existing bioprinting systems and includes data from the proposed modular bioprinting system.

Table C.1 Data from Core-and-shell Bioprinting Systems

Source	Core Nozzle	Core Material	Shell Nozzle	Shell Material	Nozzle Length	Syringe Capacity	Cells	Crosslinking Method	Commercial Bioprinter	Pressure Source	Applied Pressure	Temperature	Filament Diameter	Nozzle Speed	Viability
(Cornock et al. 2014) Coaxial additive manufacture of biomaterial composite scaffolds for tissue engineering	200-300 µm Custom Shape	2% wt/wt Alginate	900-1100 µm Custom shape	PCL	N/A	N/A	L929	Pre-crosslinked CaCO3 added for 45 mins	Scaffold Plotting System (SPS1000) Korean Institute for Machinery and Materials	Unnamed pressure controller	Alginate 1-25 kPa PCL 400-600 kPa	Alginate 23°C PCL 90-140°C	600 µm	N/A	Alginate w/ PCL shell (0.7 +- 0.7% after 2hr) Alginate in 24 G nozzle (89.2 +- 0.33%) Alginate on slide (93.0+- 0.5%)
(Gao et al. 2015) Coaxial nozzle-assisted 3D bioprinting with built-in microchannels for nutrients delivery	21G, 22G, 23G [510 µm, 410 µm, 340 µm] Straight nozzle	2-5% w/v CaCl	14.5G [1600 µm] Tapered	2-5% w/v Alginate Both cell-free and laden	N/A	N/A	L929 Mouse Fibroblasts	CaCl 2-5% w/v	XYZ Adjustable Stage	Single Four-channel Pump	N/A	N/A	Average Inner Diameter 892 µm Outer Diameter 1192 µm	Stage movement speed 750 to 1150 mm/min (straight filaments)	Microchannels 92.9 +- 2.4% (1 day) 84.7+- 3.2%(4 day) 67.1+-- 3.9 (7 days) Without Microchannels 83.8+- 2.0%(1 day) 71.6+- 1.2%(4 day) 50.2+- 1.6%(7 days)

(Jia et al. 2016) Direct 3D bioprinting of perfusable vascular constructs using a blend bioink	27-30G [210 µm - 160 µm] (30G) [160 µm] Two- and three-tiered coaxial Straight nozzle	GelMA (5 or 7%) Alginate (2 or 3%) PEGTA (2 or 3%) Photo Initiator	18-25 G [840 µm, 260 µm] (20G) [600 µm] Straight nozzle	0.3 M CaCl2	N/A	N/A	HUVECs and MSC (3x10^6/mL)	Pre-crosslinking with CaCl2 solution, CaCl2 solution spray UV light immediately after printing cell-laden constructs	Novogen MMX Bioprinter Organovo, San Diego, CA, USA	Microfluidic syringe pumps (Harvard Apparatus) 40 and 35 uL/min	N/A	20°C	Average Outer Diameter 500-1500 µm Inner Diameter 400-1000 µm (Outer Diameter 800µm, Inner Diameter 690 µm)	2-6 mm/s [120-360 mm/min]	20s UV exposure 82% 1 day,85% 3day, 90% 7day 30s 80% 1day, 88% 3day, 92% 7 day 40s 66% 1 day, 70% 3day, 75% 7 day
(Dai et al. 2017) Coaxial 3D bioprinting of self-assembled multicellular heterogeneous tumor fibers	21G [510 µm] Straight nozzle	Cell-laden Fibrinogen	16G [1190 µm] Straight nozzle	Alginate Gelatin Thrombin	N/A	N/A	GSC23	CaCl2 3% w/v receiving tank	XYZ Adjustable Stage	Two Syringe Pumps Core (3-6 mL/h) Shell (15-30 mL/h)	N/A	N/A	Average Inner Diameter 242.89+-14.76 (527.49+-13.36) µm Outer Diameter 870.87+-17.96 (886.71+-9.83) µm	N/A	Cells in core immediately after bioprinting Average – 96.366+-1.54%
(Mistry et al. 2017) Bioprinting Using Mechanically Robust Core–Shell Cell-Laden Hydrogel Strands	27G [210 µm] Straight nozzle	Cell-laden Hydrogel GelMA Collagen Matrigel	18G [840 µm] Taper nozzle	Partial crosslink PEGDA (20 kDa) and/or Alginate (various concentrations)	N/A	N/A	3T3 HepG2 HUVEC	17x10-3M CaCl UV/Irgacure 2959 or Visible/LAP	RegenHU, Switzerland	Two pumps 0.01 mL/min and 0.1 mL/min	N/A	Core Temperature 5°C	~800 µm	N/A	Visible light crosslinking 90+%
(W. Liu et al. 2018) Coaxial Extrusion Bioprinting of 3D Microfibrous Constructs with Cell-Favorable Gelatin Methacryloyl Microenvironments	28G [180 µm]	CaCl (1%) GelMA (1.5%) Cells (2x10^6/mL)	23G [340 µm]	Alginate 1%	N/A	N/A	MDA-MB-231 and MCF7 NIH/3T3 and HUVECS	Pre-crosslinking with CaCl solution	Luzbolt TAZ 4 Aleph Objects, Loveland, CO, USA	Two Single-Channel Syringe Pumps	N/A	N/A	Channel Diameter 723+-40 (300 uL/min) 583+-19 (600 uL/min) 469+-8 (200 ul/min CaCl 500Alg) 691+-37 (900 ul CaCl 500 Alginate) Wall Thickness 100 µm	Hollow Alginate 500mm/min GelMA/Alginate 500 mm/min	Day 1 43.4% ± 3.9% to 63.4% ± 3.8% for MDA-MB-231, MCF7, NIH/3T3, and HUVECs Day 1 (1.5 and 2% GelMA in cores) 64.6% ± 5.6% and 88.7% ± 4.0% for MDA-MB-231, MCF7, NIH/3T3, and HUVECs
RANGE	160 µm - 510 µm 4 straight 1 custom 1 unknown	2 Alginate (2-3%) 2 CaCl (1-5%) 3 GelMA (1.5-7%) 1 PEGTA (2-3%) 1 Photo Initiator	260 µm - 1600 µm 2 straight 1 custo	4 Alginate (1-5%) 1 PCL 1 CaCl (0.3 M) 1 Gelatin 1 Thrombin 1 PEGDA	N/A	N/A	2 L929 3 HUVEC 2 3T3 1 MSC 1 MCF7 1 MDA-	3 CaCl pre-crosslinking 3 CaCl solution (2-5%) 2 UV 1 Visible/LAP 1 CaCl spray	4 Commercial Bioprinters 2 XYZ Adjustable stage		Hydrogel 1 - 25 kPa Synthetic 400-600 kPa	Hydrogel 5-20°C Synthetic 90-140°C	Inner Diameter 228.13 µm - 1000 µm Outer Diameter 800 µm - 1500 µm	120 - 1150 mm/min	Day 0 90-98 Day 1 40-92 Day 3 70-88 Day 4

		1 Fibrinogen 1 Collagen 1 Matrigel	m 1 tapered 1 unknown				MD-231									70-89 Day 7 65-92

Table C.2 Data from Side-by-side Bioprinting Systems

Source	Nozzle One	Material One	Nozzle Two	Material Two	Nozzle Length	Syringe Capacity	Cells	Crosslinking Method	Commercial Bioprinter	Material Organization	Applied Pressure	Temperature	Filament Diameter	Nozzle Speed	Viability
(Schuurman et al. 2011) Bioprinting of hybrid tissue constructs with tailorable mechanical properties	23G 340 µm Straight nozzle	PCL (Mw 70 000–90 000)	210 µm Straight nozzle	2% w/v Alginate	N/A	N/A	Human Chondrocytes	102 mM CaCl	BioScaffolder Dispensing System (SYS+ENG, Salzgitter-Bad, Germany) Multi-head	Alginate between PCL	PCL 0.5 MPa [500 kPa]	Alginate Room PCL 160°C	N/A	N/A	Day 0 80+% Day 1 70% Day 3 65%
(Shim et al. 2012) Bioprinting of a mechanically enhanced three-dimensional dual cell-laden construct for osteochondral tissue engineering using a multi-head tissue/organ building	200 µm and 150 µm Straight nozzle	PCL (Mw 70 000-90 000)	200 µm and 150 µm Straight Nozzle	4% w/v Alginate	N/A	N/A	Human Chondrocytes and Osteoblasts	100 mM CaCl	Custom Multi-head Bioprinter	Alginate between PCL	PCL 300 kPa - 400 kPa	Alginate 20°C PCL 80°C	PCL 250 µm Alginate N/A	PCL 100 mm/min Alginate 250 mm/min	Day 1 90-94% Day 7 93.9+-0.3% (chondro) 95.6+-1.8% (osteo)
(Chen and Ozbolat 2013) A Multi-Material Bioprinting Platform towards Stratified Articular Cartilage Tissue Fabrication	250 µm Inner Diameter Straight nozzle	4% w/v Alginate	250 µm Inner Diameter 45° nozzle	Alginate Cellular Spheroids	Alginate 12.7 mm Cell Spheroid 38.1 mm 45° bend	N/A	Cartilage progenitor cells	4% w/v CaCl	Custom Multi-arm Bioprinter	Cell spheroids between alginate	Alginate 70 kPa Cell Spheroid 117 kPa	Room	N/A	Max 300 mm/s [18000 mm/min]	24 hr 99%
(Duan et al. 2013) 3D Bioprinting of heterogeneous aortic valve conduits with alginate/ gelatin hydrogels	800 µm Tapered nozzle	0.06 g/mL Gelatin 0.05 g/mL Alginate Cell 1	800 µm Tapered	0.06 g/mL Gelatin 0.05 g/mL Alginate Cell 2	From EFD Inc, East Providence, RI	N/A	Porcine Valve interstitial cells Human aortic smooth muscle cells	300 mM CaCl	Standard Fab@Home Printhead adapted for dual syringes Multi-head	Root region with Cell 1 and leaf region with cell 2	N/A	Room	N/A	5 mm/s [300 mm/s]	Day 7 84.6+-3.1%
(Tan and Yeong 2014) Direct Bioprinting of Alginate-Based Tubular Constructs Using Multi-	250 µm Straight nozzle	0.06g/mL Alginate 0.01-0.03 g/mL Xanthan gum 0.022 g/mL CaCl	300 µm Straight nozzle	500 mM CaCl	Needle DD-135N-N4	N/A	N/A	No further crosslinking	Multi-nozzle Extrusion-based technique from BioCad (RegenHu) Multi-nozzle	Circular shell of hydrogel with CaCl filling	Alginate 1.5 bar [150 kPa] CaCl 0.5 bar [50 kPa]	Room	N/A	Path Speed Alginate 500 mm/min CaCl	N/A

Nozzle Extrusion-Based Technique													100 mm/min	
(Zhao et al. 2014) Three-dimensional printing of Hela cells for cervical tumor model in vitro	250 µm Inner Diameter Straight nozzle	10% w/v Gelatin 1% w/v Alginate 2% w/v Fibrinogen + Cells	250 µm Inner Diameter Straight nozzle	Hela/Hydrogel	N/A	N/A	Hela Cells	Physical crosslinking at 25°C 3% w/v CaCl 20 U/mL thrombin	Cell Assembly System 1 Multi-nozzle	Cubic grid	N/A	10-25°C (10°C chamber and 25°C nozzle)	Average Hela/Hydrogel 500 µm	N/A	After printing 94.9+-2.2%
(Izadifar et al. 2016) Analyzing Biological Performance of 3D-Printed, Cell-Impregnated Hybrid Constructs for Cartilage Tissue Engineering	300 µm Inner Diameter Straight nozzle	PCL (Mw 48,000–90,000)	200 µm Inner Diameter Tapered nozzle	2%-5% Alginate Cells	N/A	N/A	Chondrocytes	6 100 mM CaCl Solution 160 mM CaCl aerosol	3D-Bioplotter System (EnvisionTec GmbH) Multi-head	Alternating PCL and alginate	Alginate 0.01 MPa [10 kPa] PCL 0.8 MPa [800 kPa]	Alginate 10°C PCL 65-80°C	N/A	PCL 1 mm/s [60 mm/min] Alginate 25 mm/s [1500 mm/min]	Rounded 80+% (Day 0, 3, 7, 14) Fibroblastic 80+% (Day 0) 76% (Day 7) 85% (Day 14)
(Lee et al. 2017) A Desktop Multi-Material 3D Bio-Printing System with Open-Source Hardware and Software	200 µm Inner Diameter Straight nozzle	PLGA	250 µm Inner Diameter Straight nozzle	5% w/v HA Cells	N/A	N/A	Fibroblasts	N/A	Custom Carousel Multichannel dispensing system Multi-nozzle	Cylindrical PLGA cell with hydrogel filler	PLGA 220-280 kPa HA 320-380 kPa	PLGA 130 °C	PLGA 185-269.2 µm HA 480.2 – 1447.5 µm	PLGA 200–250 mm/min HA 280 – 420 mm/min	No dead cells on surface Could not image cells deep inside
RANGE	150 µm - 800 µm 7 Straight 1 Tapered	4 Alginate (1-6%) 2 PCL (Mw 48,000–90,000) 2 Gelatin (6-10%) 1 Xanthan (1-3%) 1 Fibrinogen (2%) 1 PLGA 1 CaCl (2%)	150 µm - 800 µm 5 Straight 2 Tapered 1 45°	5 Alginate (2-5%) 1 Gelatin (6%) 1 Cell spheroids 1 Hela 1 HA (5%) 1 CaCl (500 mM)	12.7 mm	N/A	3 Chondrocytes 1 Osteoblasts 1 Fibroblasts 1 Hela 1 Human aortic smooth muscle cells 1 Porcine valve interstitial cells 1 Cartilage progenitor cells	6 100 - 300 mM CaCl solution 1 160 mM CaCl aerosol 1 Physical Crosslinking at 25°C 2 No further crosslinking	4 Multi-head 3 Multi-nozzle 1 Multi-arm	Alternating Filaments	Alginate 10 - 150 kPa PCL 220-800 kPa	Alginate 10-25°C PCL 65-160°C Hela 10-25°C PLGA 130°C	PCL 250 µm PLGA 185-269.2 µm HA 480.2-1447.5 µm	Alginate 250 - 1500 mm/min PCL 100 mm/min	Day 0 80-95 Day 1 70-95% Day 3 65-80 Day 7 80-95

Table C.3 Data from Advanced Bioprinting Systems

Source	Nozzle One	Material One	Nozzle Two	Material Two	Nozzle Length	Syringe Capacity	Cells	Crosslinking Method	Commercial Bioprinter	Applied Pressure	Temperature	Filament Diameter	Nozzle Speed	Viability
(Liu et al. 2017) Rapid Continuous Multimaterial Extrusion Bioprinting	N/A	5% GelMA 1% Alginate Cells	N/A	Dyes	N/A	N/A	HDF, HUVEC, HepG2, hMSC	Photo-crosslinked immediately after printing	Proof of concept bioprinter Movable stage	3 psi [20.7 kPa]	N/A	100-200 µm	400 mm/min	Day 0 90-95% Day 1 80-90% Day 7 70-95%
(Kang et al. 2018) Pre-set extrusion bioprinting for multiscale heterogeneous tissue structure fabrication	840, 610, 400, 250, 200 µm Inner Diameter Tapered nozzle Tetramerous cartridge in 3 ml syringe 9.3 mm Tetramerous cartridge in 10 ml syringe 15 mm	2%, 3%, 4% (w/v) Alginate	N/A	Fluorescent particles from Fisher (R0200B, G0200B, B0200; 2.0 µm, 2.0 µm, and 2.1 µm, respectively)	Tetramerous cartridge 15 mm Other cartridges 20 mm	3 mL or 10 mL	HepG2 cells, Ecs	200 mM CaCl solution	N/A Commercial Printer	15 kPa	Head 4°C	Quarter diameter approximately 260 µm, 211 µm, 161 µm, 111 µm, and 76 µm For 840, 610, 400, 250, 200 µm Inner Diameter, respectively	13.75 mm/s dispensing speed [825 mm/min]	0, 15, 30, 45, 60, or 120 min after printing Lower viability over time Lower viability with decreasing diameter Day 0 (75-95%)
(Rocca et al. 2018) Embedded Multimaterial Extrusion Bioprinting	Three 27G needles 210 µm Inner Diameter	2% Alginate	N/A	Fluorescent beads (AmeriColor)	N/A	N/A	N/A	0.05% CaCl 21 - 30% PF-127 Solution	Lulzbot TAZ 5	10 - 70 psi [68.9 - 782.6 kPa]	3D Bioprinting Process 23°C Gel-to-liquid transition 4°C	50-360 µm	1-30 m/s [60-1800 mm/min]	N/A
RANGE	200 - 840 µm 1 straight 2 tapered	3 Alginate (1-5%) 1 GelMA (5%)	N/A	Dye Fluorescent particles Fluorescent beads	N/A	**N/A**	**2 HepG2 1 HDF 1 HUVEC 1 hMSC 1 Ecs**	**1 Photo crosslinking 1 CaCl solution 1 No further crosslinking**	**2 Commercial Printer 1 Proof of concept printer**	**15-782.6 kPa**	**4-23°C**	**50-360 µm**	**60-1800 mm/min**	**Day 0 75-95% Day 1 80-90% Day 7 70-95%**

Table C.4 Summary of Existing Bioprinting Systems and Modular Bioprinting System

Group	Nozzle One	Material One	Nozzle Two	Material Two	Nozzle Length	Syringe Capacity	Cells	Crosslinking Method	Commercial Bioprinter	Applied Pressure	Temperature	Filament Diameter	Nozzle Speed	Viability
Side-by-side	150 µm - 800 µm 7 Straight 1 Tapered	4 Alginate (1-6%) 2 PCL (Mw 48,000–90,000) 2 Gelatin (6-10%) 1 Xanthan (1-3%) 1 Fibrinogen (2%) 1 PLGA 1 CaCl (2%)	150 µm - 800 µm 5 Straight 2 Tapered 1 45°	5 Alginate (2-5%) 1 Gelatin (6%) 1 Cell spheroids 1 Hela 1 HA (5%) 1 CaCl (500 mM)	12.7 mm	N/A	3 Chondrocytes 1 Osteoblasts 1 Fibroblasts 1 Hela 1 Human aortic smooth muscle cells 1 Porcine valve interstitial cells 1 Cartilage progenitor cells	6 100 - 300 mM CaCl solution 1 160 mM CaCl aerosol 1 Physical Crosslinking at 25°C 2 No further crosslinking	4 Multi-head 3 Multi-nozzle 1 Multi-arm	Natural 10 - 150 kPa Synthetic 220-800 kPa	Natural 10-25°C Synthetic 65-160°C	185 - 1447.5 µm	100 - 1500 mm/min	Day 0 80-95% Day 1 70-95% Day 3 65-80% Day 7 80-95%
Coaxial	160 µm - 510 µm 4 Straight 1 Custom 1 Unknown	2 Alginate (2-3%) 2 CaCl (1-5%) 3 GelMA (1.5-7%) 1 PEGTA (2-3%) 1 Photo Initiator 1 Fibrinogen 1 Collagen 1 Matrigel	260 µm - 1600 µm 2 Straight 1 Tapered 1 Custom 1 Unknown	4 Alginate (1-5%) 1 PCL 1 CaCl (300 mM) 1 Gelatin 1 Thrombin 1 PEGDA	N/A	N/A	2 L929 3 HUVEC 2 3T3 1 MSC 1 MCF7 1 MDA-MD-231	3 CaCl pre-crosslinking 3 CaCl solution (2-5%) 2 UV 1 Visible/LAP 1 CaCl spray	4 Commercial Bioprinters 2 XYZ Adjustable stage	Natural 1 - 25 kPa Synthetic 400-600 kPa	Natural 5-20°C Synthetic 90-140°C	Inner Diameter 228.13 µm - 1000 µm Outer Diameter 800 µm - 1500 µm	120 - 1150 mm/min	Day 0 90-98% Day 1 40-92% Day 3 70-88% Day 4 70-89% Day 7 65-92%
Advanced	200 - 840 µm 1 straight 2 tapered	3 Alginate (1-5%) 1 GelMA (5%)	N/A	Dye Fluorescent particles Fluorescent beads	N/A	N/A	2 HepG2 1 HDF 1 HUVEC 1 hMSC 1 ECs	1 Photo crosslinking 1 CaCl solution 1 No further crosslinking	2 Commercial Printer 1 Proof of concept printer	15-782.6 kPa	4-23°C	50-360 µm	60-1800 mm/min	Day 0 75-95% Day 1 80-90% Day 7 70-95%
TOTAL	150 - 840 µm 8 Straight 3 Tapered 1 Custom 1 Unknown	7 Alginate (1-6%) 2 PCL (Mw 48,000–90,000) 4 GelMA (1.5-7%) 2 Gelatin (6-10%) 2 Fibrinogen (2%) 1 PEGTA (2-3%) 1 Photo Initiator 1 Xanthan (1-3%) 1 PLGA 1 CaCl (2%)	150 - 1600 µm 7 Straight 3 Tapered 1 Custom 1 45° 1 Unknown	5 Alginate (2-5%) 2 Gelatin (6%) 2 CaCl (300 - 500 mM) 1 Cell spheroids 1 Hela 1 HA (5%) 1 PCL 1 Thrombin 1 PEGDA Dye Fluorescent particles Fluorescent beads	12.7 mm	N/A	3 Chondrocytes 4 HUVEC 2 L929 2 3T3 2 HepG2 1 Osteoblasts 1 Fibroblasts 1 Hela 1 Human aortic smooth muscle cells 1 Porcine valve interstitial cells 1 Cartilage progenitor cells 1 MSC 1 MCF7 1 MDA-MD-231 1 HDF 1 hMSC 1 ECs	10 100 - 500 mM CaCl solution 3 CaCl pre-crosslinking 3 No further crosslinking 2 160 mM CaCl aerosol 2 No further crosslinking 2 UV 2 Photo crosslinking 1 Physical Crosslinking at 25°C	4 Multi-head 4 Commercial Bioprinters 3 Multi-nozzle 2 XYZ Adjustable stage 1 Multi-arm 1 Proof of concept printer	Natural 10 - 782.6 kPa Synthetic 220 - 600 kPa	Natural 4-25°C Synthetic 65-160°C	50-1500 µm	60-1500 mm/min	Day 0 90-98% Day 1 40-92% Day 3 70-88% Day 4 70-89% Day 7 65-92%
Modular	Any	Alginate (1-6%)	N/A	Dye Fluorescent particles Fluorescent beads	Any	N/A	Any	Any	Commercial 3D printer	10 - 400 kPa	Room	N/A	10-6000 mm/min	N/A